ROLE OF BAP1 IN MESOTHELIOMA AND MELANOMA PREDISPOSITION

A Dissertation
Submitted to
the Temple University Graduate Board

In Partial Fulfillment
of the Requirements for the Degree
DOCTOR OF PHILOSOPHY

---

by
Anna-Mariya Kukuyan
May 2019

Examining Committee Members:

Joseph R. Testa, PhD, Fox Chase Cancer Center
Raza M. Zaidi, PhD, Fels Institute for Cancer Research and Molecular Biology
Xavier Graña, PhD, Fels Institute for Cancer Research and Molecular Biology
Siddharth Balachandran, PhD, Fox Chase Cancer Center
Richard T. Pomerantz, PhD, Fels Institute for Cancer Research and Molecular Biology
Haifeng Yang, PhD, External Member, Thomas Jefferson University

ABSTRACT

BAP1 (BRCA-Associated Protein1) is a tumor suppressor gene encoding a deubiquitinating enzyme (DUB) that regulates many facets of cellular biology. Genetic studies have demonstrated that somatic *BAP1* mutations occur in numerous cancer types and that germline *BAP1* mutations lead to a cancer susceptibility disorder that predisposes individuals to various tumors, in particular malignant mesothelioma (MM) and both uveal melanoma (UM) and cutaneous melanoma (CM).

The Testa laboratory has identified several families (including one in Louisiana, designated Lou) with germline *BAP1* mutations, in which there were recurrent cases of MM, UM, and CM. We generated a *Bap1* mutant mouse model with a knockin mutation identical to that observed in the Lou family (*Bap1*$^{+/Lou}$) to test whether this mutation alone confers susceptibility to ultraviolet (UV) light-induced melanomagenesis either alone or in combination with a mutation found in a well-established Hepatocyte Growth Factor (HGF)/Scatter Factor transgenic mouse model. Neither *Bap1*$^{+/Lou}$, *HGF*, nor *Bap1*$^{+/Lou}$*;HGF* mice showed a significantly higher incidence or shorter latency of UV light-induced melanoma than wild type (WT) mice. The study also suggests that germline mutation of *Bap1* alone does not cause an increased incidence of UV-induced melanomas under the conditions used in this investigation.

Recent evidence indicates that BAP1 participates in the DNA damage repair response, suggesting that BAP1's role in tumorigenesis could be particularly important in cancers associated with environmental carcinogens such as ultraviolet irradiation (UVR).

To further investigate the role of BAP1 (Bap1 in the mouse) in DNA damage, we first knocked down *BAP1* in human melanocytes as well as Melan-A and Melan-C mouse melanocytes and then exposed the cells to UVR, followed by analysis of DNA damage repair. UVR-induced and steady state levels of DNA damage were higher in *BAP1*-knockdown cells compared to shGFP-control cells. Levels of UVR-related DNA damage markers such as p53, γH2AX and CPD (cyclobutane pyrimidine dimers) were increased following BAP1 loss and UVR treatment. Cell cycle analysis by flow cytometry demonstrated that cells with knockdown of *BAP1* and post UVR treatment showed a higher proportion of cells in S/G2 phase. Such an effect could be due to BAP1 loss and consequent inability to repair DNA damage and/or cell cycle progression. These data are consistent with a role for BAP1 in UVR-induced DNA damage repair.

In MM, it is unclear to what extent *BAP1* mutations cooperate tumorigenically with mutations of other tumor suppressor genes (TSGs) implicated in MM, such as *CDKN2A* and *NF2*. While <u>germline</u> mutations of *BAP1* clearly predispose to MM, whether <u>somatic</u> mutations of *BAP1* drive a more aggressive, metastatic tumor phenotype may depend on the disease type. For such studies, we used conditional knockout (CKO) mice along with intrathoracic (IT) or intraperitoneal (IP) injection of adenovirus expressing Cre recombinase (Adeno-Cre) to excise critical homozygously floxed TSGs in the mesothelial lining. These labor-intensive experiments demonstrated that while homozygous deletion of *Bap1*, *Cdkn2a*, or *Nf2* alone in the pleural cavity (IT) of genetically engineered mouse (GEM) models gave rise to few or no MMs, inactivation of *Bap1* cooperated with loss of either *Nf2* or *Cdkn2a* to drive development of MM in ~20% of double CKO mice, and a high incidence (22/26, 85%) of MMs with short latency (12 weeks) was observed in *Bap1;Nf2;Cdkn2a* (triple)-CKO mice. The same trend was confirmed when the same gene combinations were homozygously deleted IP in these same GEM models, except that a much higher incidence of MM was observed in homozygously floxed *Bap1* (*Bap1*$^{f/f}$) mice injected IP versus IT, which may be due to a larger cell surface area of the peritoneum. Adeno-Cre treatment of normal mesothelial cells from *Bap1*$^{f/f}$;*Nf2* $^{f/f}$;*Cdkn2* $^{f/f}$ mice, but not from mice with knockout of one or any two of these tumor suppressor genes, resulted in robust spheroid formation *in vitro*, suggesting that homozygous deletion of all three of these TSGs is sufficient to drive a cancer stem cell-like potential. RNA-seq analysis of pleural MMs from triple-CKO mice revealed enrichment of many genes transcriptionally regulated by the polycomb repressive complex 2 (PRC2). Other genes upregulated in MMs from triple-CKO mice included *Vegfd* and *Pak3*, which encode proteins involved in angiogenic and cell motility pathways.

In conclusion, we hypothesize that inherited mutations of *BAP1* may increase susceptibility to certain environmental factors that may induce DNA damage and contribute to cancer development. Our data also indicate that cooperative somatic inactivation of *Bap1*, *Nf2*, and *Cdkn2a* results in rapid, highly aggressive MMs, and that deletion of *Bap1* contributes to tumorigenesis, in part, by loss of PRC2-mediated gene repression of tumorigenic target genes and by acquisition of stem-cell potential. Thus, our studies suggest a potential avenue for therapeutic intervention.

DEDICATION

This dissertation is dedicated to my mother, who was the first one to introduce me to cancer and who believed I would become a doctor one day. My current and future work is dedicated to all the children who had to lose their mothers and to all those who had to lose their loved ones to this dreaded disease.

ACKNOWLEDGMENTS

I would like to thank my mentor, Dr. Joseph R. Testa, for accepting me into his lab as a graduate student and for providing me an opportunity to learn about mesothelioma from a world expert. I thank him for nurturing the culture of asking big-picture questions and helping me understand how your research impacts other people. I highly appreciate the opportunities he afforded me to go to conferences and especially appreciated the many working hours in his office where he guided me on presentation slides, papers and grant ideas. I learned not only about science but also about philosophical ideas of life, and I am grateful for all the lessons given.

Also, I would like to thank Dr. Xavier Graña, Dr. Raza Zaidi, Dr. Siddharth Balachandran and Dr. Richard Pomerantz for their willingness to be my thesis committee members, and for their time, scientific input and enormous impact on my thesis work. I would like to thank Dr. Zaidi for collaborating with Dr. Testa on the $HGFxBap1^{Lou}$ project. I learned much from Dr. Zaidi about ultraviolet radiation, melanoma and about working with mice to develop a model for cutaneous melanoma development. I thank Dr. Zaidi for coming to Fox Chase on multiple occasions to test our UV machine and for his advice on the project. I would like to separately thank Dr. Balachandran for letting me work on one of the projects that he collaborated on with Dr. Testa. Dr. Balachandran has provided me with great support and advice during tough times and taught me the power of mindfulness. I would also like to thank Dr. Glenn Rall, Fox Chase's former postdoc and graduate student advisor, who has supported and guided me in times when it was needed most. I really appreciated this help, as I learned that working in research is just as

much about mental strength and determination as it is about perfection in one's scientific experiments.

I would like to thank Dr. Haifeng Yang for being my external committee member and for providing useful comments and criticism of this work. His advice and input proved invaluable to the final quality of this thesis.

I am deeply indebted to Eleonora Sementino, M.S. and Dr. Craig Menges, who took me under their wing and were my teachers in the practical bench skills necessary to efficiently work in the laboratory. I thank Dr. Craig Menges for intellectual advice and encouraging scientific discussions that stimulated analytical thinking and led to new ideas. I greatly appreciate his help with bench work in the final stages of my time in the laboratory, which allowed me to concentrate on writing my thesis. No words can describe how thankful I am to Eleonora Sementino, who has been my inspiration and motivation throughout the years of my stay at Fox Chase Cancer Center. She encouraged me in every difficult step during my laboratory work and even during personal life challenges. She was my main person to run to if I had any technical questions and any exciting ideas I wanted to discuss. She has contributed intellectually and realistically to this thesis, and I am honored to have her as the second author of my main paper from this thesis work.

I am also grateful to Dr. Yuwaraj Kadariya and Dr. Mitchell Cheung for their technical support. Dr. Yuwaraj Kadariya has helped enormously with mouse work and was responsible for all the Adeno-Cre injections performed. He was extremely helpful in monitoring mice on weekends, so that we rarely lost a data point. Dr. Mitchell Cheung provided the $Bap1^{+/Lou}$ and $Bap1^{f/f}$ mouse models discussed in the thesis, informed me on the genotyping necessary for the projects, obtained a UV light box used for the *in vitro* experiments, and contributed an enormous amount of time to help with the analysis of the RNA-seq data. I also thank him for answering my numerous questions in preparation of this thesis.

I am very grateful to Dr. Testa's former administrative assistant, Kathy Ireton, as she has always been there for me when I needed support and encouragement and has helped in organizing all the events necessary for the completion of my work.

I would like to thank all my biology professors at Earlham College and Temple University School of Medicine, who instilled in me curiosity and appreciation for the sciences, particularly, Dr. Wendy Tori, for teaching my first biology course and encouraging me to complete it despite my initial language difficulties and to pursue a career in biology. I will be also forever thankful to Dr. Aliester Saunders (Drexel University) for giving me the opportunity to volunteer in his laboratory and to take my first steps in a research setting.

Finally, and most importantly, I would like to thank my father, my sister, my American host-parents, my cousins, and my dear friends for their patience with my emotions and for countless phone calls supporting me and helping me build the stamina and motivation to continue my course and thesis work. Without these people, who have been my moral support from the very beginning to the very end, this work would not have been accomplished.

TABLE OF CONTENTS

Page

LIST OF TABLES

LIST OF FIGURES

LIST OF ABBREVIATIONS:

53BP1: p53 binding protein 1

AKT: AK strain transforming

ALK: Anaplastic lymphoma kinase

ASXL1/2: Additional Sex Combs Like proteins

ATF3: Cyclic AMP-dependent transcription factor

ATM: Ataxia telangiectasia mutated, a serine/threonine protein kinase

BAP1*:* BRCA1-Associated Protein 1

BAP1-TPDS: BAP1 tumor predisposition syndrome

BARD1: BRCA1-associated RING domain protein 1

Ca^{2+}: Calcium

CDK: Cyclin-dependent kinases, CDK4 and CDK6

CDKN2A: Cyclin dependent kinase inhibitor 2A

ChiP-seq: Chromatin immunoprecipitation sequencing

CHOP: Transcription factor activated upon ER stress

CKO: Conditional knockout mouse

CK5/6: Cytokeratin 5/6

CM: Cutaneous melanoma

CPD: Cyclobutane pyrimidine dimers

CRS: Cytoreductive surgery

CTLA4: Cytotoxic T-lymphocyte-associated protein 4

DNA: Deoxyribonucleic acid

EGFR: Epidermal growth factor receptor

EPIC: Normothermic early postoperative chemotherapy

ER : Endoplasmic reticulum

EZH2: Enhancer of zeste homolog 2

FCCC: Fox Chase Cancer Center

Foxg1: Forkhead box protein G1

GAPDH: Glyceraldehyde 3-phosphate dehydrogenase

GEM: Genetically modified mouse

GPX4: Glutathione peroxidase 4

GR: Glutathione reductase

GSH: Reduced glutathione

GSL: Glutamate-cysteine ligase

GSSG: Oxidized glutathione

H2AK119ub1: ubiquitilated lysine 119 of histone H2A

H3K27me1,2,3: Mono-, di- and trimethylation of histone 3

HCC: Hepatocellular carcinoma

HCF1: Host cell factor 1

HGF/SF: Hepatocyte growth factor/scatter factor

HIPEC: Hypothermic intraperitoneal chemotherapy

HR: Homologous recombination pathway

IACUC: Institutional Animal Care and Use Committees

ICC: Intrahepatic cholangiocarcinoma

IP: Intraperitoneal

IP3R3: Channel type-3 inositol-1,4,5-trisphosphate-receptor

IT: Intrathoracic

Lou: Louisiana

MCU: Mitochondrial Ca^{2+} uniporter

MM: Malignant mesothelioma

Mmp14: Matrix metalloproteinase-14

MPeM: Malignant peritoneal mesothelioma

mTOR: Mammalian target of rapamycin

NADPH : Nicotinamide adenine dinucleotide phosphate-oxidase

NER: Nucleotide excision repair

NF2: Neurofibromatosis type 2

NLS: Nuclear localization signal

Pak3: p21-activated kinase 2, beta-PAK

PcG: Polycomb group proteins

PD1: Programmed cell death protein 1

Pdgfra: Platelet-derived growth factor receptor

PDX: Patient-derived xenografts

p-pRb: Phosphorylated retinoblastoma protein

PRC2: Polycomb repressive complex 2

PR-DUB: Polycomb repressive deubiquitinase

PTEN: Phosphatase and tensin homolog

RNA: Ribonucleic acid

RNA-seq: RNA sequencing

ROS: Super-reactive oxygen species

RT-PCR: Real time polymerase chain reaction

SCGE: Single cell gel electrophoresis assay

shRNA: Short hairpin RNA

SIC: Sequential chemotherapy

siRNA: Short interference RNA

SLC7A11: light-chain subunit of the cystine/glutamate antiporter

TSG: Tumor suppressor gene

Twist1: Twist-related protein 1

Ub: Ubiquitin

ULD:UCH37-like domain

UM: Uveal melanoma

UVR: Ultraviolet radiation

VDAC: Voltage-dependent anion channel

VEGF: Vascular endothelial growth factor

Wis: Wisconsin

WT: Wild-type

WT1: Wilms tumor protein

XPA: Xeroderma pigmentosum type A

YY1: Ying Yang 1

$^{\Delta/\Delta}$: Adeno-Cre virus-exposed normal mesothelial cells from a mouse with floxed genes; or a tumor dissected out of a mouse, which was injected with Adeno-Cre

$^{f/f}$: floxed alleles of a designated gene

CHAPTER 1

1 INTRODUCTION

1.1 Overview of Malignant Mesothelioma

Malignant mesothelioma (MM) is a rare type of cancer arising from serosal cells lining the thoracic and abdominal cavities and internal organs. These mesothelial cells make up the mesothelium and secrete a lubricating fluid that prevents friction between organs. The mesothelium that lines the thoracic cavity covers the lungs and is referred to as the pleura. The mesothelium that lines the abdominal cavity and encases all the internal organs of the abdomen is the peritoneum. There is also the pericardium that lines the heart and the space around it, as well as the tunica vaginalis, which encapsulates the testicles. Thus, MM can start in any of these cavities and is named accordingly (Figure 1). The most common type of MM is pleural in origin (about 80% of cases). Peritoneal MM is the second most common type seen in patients, with MMs of the pericardium and tunica vaginalis being extremely rare (1).

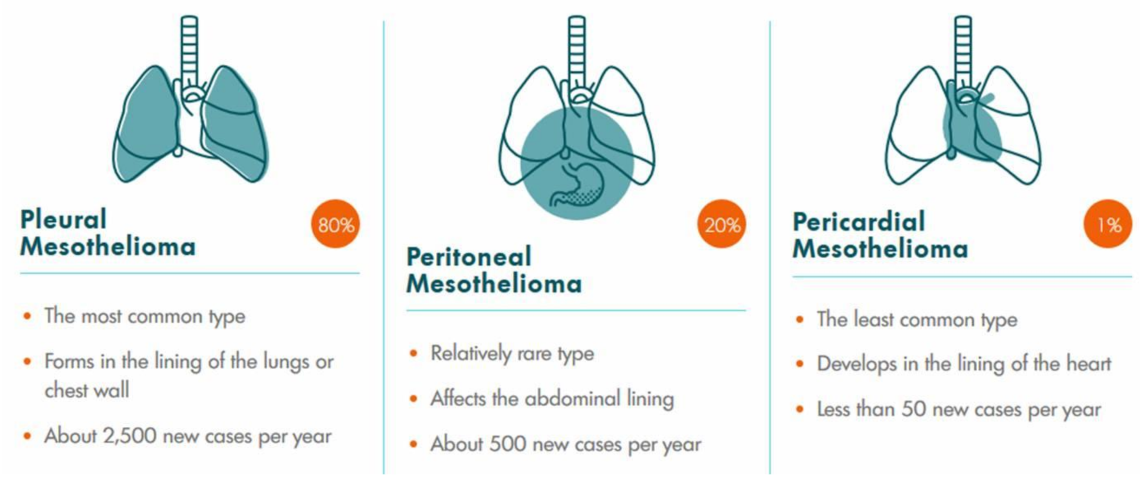

Figure1. Types of malignant mesothelioma (2). *Left*, pleural MM – predominant type (80% of cases). *Center*, peritoneal MM (20% of cases). *Right*, pericardial mesothelioma (1%).

There are three histological types of MMs depending on the predominant cell type. Epithelioid MM is the most prevalent (70%) and is usually associated with a better prognosis. Mixed or biphasic MM occurs in about 20% of MM cases and sarcomatoid tumors (~10%) are the most aggressive histotype (3). There are approximately 3,200 new cases of MM every year in the U.S., despite asbestos abatement efforts (2). Symptoms in MM patients include chest pain, shortness of breath, persistent cough and fluid buildup in the lungs (pleural effusion) or peritoneum (ascites). Life expectancy is usually short with affected individuals typically living between 6 to 24 months with a median survival of 9-12 months, even with surgery and/or chemotherapy.

MM development is etiologically linked to asbestos exposure. The term "asbestos" refers to six types of natural minerals that form bundles of fibers (4). There are many industrial applications for which asbestos has been used, including as furnace and roof insulation, car brakes and ship hull insulation, to name a few. Therefore, virtually all the industrial workers and others using asbestos products have been exposed to it; according to the World Health Organization, up to 125 million workers globally are exposed to asbestos on the job (5). When asbestos fibers are inhaled, they can become embedded into the pleura leading to inflammation (6). The mechanism of asbestos-induced inflammation and the consequent carcinogenesis is not fully understood. One hypothesis is that macrophages attempt to engulf the fibers and when they internalize a large fiber, they undergo so-called “frustrated” phagocytosis, leading to a soaking of the mesothelial lining with pro-proliferative cytokines (7). It is also hypothesized that super-reactive oxygen species (ROS) released from the macrophage can also cause DNA damage in nearby mesothelial cells leading to pro-tumorigenic genetic alterations (8).

1.2 Genetics of Mesothelioma

As mentioned previously, most MMs are pleural tumors linked to asbestos inhalation. Peritoneal MM can be caused by asbestos if it was ingested, although the majority of these cases have no known asbestos exposure history. Although asbestos is considered the primary cause of MM development, only a small fraction of asbestos-exposed individuals, including mineral fiber miners who have had a lifetime of exposure, actually develop MM (9). This leads to the question: what other factors in addition to or instead of asbestos exposure could drive MM pathogenesis. Like the majority of cancers with the exception of viral-driven tumors, somatic and germline mutations in oncogenes and/or tumor suppressor genes cause normally differentiated cells to grow uncontrollably (10). More than two decades ago, Cheng *et al.* published data revealing deletion of chromosome band 9p21 leading to the homozygous loss of *CDKN2A* (cyclin dependent kinase inhibitor 2A) in primary tumors and cell lines from MM patients (11). The *CDKN2A* gene expresses two alternatively spliced mRNA that encode both the p16INK4A and p14ARF (p19Arf in the mouse) proteins. These proteins regulate the cell cycle preventing cells from dysregulated proliferation and, thus, acting as tumor suppressors. p16INK4A binds to and inhibits the cyclin-dependent kinases (CDK) CDK4 and CDK6, which normally stimulate cell cycle progression and cell division by phosphorylating and inhibiting the pocket proteins pRb, p107 and p130. The p14ARF protein prevents degradation of another important tumor suppressor protein, p53, by binding to and inhibiting MDM2, which acts synergistically to control cell proliferation and survival (12). Most of MM cases (>80%) harbor somatic alterations of the *CDKN2A* locus (13), making this the most common genetic mutation/loss in MM.

Shortly after the discovery of *CDKN2A* deletions in MM, Bianchi *et al.* reported another frequent somatic genetic abnormality in MM when they identified mutations of the tumor suppressor gene *NF2* (neurofibromatosis type 2 gene) in about 50% of MMs (14). The *NF2* gene resides on chromosome 22 and mutations of *NF2* in MM are almost always accompanied by loss of the second copy of chromosome 22, resulting in biallelic inaction of *NF2* (13). The *NF2* gene encodes the FERM-domain protein Merlin that is involved in controlling cell shape, cell proliferation and cell adhesion through interactions with downstream effectors such as focal adhesion kinase (FAK), p21-activated kinases (PAKs) and Rac1 to name a few (15). Even though the exact mechanism of how Merlin suppresses tumor growth is yet unknown, it has been shown that it is regulated by Rac/PAK signaling which can regulate the expression of cyclin D1 (16).

In 1994, loss of the chromosomal band 3p21 n was also implicated in MM as a common genetic abnormality in MM, and it was proposed that a putative tumor suppressor gene resided at this location (17). Subsequently, Jensen *et al.* identified the BRCA1-Associated Protein 1 tumor suppressor (BAP1) through a yeast two-hybrid screen using breast cancer type 1 protein (BRCA1) as bait and located the *BAP1* gene through fluorescence *in situ* hybridization to the 3p21. In recent years somatic mutations and exonic deletions of *BAP1* have been reported in up to 60% of MM specimens (18). Interestingly, in 2011, germline mutations of *BAP1* were identified in two families with high incidence of MM, uveal melanoma, and several types of epithelial cancer, such as renal carcinoma (19). A simultaneous report described two families with heritable mutations of *BAP1* with numerous cases of atypical melanocytic tumors and occasional uveal and cutaneous melanomas (20). Contemporaneously, a third group independently reported a family with a germline *BAP1* mutation associated with uveal melanoma, lung adenocarcinoma, meningioma, and other cancers (21). Subsequently, numerous reports have expanded on the discovery of germline *BAP1* mutations in families with these and other cancers (22), now defined as the BAP1 tumor predisposition syndrome (BAP1-TPDS). In this hereditary tumor syndrome, germline pathogenic variants in *BAP1* are now known to predispose carriers to uveal melanoma, MM, cutaneous melanoma, renal cell carcinoma, and cutaneous *BAP1*-inactivated melanocytic tumors.

1.3 BAP1 structure and functions

1.3.1 BAP1 structure overview

As previously stated BAP1 was first identified by Jensen *et al.* in 1998 via a yeast two-hybrid screening for BRCA1 ring finger domain interacting proteins (23). The *BAP1* gene encodes a 729-amino acid protein composed of three main functional domains: an N-terminal UCH (ubiquitin C-terminal hydrolase) deubiquitinating (DUB) domain responsible for removing ubiquitin from ubiquitylated substrates, a host cell factor (HCF1)-binding domain or (HBM)-like motif, and a motif that shares conservation with UCH37, i.e., a UCH37-like domain (ULD). It also has the C-terminal domain with a nuclear localization signal (NLS) (18, 24). BAP1 interacts with BRCA1-associated RING domain protein 1 (BARD1), HCF1, BRCA1, Ying Yang 1 (YY1) and Additional Sex Combs Like proteins ASXL1/2 (see Figure 2A (24)).

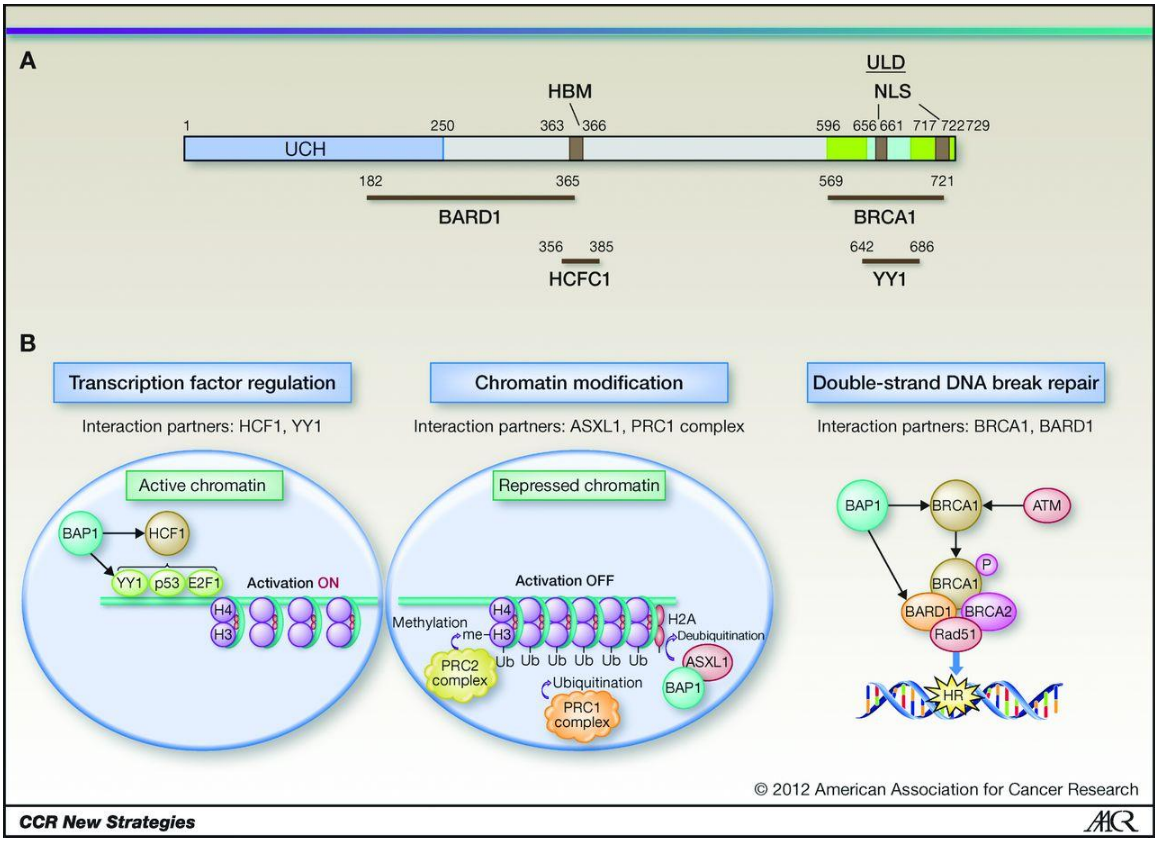

Figure 2. BAP1 structure and functions (24). (A) Structural domains of BAP1 protein: N-terminal UCH domain (blue), an HCF1-binding domain (HBM)-like motif; a motif that shares conservation with UCH37 (ULD: UCH37-like domain); and a nuclear localization signal (NLS). Interacting sites are depicted: BARD1, HCF1, BRCA1, and YY1. **(B)** BAP1 functions: *left*, BAP1 in transcription factor regulation; *center*, BAP1 during chromatin modifications; *right*, hypothesized role of BAP1 in DNA damage repair.

1.3.2 BAP1 function in transcriptional regulation

BAP1 has multiple functions and has been shown to act as a bona fide tumor suppressor *in vivo* (25). Ventii *et al*. demonstrated that BAP1 was able to extend the G1-S progression checkpoint and induce apoptotic and necrotic cell death due to the inability to repair damaged DNA (26). BAP1 tumor suppressor activity required its NLS and DUB activity (26).

In addition, Machida *et al*. reported that BAP1 could interact with HCF-1 and that this interaction is crucial for the BAP1-mediated growth regulation. HCF-1 regulates cell proliferation by playing a role in the cell cycle, specifically in G1/S phase progression as it brings together the H3K4 histone methyltransferases and E2F1 transcription factor to transcribe the genes required for S-phase (27). Machida *et al*. showed that BAP1 deubiquitinates HCF-1 and thereby negatively regulates its activity (27). Because BAP1 interacts with HCF-1, which in turn interacts with E2F1, it has been proposed that BAP1 co-regulates transcription from promoters governed by both HCF-1 and E2F1 and thereby controls cell proliferation by regulating G1/S progression (Figure 2B) (28). BAP1 also links histone-modifying enzymes to a set of transcription factors and recruits them to promoter sites to regulate gene expression through a chromatin remodeling mechanism (29, 30).

1.3.3 Role of BAP1 in epigenetic regulations.

The eukaryotic genome is packaged into nuclei as chromatin wrapped around the four core histones (H2A, H2B, H3 and H4). Chromatin can be physically remodeled in accordance with epigenetic modifications of the DNA or histone proteins to either allow or protect the DNA templates from being transcribed. BAP1 has been shown to play a role in such epigenetic modifications via regulating the decompression of the chromatin and thus influencing gene expression. There is a large and diverse family of polycomb group (PcG) proteins that epigenetically control the transcription of genes. These proteins form three distinct groups, including polycomb repressive complexes 1 and 2 (PRC1 and 2) and polycomb repressive deubiquitinases (PR-DUBs). In chromatin modification, methylation and ubiquitination of the histones play a critical role in serving as a signal for the appropriate enzymatic machinery involved in the condensation or decondensation of the DNA. As one of the subunits of the PRC1, E3 ubiquitin ligases monoubiquitinate lysine 119 of histone H2A (H2AK119ub1) repressing the chromatin and providing a stimulatory signal for the PRC2 complex (31, 32). The PRC2 complex consists of multiple components such as EZH1/2, SUZ12, and JARID2 that transfer methyl groups on histone H3 lysine 27 for mono-, di- and trimethylation (H3K27me1,2,3) and condense the chromatin. As mentioned earlier, BAP1 interacts with ASXL1. This interaction forms a PR-DUB that antagonizes the activity of the PRC1 by cleaving the ubiquitin off the histone H2A (H2AK119Ub1) and decondensing the chromatin (Figure 3) (33). Such epigenetic regulation by the PcG complexes is critical in embryonic development, stem cell pluripotency and cell differentiation. Therefore, it can be speculated that the deregulation of these processes can also affect cancer initiation and influence its progression. Unfortunately, how these complexes interact with one another mechanistically is still not known (31). It is important to note that the PRC2 proteins EZH2 and EED have been shown to be frequently overexpressed in MM and have been proposed as possible therapeutic targets for MM treatment (34). Notably, LaFave *et al.*

demonstrated a correlation between BAP1 loss and elevated EZH2 expression levels and showed that MM cells lacking BAP1 are sensitive to a pharmacologic inhibition of EZH2 (35).

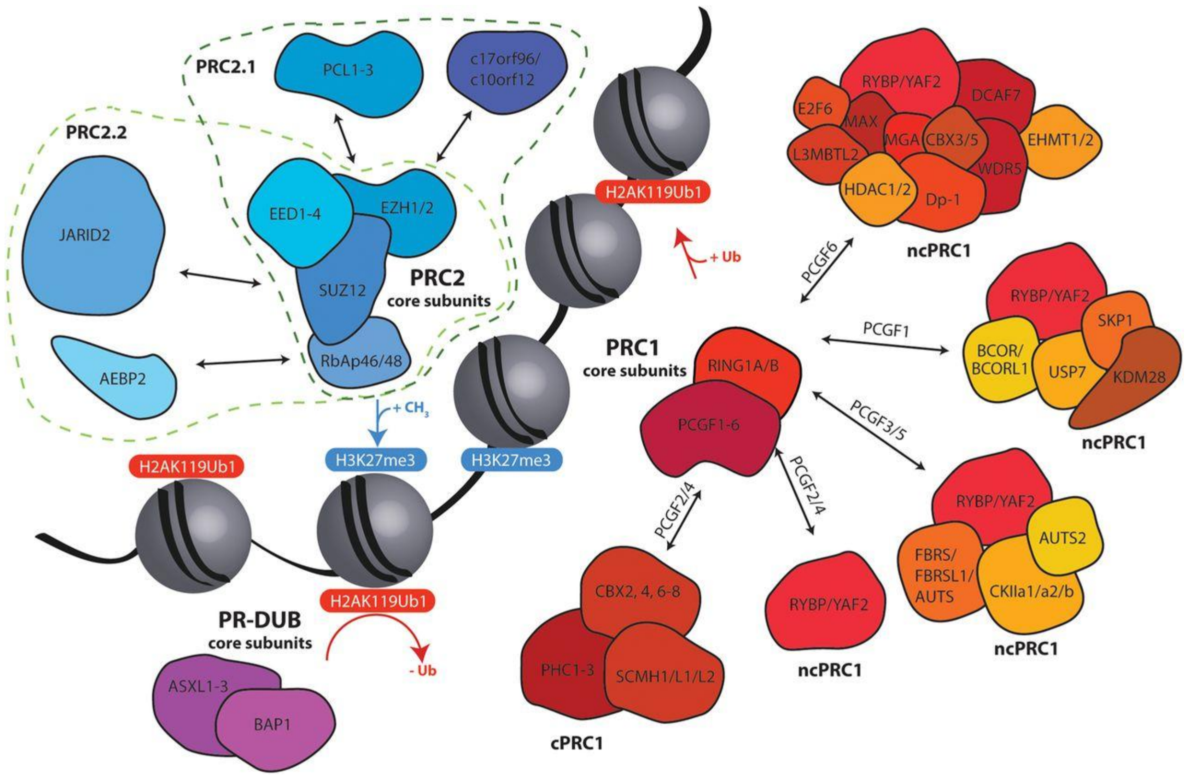

Figure 3. Three polycomb repressive complexes (31). PRC1 complex with its numerous subunit combinations (in red) adds ubiquitin on lysine 119 of histone H2A to form H2AK119Ub1, PRC2 with different possible combinations of the subunits adds methyl groups on lysine 27 of histone H3 to form H3K27me3 (in blue). PR-DUB with known subunits (in purple) deubiquitinate H2AK119Ub1 (31).

1.3.4 BAP1 in DNA damage repair

As two of the binding partners of BAP1 include BRCA1 and BARD1, which are key players in double strand DNA repair (23), BAP1 was also hypothesized to be involved in the DNA damage repair. Ubiquitin is known to be important not only in chromatin remodeling, but also in serving as a signal for initiating the DNA damage repair response such as in the double-strand break (DSB) repair (36). Specifically, ubiquitin signals the recruitment of the RING finger E3 ligases, which form the K63-linked ubiquitin chain on H2A/H2AX histones and therefore bring upon downstream factors such as p53 binding protein 1 (53BP1), BRCA1 and RAD51 homologue 1 (RAD51) (37). Subsequently, 53BP1 promotes nonhomologous end joining (NHEJ) and BRCA1 and RAD51-homologous recombination (HR) DSB repair mechanisms (38). As described earlier, BAP1 is part of the DUB complex and as a deubiquitinase, it not only plays a role in the epigenetic modification of chromatin but may also affect the DSB repair response, as has been shown for the DUBs (39). To date, only two studies have explored this possibility. In one of these reports, Yu *et al.* used a human DUB RNAi library to screen for DUBs required for HR and identified BAP1 as one of the regulators of efficient HR. The group employed ionizing radiation (IR) to examine the role of BAP1 in DSB repair. They demonstrated that BAP1 inactivation sensitizes cells to IR-induced DSBs and leads to an increased number of chromosomal breaks. Six IR-induced phosphorylation sites in BAP1 were identified and shown to be required for the recruitment of BAP1 to DSB sites (40). As a possible explanation of how BAP1 regulates HR, the investigators proposed that the BAP1 complex synergizes with the PRC1 complex to regulate the balance of ubiquitination/deubiquitination of H2A, thereby controlling chromatin modification at the site of DSB. In a second report, Ismail *et al.* also showed BAP1-mediated recruitment of PR-DUB to sites of DSB, moreover they implicated phosphorylation of BAP1 by the DNA damage response kinase, ataxia telangiectasia mutated (ATM) (41). Both studies suggest that the deubiquitinating function of BAP1 controls chromatin modification by BAP1 being part of the PR-DUB, and thereby influencing the DNA damage response (40, 41). However, BAP1's function in the DNA repair is still largely understudied and requires more investigation. The overview of the proposed function of BAP1 in DNA damage repair is summarized in Figure 4 by Yu *et al.* (40).

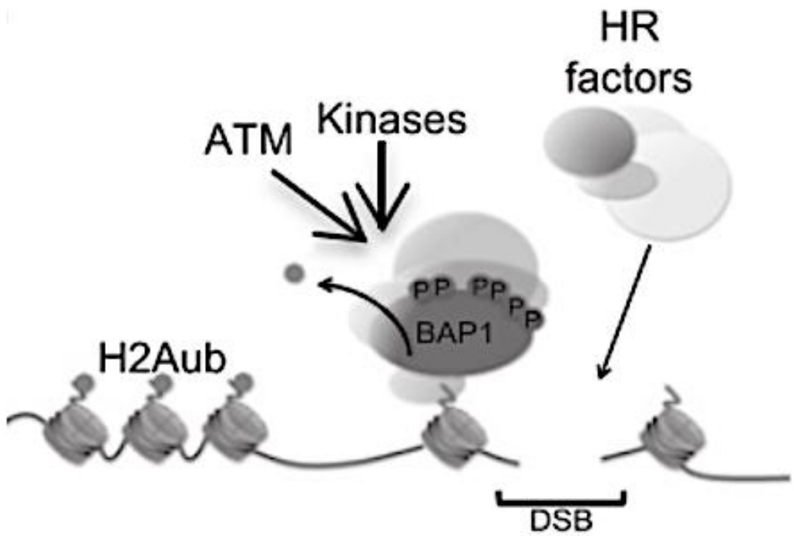

Yu H. *et al.*, *PNAS* 2014

Figure 4. Proposed by Yu H. *et al.* model of BAP1 in DNA damage repair (40). As the DNA damage occurs, BAP1 is phosphorylated at 6 sites and is then recruited to the double-strand break location, where it deubiquitinates H2A and promotes the recruitment of downstream repair proteins.

1.4 BAP1 in different mechanisms of cell death

1.4.1 BAP1 and apoptosis

Until recently, BAP1's main functions were known to be related to its nuclear localization signal and nuclear activities. However, the scientific community was interested to explore its role in the cytoplasm as well. Recently, Bononi *et al.* reported the accumulation of BAP1 in the endoplasmic reticulum (ER) (42). The group showed that BAP1 binds, deubiquitinates and stabilizes an intracellular calcium (Ca^{2+}) release channel type-3 inositol-1,4,5-trisphosphate-receptor (IP3R3), which mediates Ca^{2+} release from the ER. In doing so, BAP1 regulates Ca^{2+} flux from the ER into the cytoplasm and mitochondria. As the mitochondria overload with Ca^{2+}, they release cytochrome C, which promotes apoptosis (Figure 4, left portion of image) (42). It was proposed that when there is haploinsufficiency for BAP1, such as in normal mesothelial cells from *BAP1*-mutatuion carriers, there is not only reduced nuclear BAP1 activity, but also diminished cytoplasmic BAP1activity as well. The decreased levels of cytoplasmic BAP1 would consequently result in reduced levels of Ca^{2+} flux and, thus, negatively affect BAP1-related death pathways such as apoptosis (42). Apoptosis is crucial in maintaining the balance between healthy and damaged cells. Thus, in a situation where cells are exposed to a DNA damaging agent such as UV or asbestos, and the apoptotic pathway is not proficient due to decreased levels of BAP1, DNA damaged cells would accumulate and potentially transform into a malignancy.

1.4.2 BAP1 role in ferroptosis

Ferroptosis is a newly described forms of regulated cell death that involves a unique iron-dependent pathway that differs morphologically, biochemically, and genetically from autophagy, necrosis, and apoptosis. It is characterized by high accumulation of lipid peroxidation products and reactive oxygen species (ROS) derived from iron metabolism. It is known that upregulation of ER stress, activation of mitochondrial voltage-dependent anion channels and mitogen-activated protein kinases, and inhibition of cystine/glutamate antiporter promote ferroptosis. Nicotinamide adenine dinucleotide phosphate (NADPH) and p53 positively regulate ferroptosis by inducing ROS production and inhibiting the expression of SLC7A11 (a light-chain subunit of the cystine/glutamate antiporter), respectively.

Zhang *et al.* determined that BAP1 represses genes that are enriched in cell metabolism-associated pathways. Specifically, the group found SLC7A11 gene expression to be inversely correlated with BAP1 (43). Furthermore, they demonstrated that BAP1 reduces the levels of the ubiquitin on H2A of the promoter of SLC7A1. Even though, deubiquitination of histones is supposed to derepress chromatin and initiate transcription, the investigators found that BAP1 repressed the transcriptional activity of SLC7A1. Due to this BAP1-mediated decrease of SLC7A11 expression, cystine uptake was also reduced, resulting in low levels of glutathione, increased lipid peroxidation, and promotion of ferroptosis (Figure 5) (43).

Interestingly, Affar and Carbone speculated that since the PRC1 complex regulates H2A ubiquitination and is often overexpressed in cancer, this could lead to increased expression of SLC7A11 and therefore reduced possibility for ferroptosis (44). Looking at the components of the PR-DUB that associate with BAP1, Zhang *et al*. showed that depletion of ASXL1, but not ASXL2, decreased the expression of SLC7A11 (43). Depletion of HCF-1 had no impact on expression of SLC7A11, whereas depletion of OGT decreased SLC7A11 expression. These results suggest that some BAP1-associated components might have additional regulatory effects on BAP1-mediated ferroptosis (44).

As described above, BAP1 plays a role in two distinct pathways of programmed cell death: apoptosis and ferroptosis (Figure 5). As Affar and Carbone suggest in their review, it would be interesting to explore if these pathways act together or independently in cancer development.

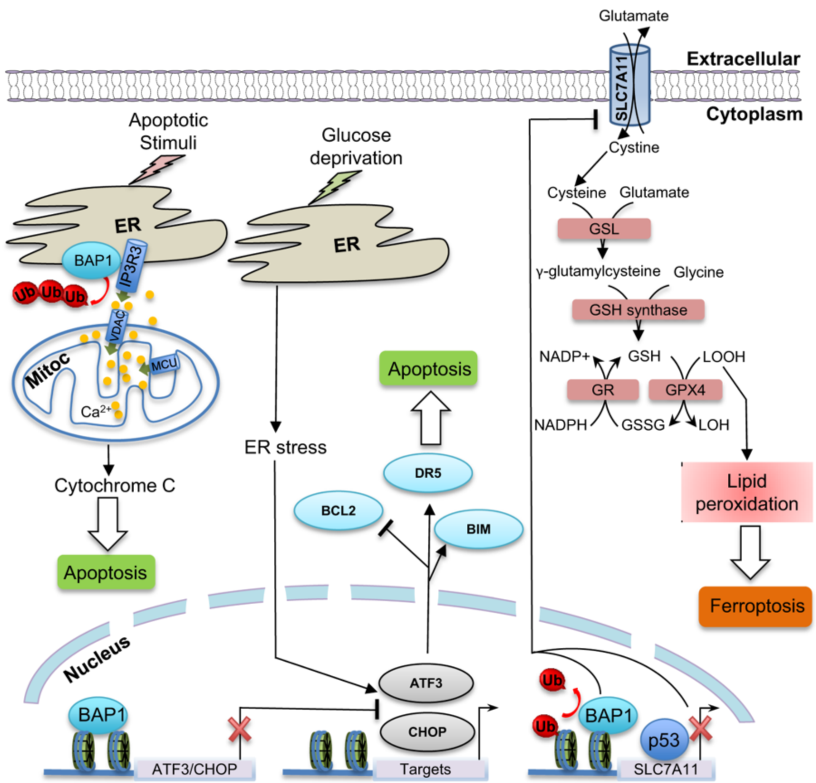

Figure 5. Role of BAP1 in cell death (44). *Left*, Under the stress-induced signals, cytoplasmic BAP1 stabilizes and deubiquitinates IP3R3, thus increasing the levels of Ca^{2+} influx into mitochondria (Mitoc), inducing the release of cytochrome C and thereby activating the apoptosis pathway. *Center*, In the nucleus, BAP1 can repress the expression of key ER stress transcription factors having pro-apoptotic functions, and inhibit apoptosis. *Right*, BAP1 deubiquitinates the promoter of *SLC7A11*, repressing its expression. SLC7A11, a cystine/glutamate antiporter, imports cysteine, a metabolite used for the synthesis of reduced glutathione. Decreased levels of SLC7A11 expression leads to reduced glutathione, diminished antioxidant capacity of the cells, lipid-ROS accumulation and ferroptosis.

1.5 BAP1 in familial cancers

Even though the main cause associated with MM is considered to be asbestos, only a small fraction of all exposed individuals develops MM (45). Testa *et al.* pursued the question of whether genetics factors contribute to MM susceptibility by studying families with high incidence of MM to find genes potentially predisposing to the disease. The group published data on two American families that were not exposed to asbestos occupationally: one in Wisconsin (Wis family) and one in Louisiana (Lou family). Germline *BAP1* mutations and somatic alterations affecting the *BAP1* locus identified in these families linked the *BAP1* gene to familial MM. Even though MM was the most prevalent cancer in these families, there were multiple other tumor types, which led the investigators to conclude that germline mutation of *BAP1* not only predisposes to MM, but also causes susceptibility to a variety of tumors as a hereditary cancer predisposition syndrome (19, 45). This syndrome, now referred to as BAP1 tumor predisposition syndrome (BAP1-TPDS) (19-21, 46), predisposes the carriers to the development of multiple malignancies, specifically MM, uveal and cutaneous melanomas, basal cell carcinoma, renal cell carcinoma, and certain other cancers (47).

Interestingly, the families described by Testa *et al.* happened to have asbestos in their houses, which was thought to be potentially associated with a modest level of exposure. The investigators hypothesized that when families with a germline *BAP1* mutation are exposed to asbestos, MM predominates. It was proposed that the environmental asbestos exposure would act as a second hit and, thus, represent an example of cancer etiology due to a gene vs. environment interaction (19). Alternatively, heterozygous germline *BAP1* mutation alone may be sufficient to cause MM, although studies with mouse models have provided little or no support for that possibility (25, 48) and epidemiological evidence is lacking. Benign melanocytic tumors and uveal and cutaneous melanomas are also of the BAP1 syndrome (20). Ultraviolet radiation (UVR) is a known cause of cutaneous melanoma (49) and basal cell carcinoma (50), whereas a role for UVR in uveal melanoma is controversial. It is possible that *BAP1*-mutant families where these skin tumors and uveal melanoma predominate have been excessive exposure to UVR, which may have acted in conjunction with mutation of *BAP1* to drive cancer via a gene vs. environment interaction. To explore this possibility, we exposed a mouse model with a heterozygous *Bap1* to UVR to assess whether there was enhanced susceptibility to melanoma, which will be discussed in a later chapter (Chapter 3).

1.6 Mouse models of MM.

As mentioned previously, MM is a rare type of cancer with a poor survival rate and inefficient treatment options. Standard chemotherapies such as cisplatin are relatively ineffective in diminishing MM growth, even when used in combination with the folate scavenger inhibitor pemetrexed (Alimta) (51). Even targeted therapies such as epidermal growth factor receptor (EGFR) inhibitors and mammalian target of rapamycin (mTOR) inhibitors have failed in MM clinical trials. Thus, MM researchers need new targets and more importantly, pre-clinical cancer models in order to identify and test novel therapies. In order to better assess a possible therapeutic approach, researchers were in need of rodent MM models. These models include orthotopic or heterotopic xenografts of human MM cell lines and patient-derived xenografts (PDX) using immunodeficient mice (52, 53). Such models are also developed to investigate the oncogenic mechanisms induced by asbestos or by the genes and signaling pathways relevant to the disease.

Spontaneous MMs in rats have been reported in 1987 with an incidence of 4.3% (7/395) of the genital and serosal mesothelial lining, with only one pleural MM identified. In a more recent paper, in 2016, 0.2-5% of spontaneous MMs of the tunica vaginalis were observed in male F344/N rats (54). Spontaneous MM in mice are also rare (55-57). Additionally, there are numerous distinct rodent models of asbestos-induced MM, which are described in the review by Didier Jean and Marie-Claude Jaurand (58), but will not be focused on in this thesis due to irrelevance to work described herein.

Genetically modified mouse (GEM) models of MM are important tools to determine the contribution of tumor suppressor gene (TSG) loss in MM pathogenesis. GEM models allow for deletion of TSGs in the heterozygous or homozygous state, alone or in combination, to determine the importance of MM-implicated driver genes, such as *Nf2*, *Bap1*, and *Cdkn2a* (encoding both p16Ink4a and 19Arf) in cancer development. Since BAP1-TPDS is associated with heterozygous germline mutations of *BAP1*, Kadariya *et al.* developed three types of heterozygous *Bap1* mutant mice to test whether such mice would be predisposed to cancer, particularly MM (25). They developed three different mouse models: one with knockout of exons 6 and 7 of *Bap1*, and two with point mutations mimicking the germline mutations found in the human families (W is and Lou) with a BAP1 syndrome. The mouse models with the various heterozygous alterations of *Bap1* developed numerous types of cancers but MM was very rare (2/93 mice) with a long latency. On the other hand, in mouse models with a heterozygous mutation or deletion of *Nf2, Bap1* or *Cdkn2a*, intraperitoneal (IP) injections of asbestos cause a higher rate shorter latency of MMs than in wild type littermates (25, 48, 59, 60). Mice with mutations/deletions of two of these genes developed even higher rates and shorter latency of MM (61).

While homozygous deletion of such TSGs often causes embryonic lethality in mice, somatic homozygous deletion in adult mice, e.g., by injection of an adenovirus expressing Cre-recombinase is not lethal. For example, Dey *et al.* demonstrated that homozygous deletion of *Bap1* lead to embryonic lethality in mice (62), whereas conditional GEM models allow for temporal deletion of both copies of a TSG after development and in adult tissue. For conditional GEM models of MM, intrathoracic (IT) or intraperitoneal (IP) injection of adenovirus expressing Cre recombinase (Adeno-Cre) allows for homozygous deletion of floxed TSGs in the mesothelial lining of both the pleural and peritoneal cavities, respectively.

In the first conditional GEM model of MM, Adeno-Cre was injected into the thoracic cavity of mice with either heterozygously or homozygously floxed *Nf2*, *Cdkn2a*, *Trp53*, *Rb*, or *Ink4a* alone or in combination to determine which TSGs were important to MM pathogenesis (63). The double mutants (*Nf2* and either *Cdkn2a*, *Tp53* or *Rb*) and triple mutants (*Nf2, Tp53*, and *Ink4a*) exhibited the highest rate of thoracic MM. Single inactivation of *Rb* induced the lowest tumor rate; however, adding homozygous *Nf2* deletion enhanced MM incidence in *Rb* mutants (63). In a different study, Guo *et al.* injected Adeno-Cre virus IP or in the bladder of mice with conditional mutants of *Tp53* and/or *Tsc1*(64). Homozygous deletions of the double (*Tp53;Tsc1*) mutants induced the highest rate of MM (64). Recently, Sementino *et al.* tested whether deletion of *Pten* would lead to MM development. Single homozygous *Pten* inactivation gave rise to 7% of pleural MMs, while double homozygous inactivation of *Tp53* and *Pten* developed MM in 56% of mice (65). An even higher incidence of MMs (92%) was observed in *Tp53$^{f/f}$;Pten$^{f/f}$* mice injected IP with Adeno-Cre.

In conclusion, these observations demonstrate a differential role of these TSGs in MM, and that homozygous inactivation of more than one of these genes can cooperate to enhance MM aggressiveness and progression compared to single or heterozygously inactivated TSGs.

Overall, we hypothesize that inherited mutations of *BAP1* may increase susceptibility to certain environmental factors such as UV light, due to BAP1's role in the DNA damage repair response. We also hypothesize that *Bap1*, *Nf2*, and *Cdkn2a* are critical tumor suppressor genes in MM pathogenesis and that mutation/deletion of these three genes in a mouse model is sufficient to drive MM pathogenesis. In this dissertation, we address the following aims: 1) determine if germline mutation of *Bap1* predisposes mice to UV-induced melanoma; 2) interrogate the role of Bap1 in UV-induced DNA damage/repair during melanomagenesis; and 3) evaluate if loss of *Bap1* cooperates with other tumor suppressor genes in a conditional mouse model of MM.

CHAPTER 2

2 MATERIALS AND METHODS

2.1 Mouse models used in the UV exposure experiments

All mouse studies were performed in accordance with a protocol approved by the Fox Chase Cancer Center (FCCC) IACUC. The *HGF/SF* mice were generously gifted by Dr. Raza Zaidi and backcrossed to the FVB background. Dr. Mitchell Cheung in Dr. Testa's laboratory created *Bap1*$^{+/Lou}$ mice with a heterozygous point mutation identical to that described in a human Louisiana BAP1 syndrome family (25). The *HGF/SF* and the *Bap1*^{Lou} mice were crossed and all pups (genotyping: wild-type, *HGF/SF*, *Bap1*$^{Lou/+}$, and *HGF/SF;Bap1*$^{Lou/+}$). All animals were kept in isolator cages. We routinely employed a single dose of erythemal UVR from a panel of FS40 lamps in neonatal or perinatal wild-type, *HGF/SF*, *Bap1*$^{Lou/+}$, and *HGF/SF;Bap1*$^{Lou/+}$ mice to induce the development of cutaneous melanoma. [Note that *HGF/SF* mice exposed to UVR in this manner develop melanoma within 8-14 months; and that any animals without obvious tumors by 24 months would be sacrificed at that time.] Mice were monitored weekly, and euthanized if tumor burden exceeded 10% of body weight or if mice exhibited overt stress (i.e., >10% weight loss, abdominal bloating, lethargy or ulceration of tumors, hunched posture, ataxia, labored or irregular respiration, inability to eat, drink, cachexia) by CO2 inhalation. [Note also that *Bap1*$^{Lou/+}$ mice have a heterozygous point mutation identical to that identified in a human Louisiana BAP1 syndrome family that exhibited several uveal melanomas (UMs) and skin cancers, as well as multiple mesotheliomas.] The treated cohorts from the various experiments were UV irradiated at 1.5 to 3.5 days of age (3-5 pups at a time) with a single UVR dose of 9.6 kJ/m2 from a bank of Phillips FS40 sunlamps (60% UVB/40% UVA). Our collaborator, Dr. Raza Zaidi (Temple University) has previously shown that this UVR dose is well tolerated by *HGF* pups (total exposure 15 min) with only occasional superficial peeling of the outer skin layer in some pups at 5 days of age but no apparent consequences. *HGF* transgenic mice have been described to develop intestinal pseudo-obstruction and prolapses. We monitored the mice to exhibit any symptoms of abdominal discomfort or developing prolapse and euthanized them upon such observation (66-68).

Genotyping of $Bap1^{Lou}$ mice: forward primer used for genotyping: 5'-AGG TGG GTG ACC CCT CTA CT-3' and the reverse primer: 5'- CAC TAG GTT GGC CAG CAT TC-3', Tm used: -58°C.

2.2 Cell culture

Normal human melanocytes were purchased from ScienCell™ and were cultured according to the company's protocol. Human *XPA*-deficient cells ($XPA^{-/-}$) were generously gifted by Dr. Richard Pomerantz laboratory. Melan-A and Melan-C cell lines were kindly gifted by Dr. Raza Zaidi and cultured in RPMI media with 10% FBS and 200nM TPA (69). LP9 human immortalized mesothelial cells were cultured in LP9 medium (FCCC Cell Culture Facility).

2.3 Stable knockdown of BAP1 in melanocytes, LP9 and 293 HEK cells

To make lentivirus, control pLKO-shGFP and pLKO expressing two independent shRNAs targeting Bap1, psPAX2, and pMD2.G plasmids were co-transfected into HEK293T cells using lipofectamine^{2000} (ThermoFisher Scientific), and supernatant was collected after 24-48 hours after transfection. Cells of interest, such as the LP9 cell line, were infected by lentivirus in medium containing polybrene (10 µg/mL) at 37ºC incubator overnight. The following morning the supernatant was removed and fresh medium was added. After 24h, the cells were selected with puromycin (cell culture facility at Fox Chase Cancer Center) until the selection was complete and the non-transduced cells (kill plate) were dead. Stable shGFP and shBAP1-expressing cell lines were passaged without puromycin for subsequent experiments. After several passages, cells were harvested and protein was extracted for immunoblot analysis. Transfected cells were exposed to UVR and used for cell cycle analysis experiments.

2.4 Transient knockdown of BAP1 via short interfering RNAs (siRNAs) in human and mouse melanocytes

Melanocytes were transfected using Lipofectamine RNAiMAX with Silencer® Pre-designed siRNAs against BAP1 (siBAP1#0 and siBAP1#5 for human cells (ambion BAP1 silencers and negative control: #4390546, #4390824 ID s15822, #4427038 ID s15820)) and siBap1#2 and siBap1#3 for mouse cells(# j-058658-11;#j-0558658-10) and Negative Control#1. siRNAs were obtained from ThermoFisher Scientific following manufacturer's instructions. 30 pmoles of siRNAs were transfected on 6-well plates. Human melanocytes were nucleofected using LONZA Amaxa® NHEM-Neo

Nucleofector® Kit with program O-30. Cells were exposed to UVR (72 hours post transfection) and harvested for western blotting analysis at different time points (6 and 24 hours post UVR) to evaluate p53 and γH2AX induction. Transfected Melan-A cells were exposed to UVR and used for comet assays.

2.5 *In vitro* UVR exposure

A UV box was built at Fox Chase Cancer Center with 2 UVB TL 20W/12 RS SLV lamps (Philips). According to the Zaidi lab, right before the UVR treatment, the cells are washed once with PBS and exposed to UVB (with no lid) for 90 sec at 20 mW/cm^2. A UV Stratalinker (Stratagene *1800*) was also used for some experiments. In these experiments, the cells were also washed with PBS once before the treatment and the lid was removed. The cells were exposed to 10mJ, 25mJ and 50mJ doses of UV per 10 cm plate.

2.6 Flow cytometry

293HEKT expressing shRNAs against BAP1 or control GFP were treated with UV or not were collected using trypsin (0.25%) and media with 10% FBS. The pellets were washed once with PBS and then fixed in 1 ml of PBS and 3 ml of cold Ethanol (200% proof). The samples were then fixed overnight. The next day the cells were spun down (1,000 rpm for 5 min) and RNase A (Qiagen, Cat No. 1901, 100ug/ml) was added to each sample (at 1mg/ml in 1X PBS). Samples were then vortexed every 10 min and incubated at room temperature for 30 min. After the incubation, the samples were spun down for 3 min and the resulting pellets were resuspended in 1ml of PI (Sigma 100mg) at a concentration of

20ug/ml in PBS. Samples were covered from light and at least 10 min passed before the samples were run on flow cytometer. Cells were then evaluated for cell cycle analysis, specifically for the S-phase population. The FlowJo program was used to generate the plots described in chapter 4.

2.7 Immunofluorescence

Human melanocytes and LP9 cells with stable BAP1 or control GFP knockdown grown on a chamber slide were fixed with 4% PFA for 15 min followed by permeabilization using 0.2% Triton -X100 in PBS for 10 min. After being washed with PBS, cells were blocked in 5% FBS/PBS for 30 min. Primary antibody in 5% FBS/PBS was added and the plates were kept at 4°C overnight. The next day, samples were washed with PBS, and a diluted secondary antibody was added for an additional 2 hours covered with foil. Cells were subsequently washed with PBST for three times before DAPI (1:1000 in PBS) was added for 10 min to stain nuclei. Samples were washed once again and a cover slip added using mounting media.

The following antibodies were used for immunofluorescence staining: RAD51 (Santa Cruz 1:50), BRCA1 (Cell Signaling 1:50), FITC-conjugated anti-rabbit secondary antibody (Invitrogen), Texas Red-conjugated anti-mouse secondary antibody (Invitrogen). Nuclei were stained with DAPI. CPD immunofluorescence was performed on LP9 cells following manufacturer’s instructions (Cosmo Bio Co kit #NMDND001).

2.8 Colony formation assay

Melan-A and Melan-C ($3x10^3$ cells per well) were seeded post UV exposure with stratalinker (Stratagene *1800*) according to manufacturer's protocol or using the UV box with UVB lamps (90 sec at dose meter $20mW/cm^2$) and left for approximately 2 weeks. The appropriate media was added every 3-4 days.

2.9 Comet assay

OxiSelect^{TM} Comet Assay Kit (3-Well Slides) was purchased from Cell Biolabs, Inc. (Cat.No: STA-350) and was used to perform the comet assay to evaluate DNA damage. The assay was conducted according to the manufacturer's protocol. In brief, treated cells were combined with the provided agarose and pipetted onto the OxiSelect^{TM} comet slide. The slide with the cells was treated with lysis buffer and alkaline solution, followed by electrophoresis under alkaline conditions. Nuclei were then stained with the DNA Dye (See Figure 6).

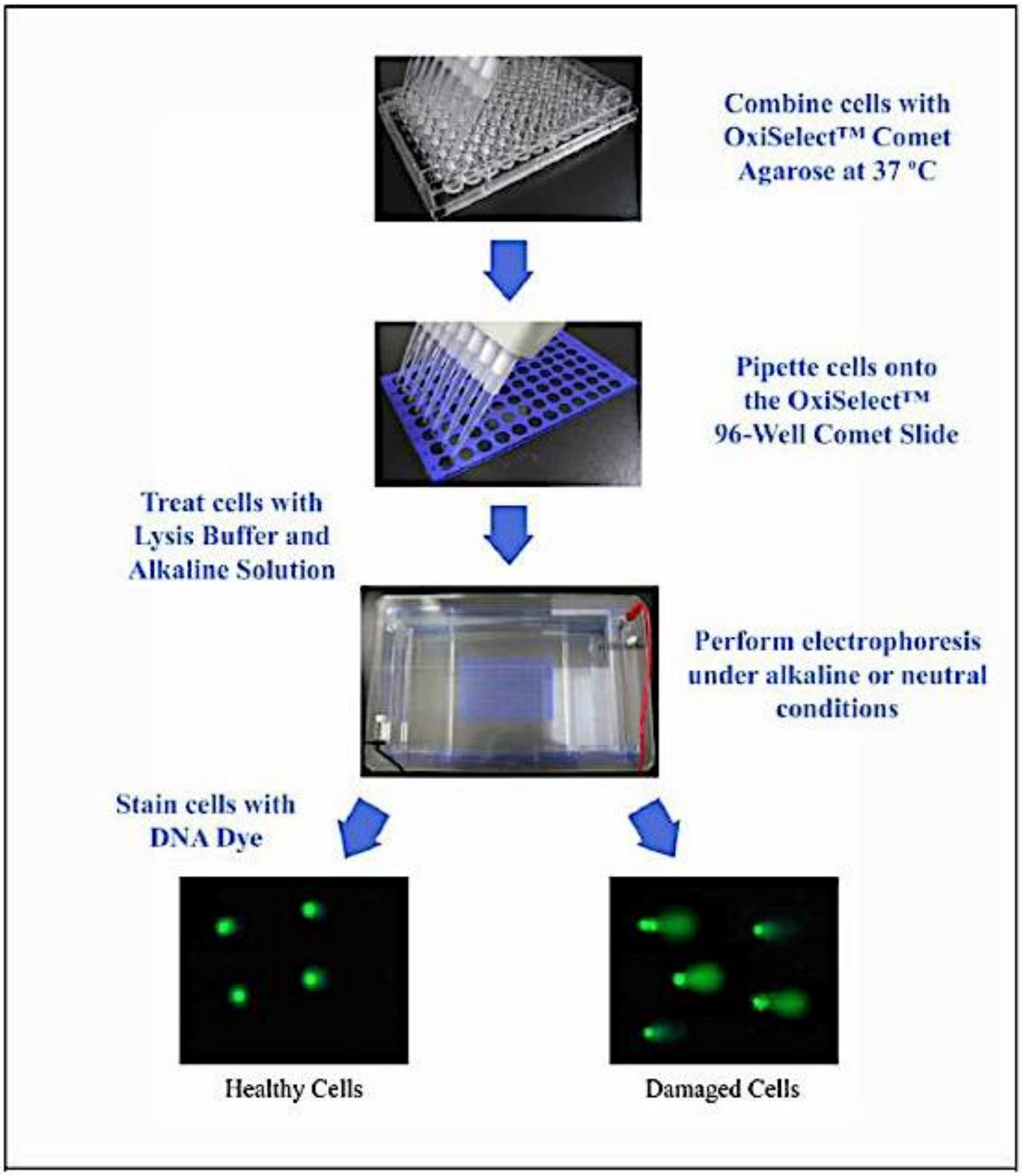

Figure 6. Comet assay principle. Cells get mixed with melted at 37C agarose, get pipetted onto the slides, cells get treated first with the lysis buffer and then alkaline solution. The slides are then placed into electrophoresis chamber to have DNA run from negative to positive electrodes under alkaline conditions. Samples are then stained and pictures are taken.

2.10 Mouse strains and genotyping

All mouse studies were performed in accordance with a protocol approved by the Fox Chase Cancer Center (FCCC) IACUC. *Nf2*$^{f/f}$*;Cdkna*$^{f/f}$ mice in FVB/N genetic background (63), a gift of Anton Berns, were maintained in our laboratory in a mixed FVB/N x 129/Sv background. The loxP sites in the *Cdkn2a* locus of these mice permit excision of exon 2, which results in inactivation of both *p16Ink4a* and *p19Arf*.

Bap1$^{f/f}$ mice in FVB/N background were developed in our laboratory using zinc finger nuclease (ZFN) technology, with the assistance of the FCCC Transgenic Mouse Facility. Custom ZFNs targeting *Bap1* were designed and validated in mammalian cells by Sigma-Aldrich (St. Louis, MO). A pair of ZFNs was identified that binds to and cuts within a site in intron 5 of *Bap1* with high efficiency and specificity. We then designed a donor DNA construct containing loxP sites in introns 6 and 7 (Figure 14A), such that upon adenovirus-mediated expression of Cre recombinase there is deletion of exon 7 of *Bap1*. The ZFN mRNAs and donor DNA were injected into the pronucleus of one-cell embryos of FVB/N mice, and embryos were then transferred into pseudo-pregnant females. DNA from pups was analyzed for correct targeting by PCR amplification of the gene and sequencing. Three founder mice with loxP sites integrated in the *Bap1* locus were identified, one of which was used for experiments reported here. Representative examples of genotyping of DNA from *Bap1* CKO mice are shown in Figure 14B.

In addition to *Bap1*$^{f/f}$, *Nf2*$^{f/f}$, and *Cdkn2a*$^{f/f}$ mice, these CKO animals were crossed to generate cohorts with the following genotypes: *Bap1*$^{f/f}$;*Nf2*$^{f/f}$, *Bap1*$^{f/f}$;*Cdkn2a*$^{f/f}$, *Nf2*$^{f/f}$*;Cdkn2a*$^{f/f}$ and *Bap1*$^{f/f}$;*Nf2*$^{f/f}$;*Cdkn2a*$^{f/f}$. The following primers and annealing temperatures were used to genotype the mice: *Bap1*$^{f/f}$ 1063: 5'-CCC TGA GAC CCA

GAA AAT CA-3’, Tm = 54.3°C; *Bap1*$^{f/f}$ 1228: 5’-GGG AGG CTC TTT GAA TTG GA-3’, Tm = 54.9°C; *Nf2*$^{f/f}$ 1048: 5’-CTT CCC AGA CAA GCA GGG TTC-3’, Tm = 58.0°C; *Nf2*$^{f/f}$ 1049: 5’-GAA GGC AGC TTC TTC CTT AAG TC-3’, Tm = 53.2°C; *Cdkn2a*$^{f/f}$ 1025: 5’-GCA GTG TTG CAG TTT GAA CCC-3’, Tm = 57.4°C; and *Cdkn2a*$^{f/f}$ 1026: 5’-TGT GGC AAC TGA TTC AGT TGG-3’, Tm = 55.8°C.

2.11 Adeno-Cre injections

Ad5CMVCre (Adeno-Cre) virus was obtained from the Viral Vector Core of the University of Iowa. Mice 8-12-weeks of age were injected intrathoracically (63), specifically intrapleurally, or intraperitoneally with Adeno-Cre virus (50 μl of 3-6 x 10^{10} PFU), with approximately equal numbers of mice of each gender in each cohort. Mice were monitored daily and were euthanized upon visible signs of distress, including extreme fatigue, labored breathing, or when mice exhibited a 10% change in body weight. Tissues of all organs of the pleural and peritoneal cavities were collected from sacrificed mice, and tumor specimens were subjected to histopathological assessment. Portions of tumors were also saved in both O.C.T. Compound and RNA*later* Solution (Thermo Fisher Scientific, Waltham, MA) and immediately frozen at -80°C.

2.12 Tumor histopathology, immunohistochemistry and RT-PCR analysis

The histopathological procedures in our laboratory are essentially the same as previously described (23). In summary, after paraffin embedding, sectioning and deparaffinization, hematoxylin and eosin (H&E)-stained sections were used for histopathologic evaluation, and unstained sections were used for immunohistochemistry (IHC). For IHC, sections were subjected to heat-induced epitope retrieval using citrate buffer (pH 6.0) for 20 min.

MMs were diagnosed by two independent pathologists (Andres J. Klein-Szanto and Qi Cai). To confirm the diagnosis of MM, IHC was performed for various mesothelial markers, including mesothelin, (Santa Cruz Biotechnology, Dallas, TX), and TROMA-1 (DSHB, University of Iowa, Iowa City, IA). In addition, reverse transcription-PCR (RT-PCR) analysis was also performed to analyze mesothelial markers, including *Wt1*, *Msln* (mesothelin), and *Krt18/19* (cytokeratin 18/19). RT-PCR analysis for *Msln* used primers 5′-ATCAAGACATTCCTGGGTGGG-3′ and 5′-CGGTTAAAGCTGGGAGCAGAG-3′. To assess cell proliferation, IHC staining was performed using Ki-67 antibody (Dako/Agilent, Santa Clara, CA).

2.13 Immunoblot analysis and antibodies

Protein lysates were prepared using cell lysis buffer (Cell Signaling) supplemented with 2 mM PMSF. All protein lysates were incubated for 15 min on ice with frequent vortexing before being cleared by centrifugation for 10 min at 4°C. Bradford reagent was used to measure protein concentrations. Then 50 μg cell lysates were loaded into NuPAGE 4-12% Bis-Tris gels (Invitrogen) and transferred nitrocellulose membranes

(BioRad). Membranes were blocked with 5% non-fat milk in TBST for 1 hour and then incubated with primary antibodies at 4°C overnight. After washing three times in TBST, membranes were incubated with secondary antibody at room temperature for 1 hour, and further washed three times. Immunoblots were developed using Immobilon Western Chemiluminescent HRP Substrate (EMD Millipore, Ontario Canada; P90720, Cat. No. WBKLS0500). The following antibodies were used.

A Bap1 antibody specific for mouse origin was purchased from Bethyl Laboratories (A302-243, 1:2000). A Bap1 antibody specific for human origin (sc-28383, 1:2000), p19ARF (sc-32748 1:1000), Actin (sc-47778, 1:50,000), Gapdh (sc-32233, 1:50,000) were purchased from Santa Cruz Biotecnology.

Nf2 (#6995 1:1000), Akt (#9272S, 1:1000), P-Akt (#4060, 1:1000), p53 (#2527, 1:2000) and γH2AX (Bethyl, A300-081A,1:2000) antibodies were purchased from Cell Signaling. A p16 antibody was purchased from Abcam (ab189034 1:1000). Anti-rabbit IgG HRP linked antibody (#7074) and anti-mouse IgG HRP linked antibody (#7076) were purchased from Cell Signaling, while anti-rat IgG HRP linked antibody was purchased from Santa Cruz Biotecnology (sc-2006 1:2000).

2.14 Spheroid growth assay

Primary normal mesothelial cells were isolated from individual CKO mice, 10-12 weeks of age, with each of the following genotypes: *Bap1*$^{f/f}$, *Nf2*$^{f/f}$, *Cdkn2a*$^{f/f}$, *Bap1*$^{f/f}$;*Nf2*$^{f/f}$, *Bap1*$^{f/f}$;*Cdkn2a*$^{f/f}$, *Nf2*$^{f/f}$;*Cdkn2a*$^{f/f}$, and *Bap1*$^{f/f}$;*Nf2*$^{f/f}$;*Cdkn2a*$^{f/f}$. The mesothelial cells were isolated by sacrificing animals and adding trypsin (0.25% Trypsin-EDTA, Gibco, 25200-056) to the peritoneal cavity, according to the method of Bot *et al.*

(70). Normal mesothelial cells at passage 2 were then seeded in 6-well plates (Thermo Fisher Scientific BioLite 6-well Multidish, Cat. #130184) and treated with 4×10^{10} PFU/ml of either control Ad5CMVempty (Adeno-CMV) or Adeno-Cre virus for 1 h. Cells were then washed in PBS, cultured in normal mesothelial media (71) for 72 h, trypsinized and then counted. Mesothelial cells (5,000) were seeded in each well of a 6-well non-adherent plate (Corning, Costar) in serum-free DMEM/F12 media supplemented with B27 (Invitrogen), EGF (10 ng/mL), basic FGF (10 ng/mL) and penicillin/streptomycin, as described (61). The experiment was performed in triplicate for each cell genotype. Spheroids were photographed using light microscopy after 9 days of culture.

2.15 RNA-seq analysis

Snap-frozen primary MMs from 6 *Nf2*$^{f/f}$*;Cdkn2a*$^{f/f}$ mice and 6 *Bap1*$^{f/f}$*;Nf2*$^{f/f}$*;Cdkn2a*$^{f/f}$ mice stored in RNA*later* at -80°C were used for RNA-seq analysis. The RNA was isolated in Trizol using a homogenizer and then processed and purified with RNeasy following the manufacturer's protocol (Qiagen Cat. No. 74104). RNA-seq was carried out with a HiSeq Sequencing System and the following reagents: TruSeq Stranded mRNA Library Kit, HiSeq Rapid SR Cluster Kit, HiSeq Rapid SBS Kit v2 (Illumina, San Diego, CA). Stranded mRNA-seq libraries were prepared using 1000 ng of total RNA for each sample according to Illumina's product guide. In brief, mRNAs were enriched twice using poly-T based RNA purification beads and subjected to fragmentation at 94°C for 8 min via divalent cation method. The first strand cDNA was synthesized using Invitrogen SuperScript II reverse transcriptase (Thermo Fisher Scientific) and random primers at

42°C for 15 min, followed by second strand synthesis at 16°C for 1 h. During second strand synthesis, dUTP was used to replace dTTP, such that the second strand was quenched during amplification. A single ‘A’ nucleotide was added to the 3’ ends of the blunt fragments at 37°C for 30 min. Adapters with Illumina P5, P7 sequences as well as indices were ligated to the cDNA fragment at 30°C for 10 min. After AMPure bead purification (Beckman Coulter, Indianapolis, IN), a 15-cycle PCR reaction was used to enrich the fragments. PCR was set at 98°C for 10 sec, 60°C for 30 sec, and extended at 72°C for 30 sec. Libraries were again purified using AMPure beads, followed by quality check using a Bioanalyzer (Agilent, Santa Clara, CA) and quantified with Invitrogen Qubit (Thermo Fisher Scientific). Sample libraries were subsequently pooled and loaded onto the sequencer. The generated single-end reads were aligned to the mm10 mouse genome using TopHat2. Raw sequence counts for each gene were then produced with HTseq and differentially expressed genes were identified by DESeq2 (72), after filtering out pseudogenes and unannotated Ensembl identifiers. Heatmaps of RNA-seq data are constructed from $\log_2(x+1)$-transformed counts per million (CPM), standardized across rows, using the “heatmap.2” function from the R gplots library.

CHAPTER 3

3 BAP1 ROLE IN MELANOMA DEVELOPMENT

3.1 Introduction

The Testa laboratory and collaborators identified two families (Louisiana: Lou, and Wisconsin: Wis) with germline *BAP1* mutations that were predisposed to MM and other types of cancer, including various carcinomas (19). The Lou family, unlike the Wis family, developed two uveal melanomas (UMs) and several skin cancers of unknown types, possibly cutaneous melanomas (CMs) or squamous cell carcinomas. One reason why the Lou family, but not the Wis family, developed UMs and skin cancers might be that the Lou family was exposed to UVR year-round in connection with residing in a subtropical area. The hypothesis is that the concurrence of a genetic predisposing factor (a germline inactivating mutation of *BAP1*) and environmental exposure to UVR contributed to the multiple uveal and skin cancers seen in this family, whereas the presence of multiple MMs in both families was related to asbestos in the home. Thus, this may be an example of gene vs. environment interaction. To test this possibility, we used a *Bap1*-mutant mouse model with a knockin mutation identical to that observed in the Lou family to evaluate whether this mutation (from here on out, referred to as $Bap1^{+/Lou}$) alone confers susceptibility to UVR-induced melanomagenesis, or when combined with a mutation found in a well-established Hepatocyte Growth Factor (HGF)/Scatter Factor transgenic mouse model (from here on, called HGF^{Tg} mice). These HGF^{Tg} mice have been previously shown to develop melanomas within 12 months following UVR given shortly after birth (73).

Bap1$^{+/Lou}$ mice were crossed to *HGF*^{Tg} mice and the following 4 genotypes were obtained: WT, *Bap1*$^{+/Lou}$, *HGF*^{Tg} alone, and *Bap1*$^{+/Lou}$;*HGF*^{Tg} double mutants. Newborn pups were exposed to UVR 3-4 days after birth and then monitored for melanoma formation for up to 24 months (Figure 7). Since the *Bap1*$^{+/Lou}$ mouse mimics the germline genetics of a human BAP1-TPDS family that developed multiple uveal and skin cancers, and *HGF*^{Tg} mice are susceptible to UVR-induced CM, we hypothesized that *Bap1*$^{+/Lou}$;*HGF*^{Tg} mice would develop CMs more rapidly and/or aggressively after being exposed to UV than WT, *Bap1*$^{+/Lou}$, or *HGF*^{Tg} mice. For this project, I thank Dr. Raza Zaidi for providing the *HGF*^{Tg} mice and instructions on the proper UVR dosing of mice (Figure 7).

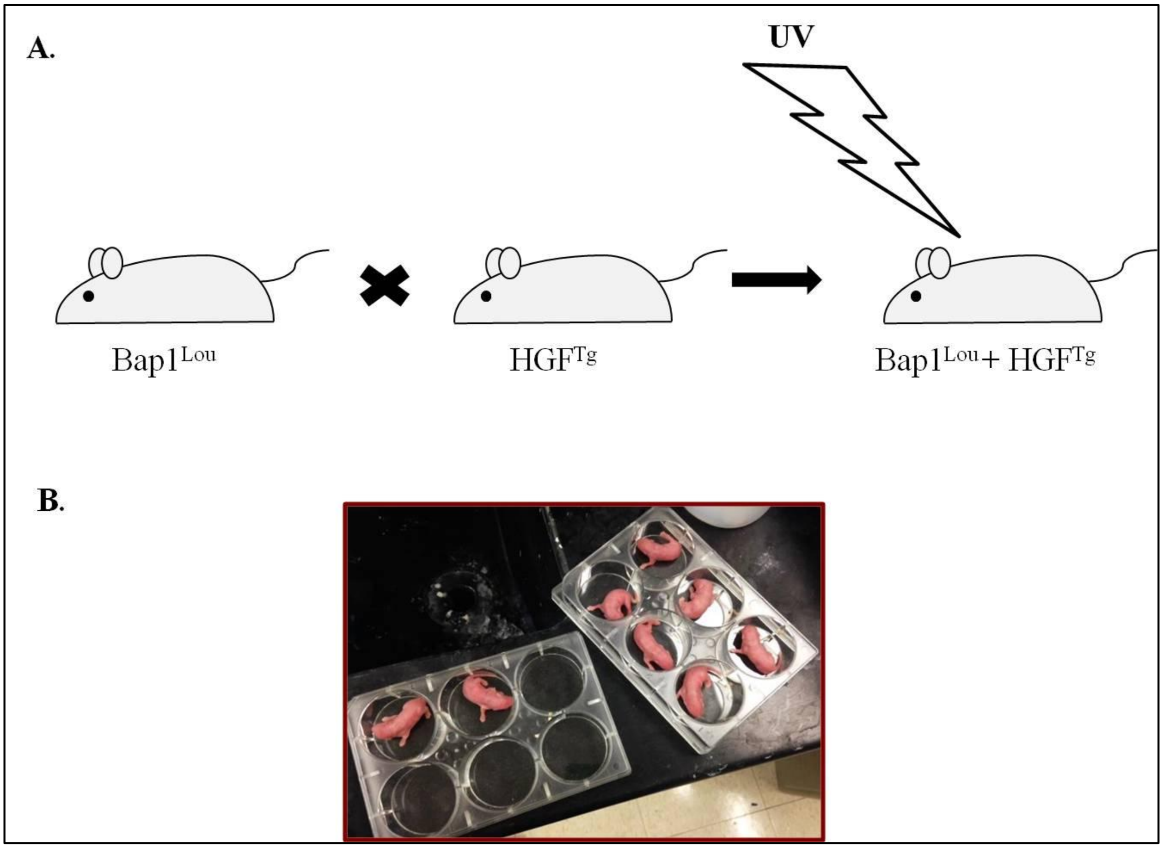

Figure 7. Experimental setup. (A) Schematic diagram of the mating crosses to obtain the necessary genotypes for further UVR exposure. **(B)** Experimental procedure: pups are getting prepared for the UVR exposure on day 3-4 after birth. To ensure pups' relative immobility for a 15-min exposure time, they are placed into 6-well plates.

3.2 Results

WT, *Bap1*$^{+/Lou}$, *HGF*^{Tg} and *HGF*^{Tg}*;Bap1*$^{+/Lou}$ mice were exposed to UVR (9.6 kJ/m^2 for 15 min) neonatally (day 3-4) and observed for any skin malformations mimicking possible melanoma. Altogether, 21 *HGF*^{Tg} mice, 26 *Bap1*$^{+/Lou}$ mice, 22 *HGF;Bap1*$^{+/Lou}$ mice and 26 WT (*Bap1*$^{+/+}$) mice were neonatally exposed to UVR at Fels Institute and Fox Chase Cancer Center. When the *HGF* transgene is expressed in mice, it was previously shown that about one third of the animals develop rectal prolapses and intestinal pseudo-obstruction (68). Unfortunately, possibly due to genetic drift in this murine line, we observed rectal prolapses and intestinal pseudo-obstructions in ~70% of our *HGF*^{Tg} mice in our colonies at both Fels Institute and Fox Chase Cancer Center at around 2 months of age, independent of UVR exposure. Unfortunately, these mice would die or would have to be euthanized before development of any signs of melanoma. Despite this setback, we were able to replicate previous results that UV-exposed *HGF*^{Tg} mice developed CM at approximately 13 months, although with a much lower penetrance (2/21 mice) than reported by Noonan *et al.* (73). However, this lower incidence was due to the fact that 70% of our *HGF*^{Tg} animals were lost due to rectal prolapses and intestinal pseudo-obstructions. Interestingly, *Bap1*$^{+/Lou}$ mice also developed melanomas (2 mice, at ages 14 and 26 months), showing that a single copy mutation of *Bap1* after a single dose of UVR is sufficient to give rise to CM, albeit at a low penetrance. Additionally, only 2 *HGF*^{Tg}*;Bap1*$^{+/Lou}$ mice developed CM at ~14 months after UVR exposure. UVR-exposed WT mice did not develop any CMs, consistent with previous findings (74). While there was a trend for increased CM formation in each of the UVR-exposed GEM models versus WT mice, the numbers are insufficient to determine statistically significant differences among the groups.

Table 1. Cutaneous melanoma incidence after UVR exposure in *Bap1*$^{+/Lou}$, *HGF*^{Tg}, and *HGF*^{Tg}*;Bap1*$^{+/Lou}$ mice.

Genotype	WT	*Bap1*$^{+/Lou}$	*HGF*^{Tg}	*HGF*^{Tg}*;Bap1*$^{+/Lou}$
Melanomas	0/26	2/26	2/21[a]	2/22[a]
Median survival in months	24	20	13	14

[a]Note that only ~70% of 21 *HGF*^{Tg} mice and 22 *HGF*^{Tg}*;Bap1*$^{+/Lou}$ mice needed to be sacrificed 2-3 months after birth due to rectal prolapses and/or intestinal pseudo-obstructions, so tumor penetrance for each genotype was actually 2 out of 6 or 7 mice (~30%).

3.3 Discussion

The fact that 2 *Bap1*$^{+/Lou}$ mice, but no WT mice, developed UVR-induced CMs, suggests that individuals with germline mutations of *BAP1* may be more susceptible to sunlight-related CM than individuals who do not harbor such mutations. Unfortunately, due to the low number of mice that survived long enough to develop UVR-induced CMs, it was not possible to tease out statistical significant differences in the latency or incidence of tumors between the various genotypes of mice. However, it would be interesting to test whether *Bap1*$^{+/Lou}$ mice would develop CM without UVR exposure, or if the UVR is the necessary environmental second hit, in favor of a gene vs. environment interaction model. It is noteworthy that in the FVB background, no spontaneous melanomas have been observed in aged *Bap1*$^{+/Lou}$ mice, although we are investigating if any CMs will occur in *Bap1*$^{+/Lou}$ mice in other strain backgrounds (Sv129S and C57/B6).

HGF^{Tg}*;Bap1*$^{+/Lou}$ mice did not show a higher incidence or shorter latency of UVR-induced CM than *HGF*^{Tg} mice. On its own, this would suggest that germline *Bap1* mutations do not enhance UVR-induced melanomagenesis in the *HGF*^{Tg} mouse model. However, in our hands, the *HGF*^{Tg} mouse was a flawed GEM model of melanoma due to the very high incidence of prolapses and intestinal pseudo-obstructions observed, resulting in too few mice that were able to survive long enough to be tested to see if they would develop CM. Instead, most of the animals had to be culled due to these issues, making it impossible to draw definitive conclusions. However, recent work with another model revealed that deletion of *Bap1* specifically in melanocytes was found to cooperate with a constitutively active, oncogenic form of BRAF (*Braf*^{V600E}) and UVR to cause cutaneous melanoma in mice, although at only a very low frequency (75). In addition, *Bap1*-null melanoma cells derived from mouse tumors proved to be more aggressive and metastasize to distant sites more readily than those from their wild-type animals. In future studies, we would like to cross *Bap1*$^{+/Lou}$ mice to other tumor suppressor genes, such as *CDKN2A*, known to be involved in predisposing to CM and subsequently exposing mice to one or more doses of UVR. We hypothesize that *Bap1*$^{+/Lou}$;*Cdkn2a*$^{+/-}$ mice would develop more CMs with a more rapid progression compared to animals with only one gene being inactivated. We would also expect *Bap1*$^{+/Lou}$ mice to develop more CMs if given multiple doses of UVR during their lifetime rather than only one neonatal dose.

CHAPTER 4

4 BAP1 IN DNA DAMAGE REPAIR

4.1 Introduction

BAP1 functions as a tumor suppressor, in part, due to its role in DNA damage repair. Yu *et al.* showed that, as a deubiquitinase, BAP1 is required for efficient assembly of the homologous recombination (HR) factors BRCA1 and RAD51 at DNA damage sites (40). Furthermore, Ismail *et al.* found that BAP1 mediates rapid poly(ADP-ribose)-dependent recruitment of the polycomb deubiquitinase complex PR-DUB to DNA damage foci (41). Additionally, BAP1 was identified as a phosphorylation target for the DNA damage response kinase ATM (40, 41). These results highlight the importance of BAP1 at sites of DNA damage and suggest that loss of *BAP1* may allow for increased DNA damage, contributing to tumorigenesis, particularly in cancers associated with environmental carcinogens such as asbestos and UVR, which are known to induce DNA damage. One limitation of the studies linking BAP1 to DNA damage repair is that these phenomena were performed in chicken and human cancer cells, not cells such as normal melanocytic or mesothelial cells that have particular relevance to the *BAP1* syndrome. Also, it has not been previously explored if BAP1 is necessary for a UVR-induced DNA damage repair pathway, i.e. nucleotide excision repair (NER). Notably, David Livingston's group demonstrated that BRCA1 is required for UVR-induced DNA damage post-replication repair (76). Since BAP1 has been shown to be a protein associated with BRCA1 (23), we speculated it could also be required for UVR-induced DNA damage repair. Therefore, we hypothesized that inherited mutations of *BAP1* may increase susceptibility to certain environmental factors, including asbestos and UVR due to BAP1's role in the DNA damage repair response.

4.2 Results

To further understand the role of BAP1 in UVR-related DNA damage repair, one environmental cause of CM, we knocked down *BAP1* in normal human and mouse melanocytes, and subsequently exposed them to UVR *in vitro* (Figure 8A). Using immunofluorescence, we tested for BRCA1 and BAP1 recruitment to UVR-induced DNA damage sites and for accumulation of Rad51 and BRCA1 in BAP1-deficient cells (Figure 8B).

A. B.

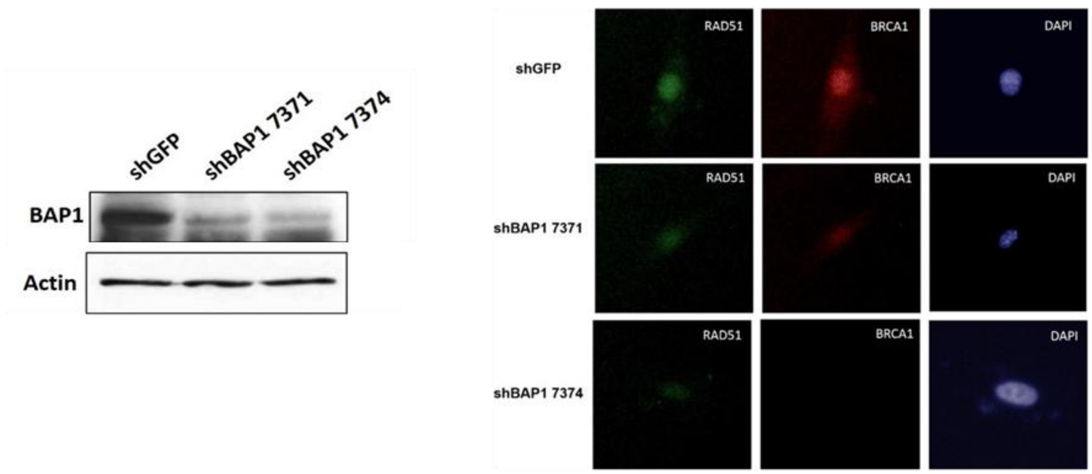

Figure 8. BAP1 deficiency affects recruitment of BRCA1 and Rad51 to UVR-induced DNA damage sites. (A) Western blot analysis of *BAP1* knock down in human melanocytes. BAP1 levels decreased following knockdown of *BAP1* with each of 2 different shRNAs, while actin levels stayed the same. **(B)** BAP1 contributes to BRCA1 and Rad51 recruitment to UVR-induced DNA damage sites in human melanocytes. Immunofluorescent staining against RAD51 (FITC), BRCA1 (Texas Red) and nucleic acid (DAPI) in control human melanocytes following treatment with *shBAP1* or *shGFP*. Images are pseudo-colored.

Normal human melanocytes were purchased from ScienCell™ and were propagated according to the manufacturer's protocol. To establish *BAP1*-deficient melanocytes, lentivirus expressing 2 independent shRNAs targeting *BAP1*, or a shRNA targeting GFP as a control, were prepared and used to transduce the human melanocytes. Cells were selected with puromycin 48 hours post-infection, with non-transduced cells (kill plate) dead. shGFP and sh*BAP1*-expressing melanocytes were passaged without puromycin for subsequent experiments. After several passages, *shGFP* and *shBAP1*-expressing melanocytes were harvested, and protein was extracted for immunoblot analysis. As shown in Figure 8A, both cell lines expressing shRNA against *BAP1* (7371 and 7374) exhibited markedly reduced BAP1 protein when compared to control *shGFP*-treated melanocytes. To determine whether BAP1 deficiency affects DNA repair in melanocytes, as previously reported in other cell lineages, *shGFP* and *shBAP1*-expressing cells were exposed to UVR. After 24 hours, the cells were fixed and immunofluoresence was used to determine if Rad51/BRCA1 foci accumulation was altered, as previously described (40). Preliminary analysis demonstrated weaker Rad51/BRCA1 accumulation in the nucleus of *BAP1*-deficient melanocytes when compared to *shGFP*-treated control cells, consistent with BAP1 having a tumor suppressor role in DNA repair after UVR (Figure 8B). These preliminary data support a role for BAP1 in maintaining genomic integrity in melanocytes and could help to explain why a higher incidence of CM is observed in individuals with germline mutations in this tumor suppressor gene. These data suggest that BAP1 is necessary for BRCA1 and RAD51 recruitment to DNA damage in normal human melanocytes upon UVR-induced DNA damage.

Next, we sought to explore whether the ability of cells to survive and propagate post UVR-induced DNA damage is dependent on *BAP1* status. We performed a colony formation assay on UVR-exposed Melan-A cells. Melan-A cells were transduced with shRNAs against GFP (control group) and *BAP1* in the same manner as described above. The colonies were then compared between the shGFP control group versus *Bap1*-deficient cells (Figure 9). Four different UVR doses were used (0, 5, 10 and 20 mJ), and then equal numbers of cells ($3x10^3$ cells/well) were seeded on 6-well plates and colonies were allowed to grow for approximately 2 weeks. As shown in Figure 9A, there was no distinguishable difference in colony formation between *shGFP*-treated and *shBap1* 7173-treated Melan-A cells exposed to 0 or 5 mJ of UVR. However, when treated with 10 or 20 mJ of UVR, *Bap1*-deficient Melan-A cells formed less colonies than shGFP control cells (Figure 9A). A similar result was obtained with Melan-C cells (Figure 9B). These data suggest that cells lacking *Bap1* are unable to repair damage caused by UVR, and therefore cannot re-enter the cell cycle and form colonies. We also obtained transient *BAP1* knockdown with short interference RNA (siRNA) in human melanocytes using the LONZA Amaxa® NHEM-Neo Nucleofector® Kit (see Chapter 2). These cells were then used to compare DNA damage markers (p53 and γH2AX) between the siControl and si*Bap1* groups. We demonstrated p53 protein induction and γH2AX increases post UVR (20mJ) in human melanocytes with transient *BAP1* knockdown (Figure 10), confirming the UVR stress response. Note that while siBap1#5 gave good knockdown at both 6 and 24 hours, siBap1#0 did not appear to work in this experiment. UVR exposure changes dipyrimidines of DNA into cyclobutane pyrimidine dimers or (6-4) photoproducts. To confirm the UVR-induced DNA damage, we stained UVR-exposed cells for CPD markers, and indeed confirmed their presence post UVR treatment (Figure 11). In retrospect, it would have been useful to evaluate the levels of CPD post UVR in Bap1-deficient cells to determine if Bap1 is necessary for nucleotide excision repair in this setting.

A

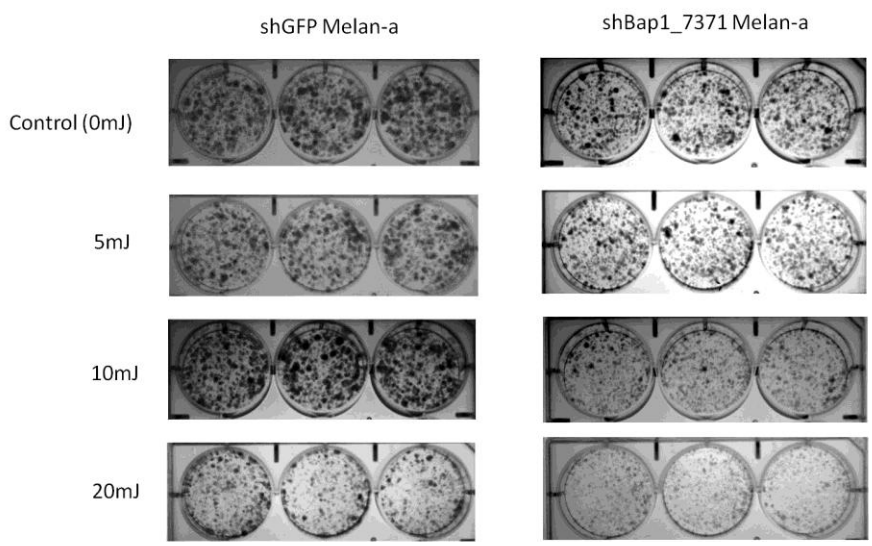

B

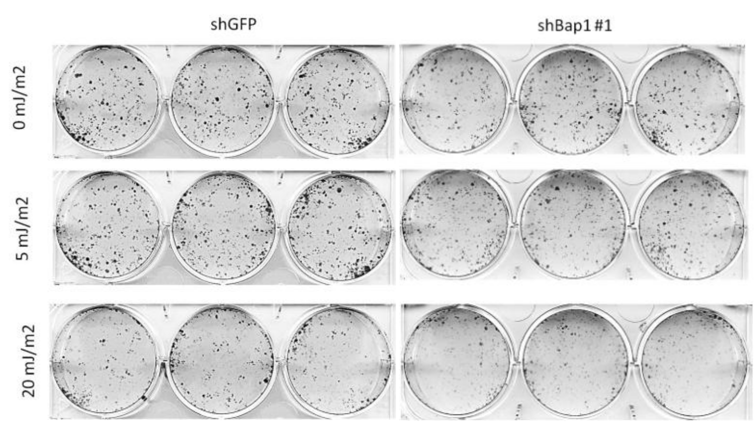

Figure 9. Bap1 clonogenic assay. (A) and **(B)** Mouse melanocytes (Melan-A and Melan-C, respectively) infected with lentivirus expressing either *shGFP* or *shBAP1* and exposed to different UVR doses. *BAP1* knockdown decreases the colony formation after UVR exposure.

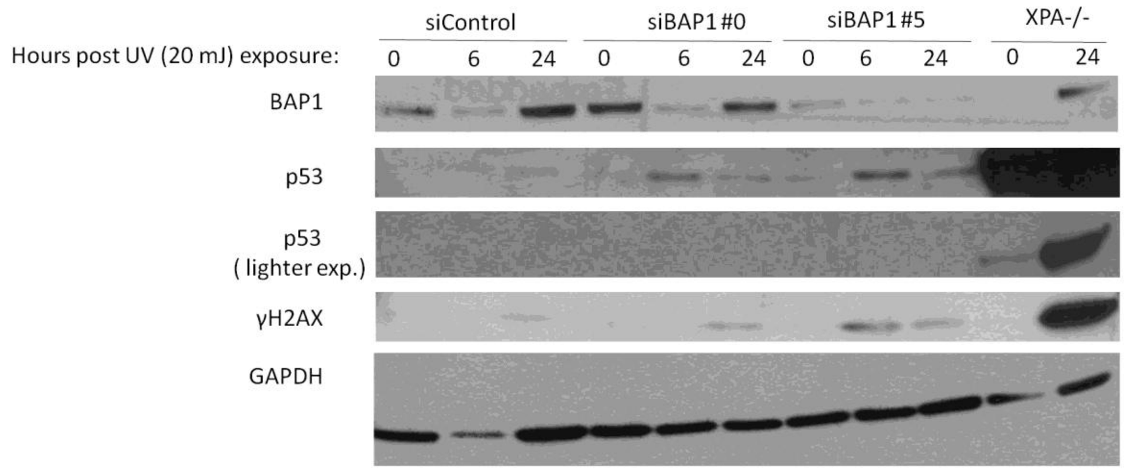

Figure 10. Western blot analysis confirming DNA damage stress response in human melanocytes. Human melanocytes with transient *BAP1* knockdown (*siBAP1#0* and *siBAP1#5*) exhibit higher levels of p53 and γH2AX marker of DNA damage post UVR exposure compared to siControl. $XPA^{-/-}$ cells are used as a positive control.

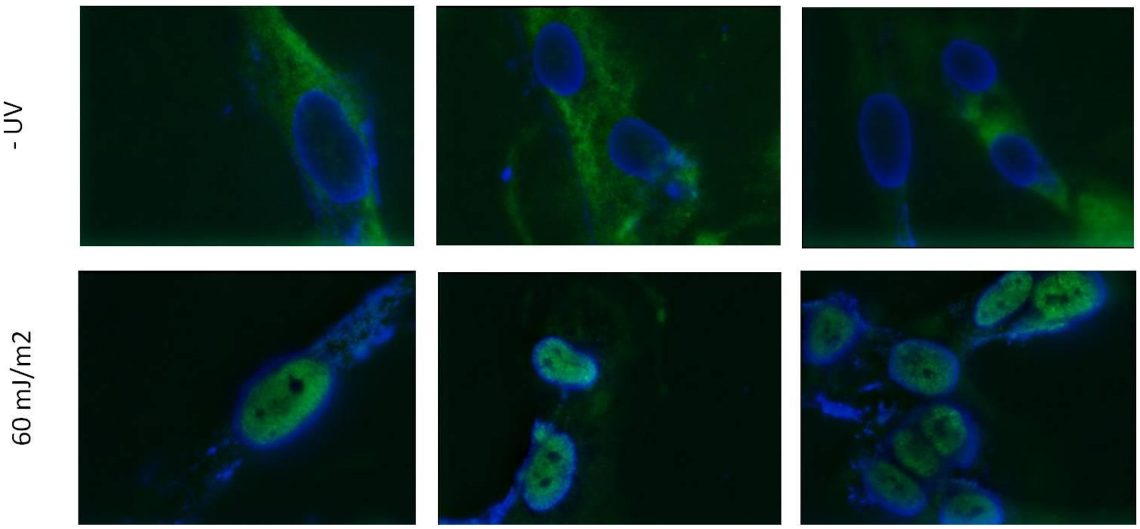

Figure 11. Immunofluorescence analysis of CPD post UVR exposure in LP9 cells. CPD is increased in LP9 cells exposed to UVR. Induction of CPD (green in nuclei) post UVR-treatment (60 mJ/m^2) in triplicate per group. DAPI, blue; CPD, green.

To further implicate BAP1 in UVR-induced DNA damage repair, we conducted a comet assay, or a single cell gel electrophoresis assay (SCGE), which measures DNA damage in individual cells. When undergoing electrophoresis, damaged cellular DNA with fragments and strand breaks forms a classic "comet tail" shape as it gets separated from the intact DNA (Cell Biolabs). For this experiment, we first used Melan-C cells and performed an UV dose escalation experiment to determine the optimal dose to cause DNA damage as determined by comet tails. We used doses of 0, 15, and 20 mJ/m^2, and demonstrated that "tails" were longer and better differentiated at 20 mJ/m^2 than at 15 mJ/m^2; thus, the higher dose was chosen for subsequent experiments (data not shown). Melan-A cells with transient knockdown of *Bap1* via siRNA#2 or #3 or control siRNA (Figure 12A) were exposed to 20 mJ/m^2 UVR, and a comet assay was performed after 16 hours. As expected, *Bap1* knockdown cells exhibited longer "comet tails" than the siRNA control cells post UVR exposure (Figure 12B). To quantify these results, the Olive Tail Moment (Olive Tail Moment = Tail DNA% x Tail Moment Length) was measured with comet assay software (CometScore) and was determined for siControl and si*Bap1* cells. *Bap1* knockdown cells had higher Olive Tail Moments when compared to that for siControl groups post UVR exposure (Figure 12C). These data indicate that there is more UVR-induced DNA damage when *Bap1* is absent or deficient in a cell, and that Bap1 is an important player in the UVR DNA damage repair.

Because there was significantly more damaged DNA in UVR-treated *Bap1*-deficient cells, we hypothesized that these cells are not able to efficiently repair DNA damage and, thus, may arrest in S-phase of the cell cycle, where NER occurs. To test this hypothesis, we stably knocked down *Bap1* using shRNA in 293 HEK-T cells (Figure

13A), exposed them to UVR, and analyzed their cell cycle using flow cytometry. 293 HEK-T cells were transduced with lentivirus expressing shGFP control shRNA or two different shRNAs (7371 and 7374) targeting *BAP1* and then selected with puromycin until a non-transduced 293 HEK-T kill plate contained no cells. The resulting cell lines will be referred to as shGFP, *shBAP1* #7173, and *shBAP1*#7374 from this point on. As cells acquired the knockdown, they were exposed to UVR (~90 sec at dose meter 20 mW/cm^2), and after 24 hours, the samples were collected (UVR-treated group and non-UVR-treated), fixed overnight, and then stained with PI for cell cycle analysis using flow cytometry. There was a higher content of cells in the S phase in the groups with *Bap1* knockdown, compared to the non-UVR-treated control groups (Figure 13B).

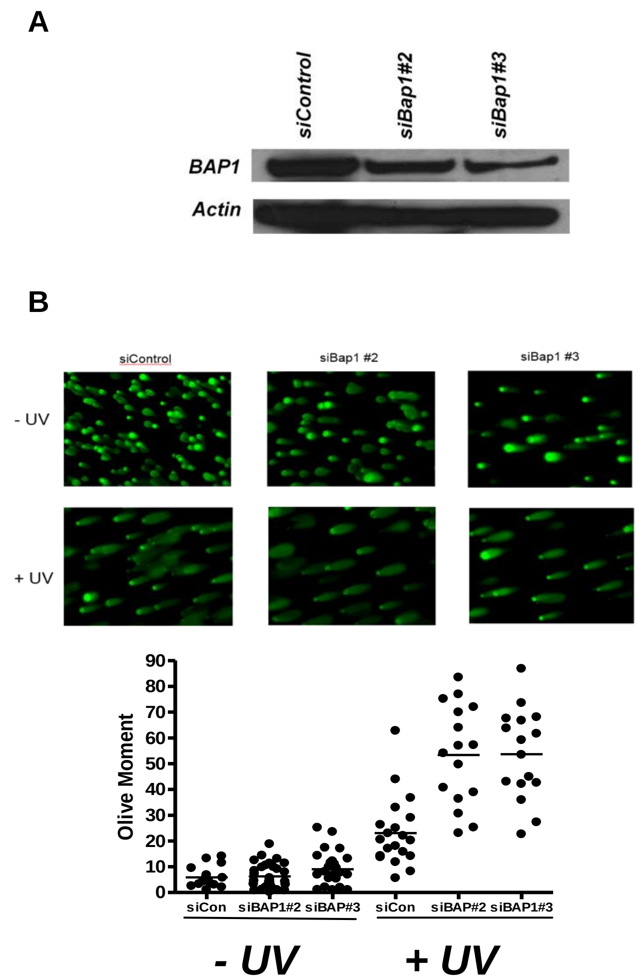

Figure 12. Comet assay analysis demonstrates Bap1 defficiency results in more cells with unrepaired DNA. (A) Immunoblot of transient *Bap1* knockdown via short interference RNA against *Bap1* in mouse melanocytes (Melan-A). **(B)** Images of comet assay post single 20 mJ/m^2 UVR treatment of control and *Bap1* knockdown cells. Dot plot of data shown in **B** comparing non-UVR-treated (-UV) with UVR-treated (+UV) siControl and *siBap1#2* and #3 cells.

A

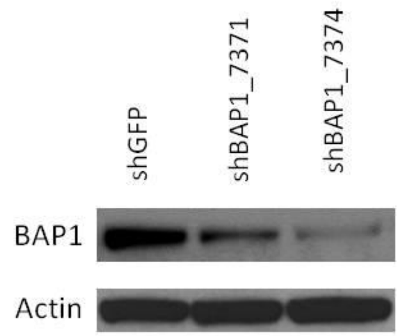

B

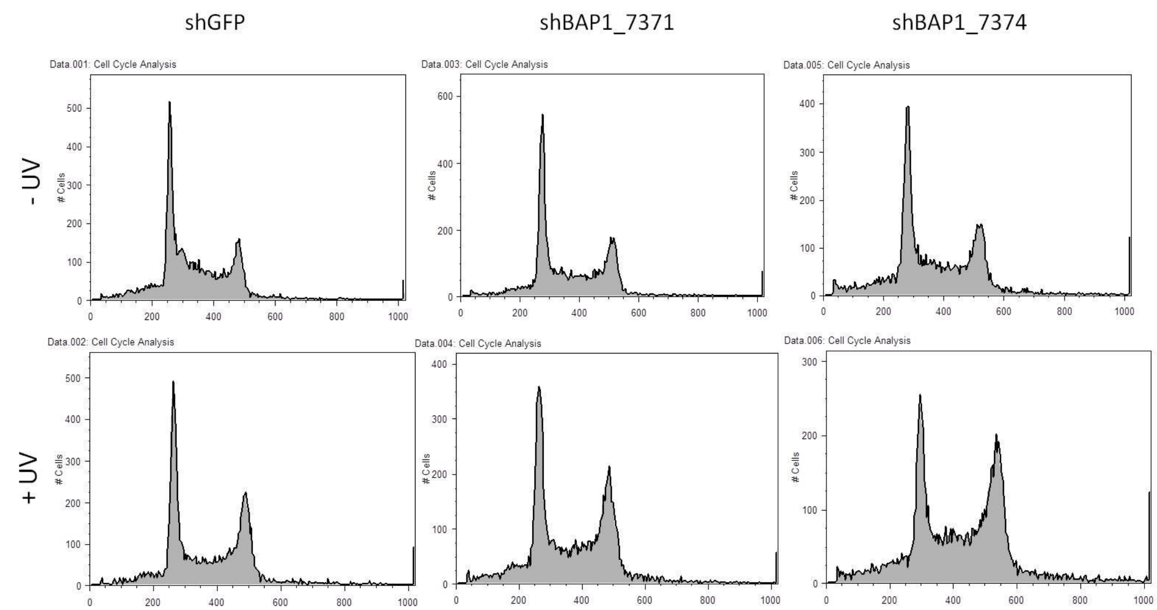

Figure 13. BAP1 deficiency leads to UVR-induced S phase arrest in 293 HEK-T cells. (A) shRNA knockdown of *BAP1* in 293 HEK-T cells. **(B)** Flow cytometry plots of cell cycle analysis 24 hours post UVR-treatment vs. non-treated 293 HEK-T cells.

4.3 Discussion

An important tumor suppressor function of BAP1 is its role in DNA damage repair. BAP1 has previously been shown to interact with BRCA1 and to contribute to DNA damage repair via the HR pathway (40). The role of BAP1 in other types of repair pathways, such as NER caused by UVR exposure, has not been formally tested in cells of origin of the cancers found in the *BAP1* syndrome.

Our experiments provide evidence that confirms a significant role for BAP1 in UVR-induced DNA damage repair. We demonstrate that cell cycle progression, DNA damage and DNA adduct repair are all altered in *BAP1*-deficient cells. Moreover, we implicate BAP1 in UVR-induced DNA damage repair in melanocytes, the cell of origin of CM and UM, two cancers included in the *BAP1* syndrome. However, further experiments are needed to elucidate the exact mechanism of how BAP1 aids in NER and what other proteins or pathways act in concert with BAP1 to repair DNA adducts. Knowing that BAP1 is a deubiquitinase that regulates gene expression by controlling chromatin condensation, perhaps it participates in the DNA damage repair via this mechanism. It would be interesting to perform ChiP-seq analysis in cells exposed to UVR, to determine if BAP1 is bound to chromatin at sites of DNA damage and/or to analyze the ubiquitin amounts at the locations of DNA damage.

From the experiments described above we can conclude that knockdown of *BAP1* in melanocytes sensitizes cells to UVR-induced apoptosis/arrest, prevents UVR-induced DNA damage repair and leads to the arrest of cells in S phase. These data support a role for BAP1 in maintaining genomic integrity in melanocytes and could help to explain why a higher incidence of CM is observed in individuals with germline mutations in this tumor suppressor gene.

CHAPTER 5

5 INACTIVATION OF *BAP1* COOPERATES WITH LOSSES OF *NF2* AND *CDKN2A* TO DRIVE THE DEVELOPMENT OF PLEURAL MALIGNANT MESOTHELIOMA IN CONDITIONAL MOUSE MODELS

5.1 Introduction

Pleural malignant mesothelioma is an aggressive, treatment-resistant cancer, which is causally related to asbestos exposure. Despite asbestos abatement efforts, MM rates have remained stable in the U.S. since 1994, causing ~3,200 deaths annually (77). Furthermore, a marked increase in MM has been predicted in developing countries, where usage of asbestos is increasing dramatically.

At the somatic genetic level, early cytogenetic and deletion mapping studies had revealed several prominent sites of chromosomal loss in human pleural MM, including 3p21, 9p21 and 22q12, and these recurrent abnormalities often occurred in combination in a given tumor, suggesting a multi-step pathogenetic process (78). The critical tumor suppressor genes at two of these sites, i.e., *CDKN2A* at 9p21 and *NF2* at 22q12, were discovered more than two decades ago (11, 14, 16, 60, 79), whereas the identity of the crucial 3p21 gene in MM remained a mystery until 2011, when *BAP1* was identified as the critical MM tumor suppressor at this locus (18, 80). In a recent comprehensive study as part of The Cancer Genome Atlas, various somatic genetic alterations of *BAP1*, *NF2* and *CDKN2A* were observed in combination in 25 of 74 (34%) pleural MMs (81).

The alterations of *CDKN2A* involve heterozygous or homozygous deletions of all or part of the locus (11). Abnormalities of *NF2* in MM frequently are biallelic, consisting of both an inactivating mutation and loss of the second allele (13). Biallelic losses of *CDKN2A* have been documented in ~40% of primary MMs (18) and up to 90% of MM cell lines (11). Inactivating *NF2* mutations have been reported in 20-55% of cases (13, 14, 18, 79). Using Sanger sequencing, somatic inactivating mutations of the *BAP1* tumor suppressor were initially reported in 20-25% of sporadic MMs (18, 80), but more recent studies with other platforms such as targeted next generation sequencing and multiplex ligation-dependent probe amplification have uncovered *BAP1* alterations in about 60% of cases, with a preponderance of exonic deletions (47).

The *CDKN2A* locus encodes the tumor suppressors p16INK4A and p14ARF, which regulate the Rb and p53 cell cycle pathways, respectively. In MM, the deleted region of *CDKN2A* typically includes exon 2 (11), which encodes portions of p16INK and p14ARF, and is thus predicted to affect both Rb and p53 pathways. Re-expression of p16INK4A in MM cells results in cell cycle arrest and tumor suppression/regression (82), while re-expression of p14ARF in MM cells induces G1 arrest and apoptosis (83). Underscoring the relevance of *Cdkn2a* to MM pathogenesis, heterozygous *Cdkn2a* knockout mice treated with asbestos develop MM at a significantly accelerated rate compared to asbestos-treated wild-type (WT) littermates (80). Additionally, mice deficient for both p16Ink4a and p19Arf exhibit enhanced asbestos-induced MM formation relative to mice deficient for either 16Ink4a or 19Arf alone (80).

Loss of the *NF2* product, merlin, in MM leads to cell cycle progression by upregulation of cyclin D1 both transcriptionally (84) and post-transcriptionally via activation of mTORC1 (85). NF2 also inhibits Pak and FAK signaling, which play key roles in cell migration and spreading, respectively, and inactivation of *NF2* in MM cells promotes invasiveness and spreading (86, 87). *Nf2*$^{+/-}$ mice treated with asbestos develop MM at an accelerated rate compared to asbestos-treated WT mice, suggesting that merlin inactivation contributes significantly to MM development (60, 63, 88). Moreover, mice with heterozygous losses of both *Nf2* and *Cdkn2a* show further acceleration of asbestos-induced MM, with resulting tumors exhibiting increased cancer stem cells and enhanced tumor spreading capability compared to those observed in mice with losses of only one or the other of these genes (61). Similarly, conditional knockout (CKO) mice harboring homozygous deletions of both *Nf2* and *p16Ink4a/19Arf* in the mesothelial lining of the thoracic cavity developed a high incidence of pleural MM that showed increased pleural invasion compared to *Nf2;Tp53* CKO mice (63).

BRCA1-associated protein-1 (BAP1) was discovered as an ubiquitin hydrolase that associates with the RING finger domain of BRCA1 and enhances BRCA1-mediated inhibition of breast cancer cell growth (23). BAP1 interacts with ASXL family members to form the polycomb group (PcG) repressive deubiquitinase (PR-DUB) complex involved in stem cell pluripotency and other developmental processes (33). BAP1 also interacts with and deubiquitinates the transcriptional regulator host cell factor 1 (HCF-1) (89). Importantly, BAP1 has been shown to form complexes with numerous transcription factors and cofactors, including transcription factor YY1 (90). The BAP1 ubiquitin carboxyl hydrolase activates transcription in an enzyme-dependent manner and regulates the expression of a variety of genes involved in numerous processes, including cell proliferation, DNA damage and inflammatory responses, metabolism, and various mechanisms of cell death (28, 44, 91-93). In animal models, asbestos exposure induces a significant increase in the incidence of MM in heterozygous *Bap1*-mutant mice compared with asbestos-exposed WT littermates (41, 94).

MM patients with germline *BAP1* mutations have an improved long-term survival compared to MM patients without such heritable mutations (71, 95). However, it remains unclear whether somatic *BAP1* mutations/deletions are associated with a poor prognosis in sporadic MM, as is the case in uveal melanoma and renal cell carcinoma (96, 97). While most human MMs exhibit somatic alterations of *BAP1*, *NF2* and/or *CDKN2A*, currently it is not known if inactivation of *BAP1* cooperates with loss of *NF2* and/or *CDKN2A* to drive a more aggressive MM phenotype. Here we address these questions experimentally using CKO models.

5.2 Results

The injection of Adeno-Cre virus into the pleural space of Rosa26 LacZ (R26R) reporter mice has been previously reported to result in efficient β-galactosidase expression of the mesothelial cell lining of the chest cavity (63). Locotemporal expression of Cre recombinase by IT injection of Adeno-Cre was used to induce mesothelial cell-specific loss of Bap1, Nf2, and/or Cdkn2a in homozygous single-gene CKO mice and in homozygous compound CKO mice. The injection scheme used for the CKO mice is depicted in Figure 14C. Tumors that arose in most mouse cohorts were mainly MMs, although other neoplasms were also observed (Table 2).

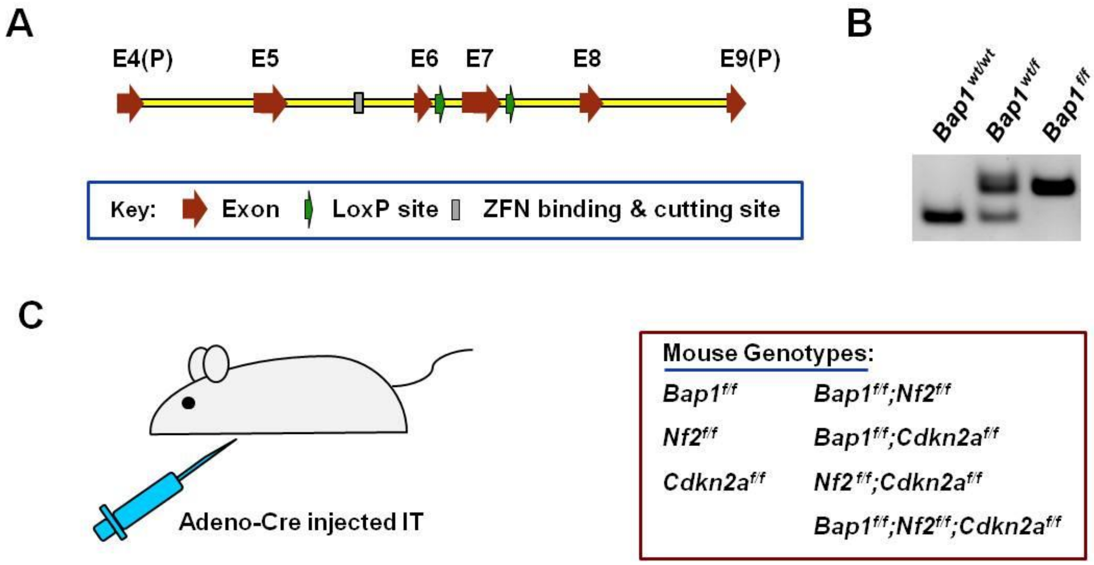

Figure 14. Generation of *Bap1* conditional knockout (CKO) mouse with zinc finger nuclease (ZFN) technology, and experimental schema used for crosses with other CKO mice. **(A)** Schematic drawing of *Bap1* loxP donor DNA sequence. Donor DNA contains region spanning part of exon 4, E4(P), to part of exon 9, E9(P). LoxP sites were inserted into introns 6 and 7. A pair of ZFNs was identified that binds to and cuts within a site in intron 5 of *Bap1* with high efficiency and specificity. A donor DNA construct was then designed that contained two loxP sites, one in intron 6 and one in intron 7, as shown, such that expression of Adeno-Cre in the mouse mesothelial cell lining the pleural cavity excises exon 7 of *Bap1*.**(B)** Genotyping of DNA from wild type (wt) mouse as well as heterozygous (wt/f) and homozygous (f/f) *Bap1* CKO mice. **(C)** Strategy used to homozygously excise *Bap1*, *Nf2*, and/or *Cdkn2a* via intrathoracic (IT) injection of Adeno-Cre virus in mice with the various genotypes shown.

Table 2. Summary of tumors observed in homozygous conditional knockout mice arising after intrathoracic (IT) injection of Adeno-Cre.

Genotype[a]	*Bap1*$^{f/f}$	*Bap1*$^{f/f}$; *Nf2*$^{f/f}$	*Bap1*$^{f/f}$; *Cdkn2a*$^{f/f}$	*Nf2*$^{f/f}$; *Cdkn2a*$^{f/f}$	*Bap1*$^{f/f}$;*Nf2*$^{f/f}$; *Cdkn2a*$^{f/f}$
No. mice injected	32	42	27	24	26
MM[b]	1 (3.1%)	7[c] (16.6%)	6 (22.2%)	15[d] (62.5%)	22 (84.6%)
Epithelioid	0	0	0	0	0
Mixed (Biphasic)	0	6	1	4	8
Sarcomatoid	1	1	5	11	14
Lymphoma	1	0	0	0	0
Adenocarcinoma	2	0	2	0	0
HCC / ICC	0	28[c,e]	0	2[d]	0
Hemangiocarcinoma	0	0	2	0	0
Other causes of death[f]	29	10	17	9	4

[a]In the other two single-gene CKO mouse cohorts, MM was observed in 0 of 12 *Cdkn2a*$^{f/f}$ mice and 2 of 15 *Nf2*$^{f/f}$ mice, frequencies similar to a previous report (63). [b]Abbreviations: HCC, hepatocellular carcinoma; ICC, intrahepatic cholangiocarcinoma; MM, malignant mesothelioma; [c]1 mouse had both MM and HCC, and 2 mice had MM as well as HCC and ICC; [d]1 mouse had both MM and ICC, and 1 mouse had MM and HCC; [e]14 of the 28 mice had both HCC and ICC; [f] mostly aged mice, with moribund animals often found to have plaques, bladder obstructions, or lymphoproliferative lesions.

A

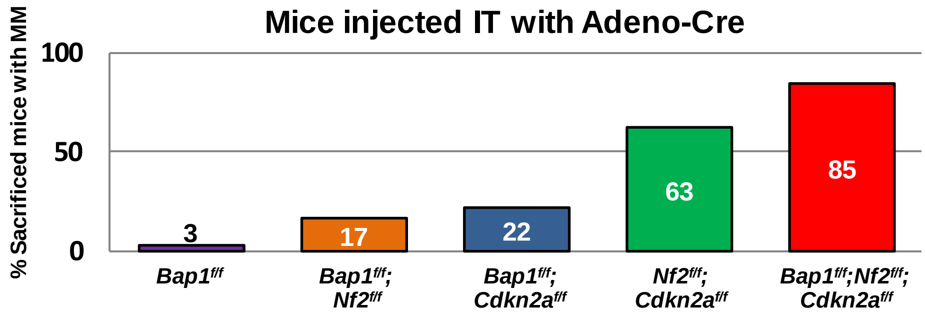

B

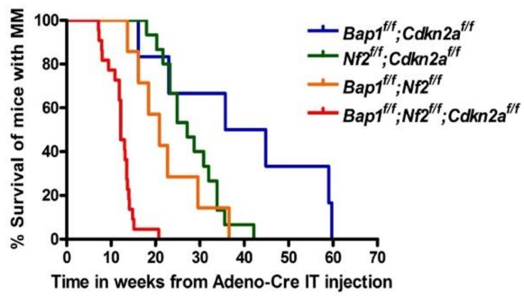

Genotype	% Mice with MM	Median Survival in Weeks
Bap1$^{f/f}$;Cdkn2a$^{f/f}$	6 / 27 (22%)	40
Bap1$^{f/f}$;Nf2$^{f/f}$	7 / 42 (17%)	21
Nf2$^{f/f}$;Cdkn2a$^{f/f}$	15 / 24 (63%)	27
Bap1$^{f/f}$;Nf2$^{f/f}$;Cdkn2a$^{f/f}$	22 / 26 (85%)	12

Figure 15. Incidence and survival of pleural MM in various mouse genotypes following IT injections with Adeno-Cre virus. (A) Incidence of MM in the various CKO mouse cohorts. **(B)** Kaplan-Meier curves depict survival of mice succumbing to MM arising after IT injections with Adeno-Cre. Note rapid development of MM in *Bap1;Nf2;Cdkn2a* triple knockout mice, with the median survival being only 12 weeks, which was significantly different (p<0.0001) from that of any of the other compound CKO mice. The survival differences between the other three double knockout combinations of CKO mice were not statistically significant.

In the cohorts of mice with homozygous knockout of a single gene only, few MMs were observed. Among 32 *Bap1*$^{f/f}$ CKO mice injected IT with Adeno-Cre, a single slow growing, well differentiated MM was observed in an animal 45 weeks after injection. Interestingly, this MM acquired loss of *Nf2* and p16Ink4a expression during tumor formation (Figure 16). MMs were observed in 2 of 15 *Nf2* $^{f/f}$ mice and 0 of 12 *Cdkn2a*$^{f/f}$ mice injected with Adeno-Cre, results comparable to those reported in an earlier study (63).

Among the IT-injected mice with homozygous inactivation of two genes, MMs were observed in 7 of 42 (16.6%) *Bap1;Nf2* CKO mice, 6 of 27 (22.2%) *Bap1;Cdkn2a* CKO mice, and 15 of 24 (62.5%) *Nf2;Cdkn2a* CKO mice. The highest incidence of MM (22 of 26, 84.6%) was observed in *Bap1;Nf2;Cdkn2a* "triple knockout" mice. A summary of MM incidence among *Bap1* CKO mice and mice with the various compound CKO genotypes is shown in Figure 14A.

With regard to histological subtype, notably no epithelioid MMs were observed in any of the mouse cohorts. Sarcomatoid MMs predominated in most cohorts, with the exception being *Bap1;Nf2* CKO mice, in which 6 of 7 MMs showed mixed (biphasic) histology.

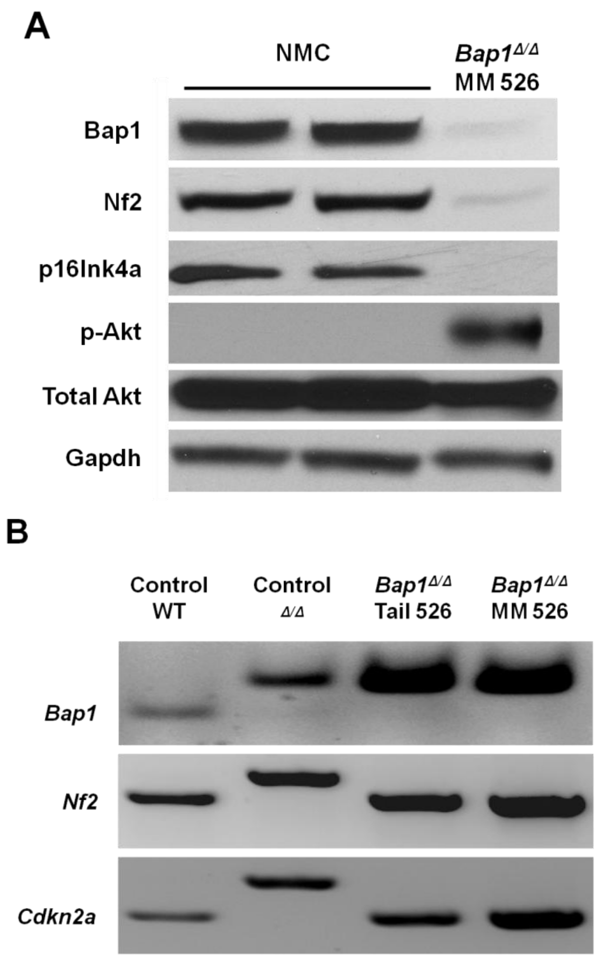

Figure 16. Characterization of MM from *Bap1*$^{f/f}$ mouse, which was detected 45 weeks after IT injection of Adeno-Cre virus. (A.) Immunoblot confirming loss of Bap1 expression in MM from *Bap1* conditional knockout mouse 526, with tumor showing greatly reduced or undetectable expression of Nf2 and p16Ink4a. **(B.)** Demonstration that loss of expression of Nf2 and p16Ink4a is acquired, not due to excision of floxed *Nf2* and *Cdkn2a* alleles. Control WT and control$^{\Delta/\Delta}$ lanes depict sizes of wild type and homozygously floxed *Bap1*, *Nf2*, and *Cdkn2a* alleles. DNA from *Bap1*$^{\Delta/\Delta}$ tail and matching MM from mouse 526 verify that *Bap1*, but not *Nf2* or *Cdkn2a*, has floxed alleles.

The MM latency varied between 21 and 40 weeks among the different compound double CKO mice. A markedly shorter MM latency, 12 weeks, was observed in *Bap1;Nf2;Cdkn2a* triple-CKO mice, a highly significant difference (log rank test, $p<0.0001$) from the 27 weeks observed for *Nf2;Cdkn2a* CKO mice or for any of the other compound double knockout mice. The MM survival differences between the three cohorts with different double knockout combinations were not statistically significant. Kaplan-Meier survival curves of IT-injected mice that developed MM are shown in Figure 15B. Additionally, MMs from *Bap1;Nf2;Cdkn2a* CKO mice were consistently high-grade, very invasive, and highly proliferative tumors (Figure 17A,B), whereas MM morphology was generally more variable and less hypercellular in the other mouse cohorts.

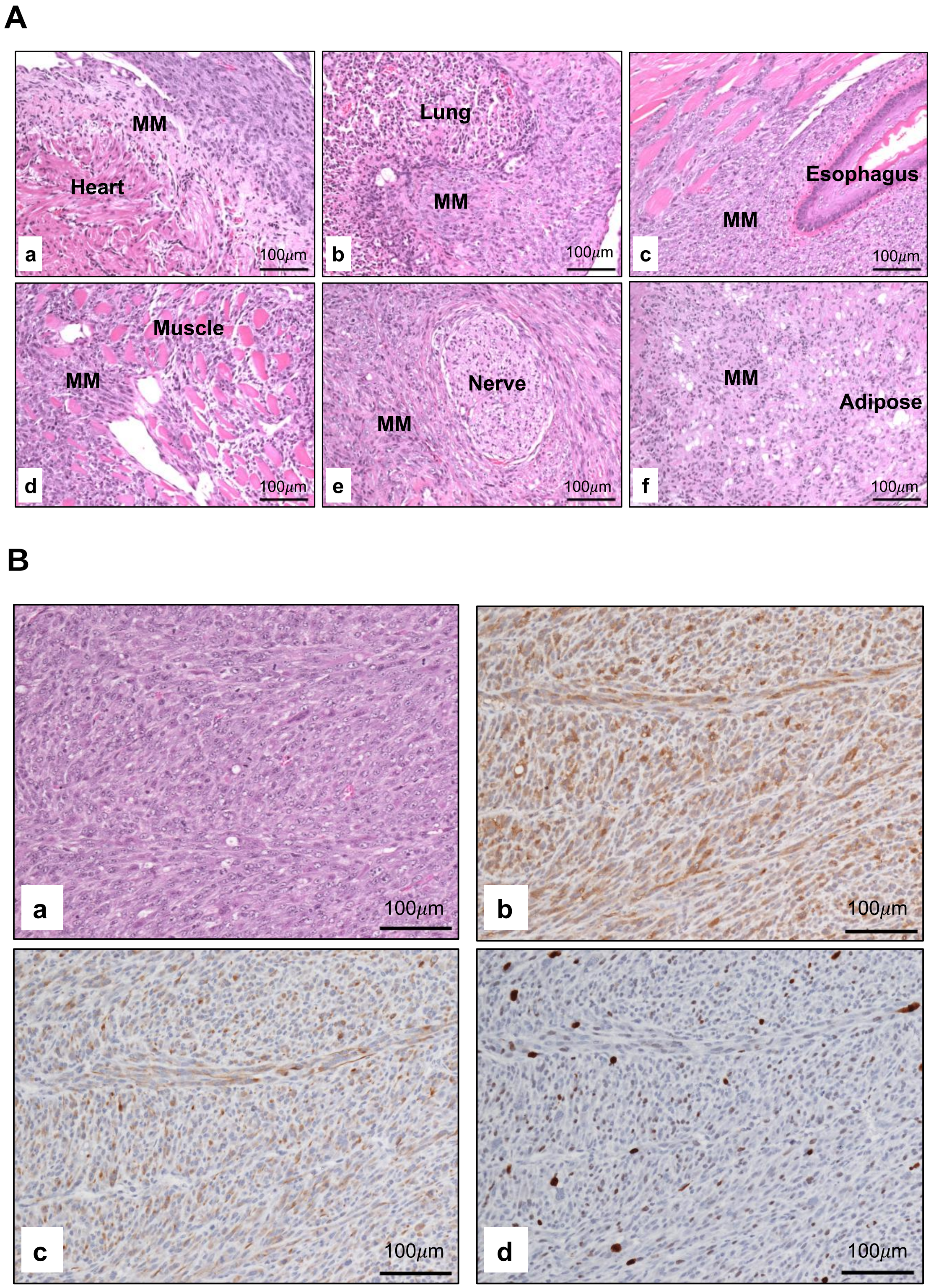
A
MM
Heart
a
100μm
Lung
MM
b
100μm
Esophagus
MM
c
100μm
Muscle
MM
d
100μm
Nerve
MM
e
100μm
MM
Adipose
f
100μm
B
a
100μm
b
100μm
c
100μm
d
100μm

Figure 17. Histopathological assessment of representative high-grade MMs from *Bap1;Nf2;Cdkn2a* CKO mice. (A) Histopathology of highly invasive, disseminated MM that arose in a *Bap1;Nf2;Cdkn2a* CKO mouse following IT injection of Adeno-Cre. Note MM invasion affecting multiple organs including the heart (a), lung (b), esophagus (c), skeletal muscle (d), nerve (e), and mediastinal adipose tissue (f). **(B)** Serial sections of a MM from a *Bap1;Nf2;Cdkn2a* CKO mouse showing H&E staining (a), and IHC for mesothelin (b), cytokeratin 8 marker TROMA-1 (c), and nuclear proliferation marker Ki-67 (d).

In addition to MMs, various other tumor types were also observed in mice injected IT with Adeno-Cre (Table 2). Among mice with homozygous inactivation of Bap1 alone in the thoracic cavity, 2 lung adenocarcinomas and 1 lymphoma were seen. The remaining mice died of other age-related diseases, including bladder obstructions or lymphoproliferative diseases. Among the compound CKO mice, most notable was the cohort with inactivation of both *Bap1* and *Nf2*, which showed a high incidence (28 of 42, 66.7%) of hepatocellular carcinoma (HCC) and intrahepatic cholangiocarcinoma (ICC) (Figure 18), with these tumors generally arising later than MMs in this cohort (median 35 weeks vs. 21 weeks, respectively). Altogether, 28 *Bap1;Nf2* CKO mice developed hepatic cancers, including 7 with HCC alone, 4 with ICC alone, 14 with both HCC and ICC, 1 with HCC and MM, and 2 with HCC, ICC, and MM.

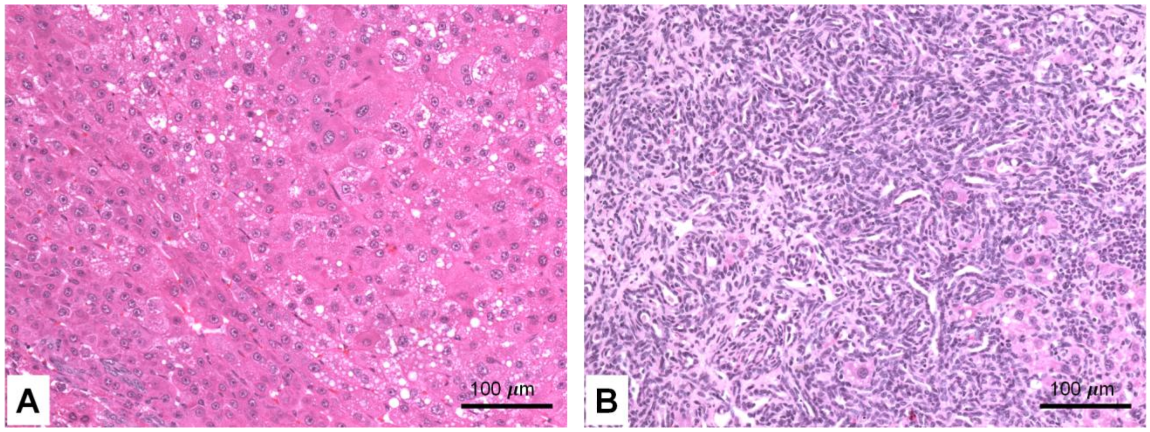

Figure 18. Representative H&E images. (A) Histopathology depicting a hepatocellular carcinoma and **(B)** an intrahepatic cholangiocarcinoma from two different Adeno-Cre-injected *Bap1*$^{f/f}$;*Nf2*$^{f/f}$ mice.

Since the triple-CKO cohort of mice had the shortest latency and most aggressive types of tumors comparing to the double CKO (*Nf2;Cdkn2a*), we wanted to further investigate the additive effect of *Bap1* loss to *Nf2;Cdkn2a* inactivtion. We decided to run a Western blot analysis to compare 6 tumor samples from *Nf2*$^{f/f}$*;Cdkn2a*$^{f/f}$ and from *Bap1*$^{f/f}$*;Nf2*$^{f/f}$*;Cdkn2a*$^{f/f}$ mice (Figure 19). As expected, we saw the deletion of *Nf2* and *Cdkn2a* (p16Ink4a and p19Arf) in all the groups, and *Bap1* in the triple-CKO group. However, we also noticed that out of 6 MM samples from Nf2;Cdkn2a mice, 4 lost the expression of *Bap1*. It is a very significant observation, as it can be speculated that spontaneous loss of Bap1 expression is necessary for tumor development. We also assessed the status of Akt in our tumors, because Akt activation occurs frequently in human and murine MMs. Akt activation was seen in all MMs examined, as indicated by expression of phosphorylated (active) Akt (Figure 19). This is notable because Akt activation plays a central role in oncogenesis due to its pro-survival role.

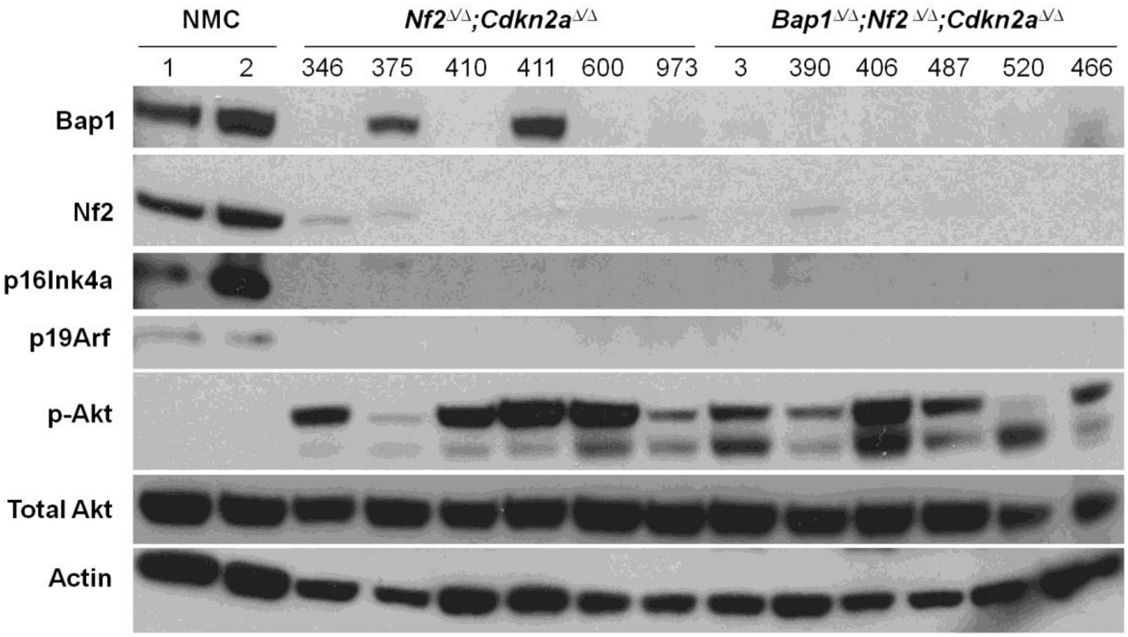

Figure 19. Western blot analysis of normal mesothelial cells (NMC) and MMs from *Nf2;Cdkn2a* and *Bap1;Nf2;Cdkn2a* CKO mice. Immunoblots confirm loss of expression of proteins encoded by conditionally knocked out genes *Bap1*, *Nf2* and *Cdkn2a* (p16Ink4a and p19Arf) in all tumors. Acquired loss of expression of Bap1 was also observed in 4 of 6 MMs from *Nf2;Cdkn2a* CKO mice. Phosphorylated Akt, indicative of Akt activation, is seen in all MMs.

To assess the cooperativity of Bap1, Nf2, and Cdkn2a losses *in vitro*, we next used a spheroid growth assay. Primary normal mesothelial cells were isolated from *Bap1*$^{f/f}$, *Nf2*$^{f/f}$, *Cdkn2a*$^{f/f}$, *Bap1*$^{f/f}$*;Nf2*$^{f/f}$, *Bap1*$^{f/f}$*;Cdkn2a*$^{f/f}$, *Nf2*$^{f/f}$*;Cdkn2a*$^{f/f}$, and *Bap1*$^{f/f}$*;Nf2*$^{f/f}$*;Cdkn2a*$^{f/f}$ mice. The mesothelial cells were then exposed to either control Adeno-CMV or Adeno-Cre virus for 1 h, seeded in non-adherent plate in serum-free stem cell medium (61), and photographed after 9 days. There was little or no evidence of spheroid formation in cultured WT mesothelial cells or mesothelial cells with Adeno-Cre-induced homozygous inactivation of one or various combinations of two tumor suppressor genes (Figure 20; data not shown for cells from *Nf2*$^{f/f}$, *Cdkn2a*$^{f/f}$, *Bap1*$^{f/f}$*;Nf2*$^{f/f}$ and *Bap1*$^{f/f}$*;Cdkn2a*$^{f/f}$ mice). In contrast, the Adeno-Cre-treated mesothelial cells from *Bap1*$^{f/f}$*;Nf2*$^{f/f}$*;Cdkn2a*$^{f/f}$ mice, i.e., with inactivation of all three of the putative MM driver genes, showed multiple large spheroids, indicative of stem cell features (Figure 20).

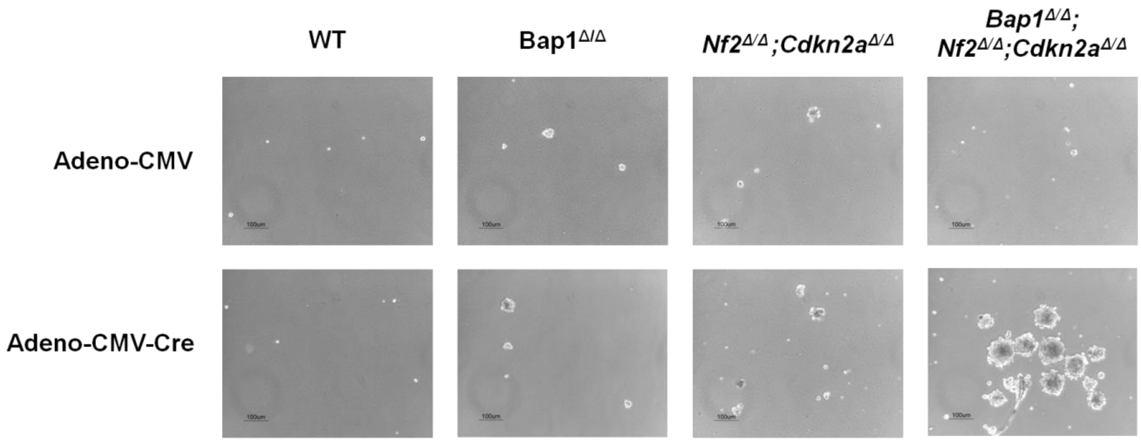

Figure 20. Spheroid assay on NMCs treated with Adeno-CMV or Adeno-Cre. Adeno-CMV-Cre virus-exposed normal mesothelial cells from *Bap1*$^{f/f}$*;Nf2*$^{f/f}$*;Cdkn2a*$^{f/f}$ mice (referred by $^{"\Delta/\Delta"}$) harbor more and much larger stem cell-like spheroids than do those from wild-type (WT), *Bap1*$^{f/f}$, and *Nf2*$^{f/f}$*;Cdkn2a*$^{f/f}$ mice. Equal numbers of mesothelial cells from mice with the various cited genotypes were seeded on non-adherent 6-well plates in stem cell media, and spheroids were photographed after 9 days.

Given the striking shift in MM latency between *Bap1;Nf2;Cdkn2a* CKO mice and *Nf2;Cdkn2a* CKO mice, as well as the consistently more aggressive nature of the MMs in triple-CKO mice, we performed RNA-seq analysis on MMs from these two cohorts to shed light on the contribution of *Bap1* inactivation in this experimental setting. Considering that Bap1 plays a role in chromatin remodeling and transcription regulation (33, 89, 90), and the fact that many of the top differentially expressed genes were significantly enriched for PRC2 targets based on a study by Sashida and colleagues (98). Among the top 390 differentially-expressed genes between MMs from triple-CKO and double-CKO, we found 138 PRC2 targets. Under the null hypothesis of no association between differential expression and PRC2 target classification, we would expect to see 48 PRC2 targets among the top 390. So the top 390 differentially-expressed genes are over-enriched 2.87 fold (p-value = 2 x 10-32, two-sided hypergeometric test). This analysis showed that the MMs from *Bap1;Nf2;Cdkn2a* CKO mice exhibit a set of significantly upregulated genes that are direct targets of PRC2. The RNA-seq analysis was performed on 6 MMs from *Bap1;Nf2;Cdkn2a* CKO mice versus 6 MMs from *Nf2;Cdkn2a* CKO mice. However, we subsequently determined that 4 of the 6 MMs from *Nf2;Cdkn2a* CKO mice acquired loss of Bap1 expression. Reevaluation of the RNA-seq data, comparing only the 2 MMs from *Nf2;Cdkn2a* CKO mice that retained expression of Bap1 versus the 6 MMs from the *Bap1;Nf2;Cdkn2a* CKO showed even higher statistical significance for differences in the expression of PRC2-upregulated genes. A heatmap of genes upregulated in MMs from these 2 *Bap1;Nf2;Cdkn2a* CKO mice compared to those from *Nf2;Cdkn2a* CKO mice is shown in Figure 21. Validation by RT-PCR analysis of two representative upregulated genes, *Mmp9* and *Gli2*, and an example of a downregulated gene, *Diras1*, is depicted in Figure 22.

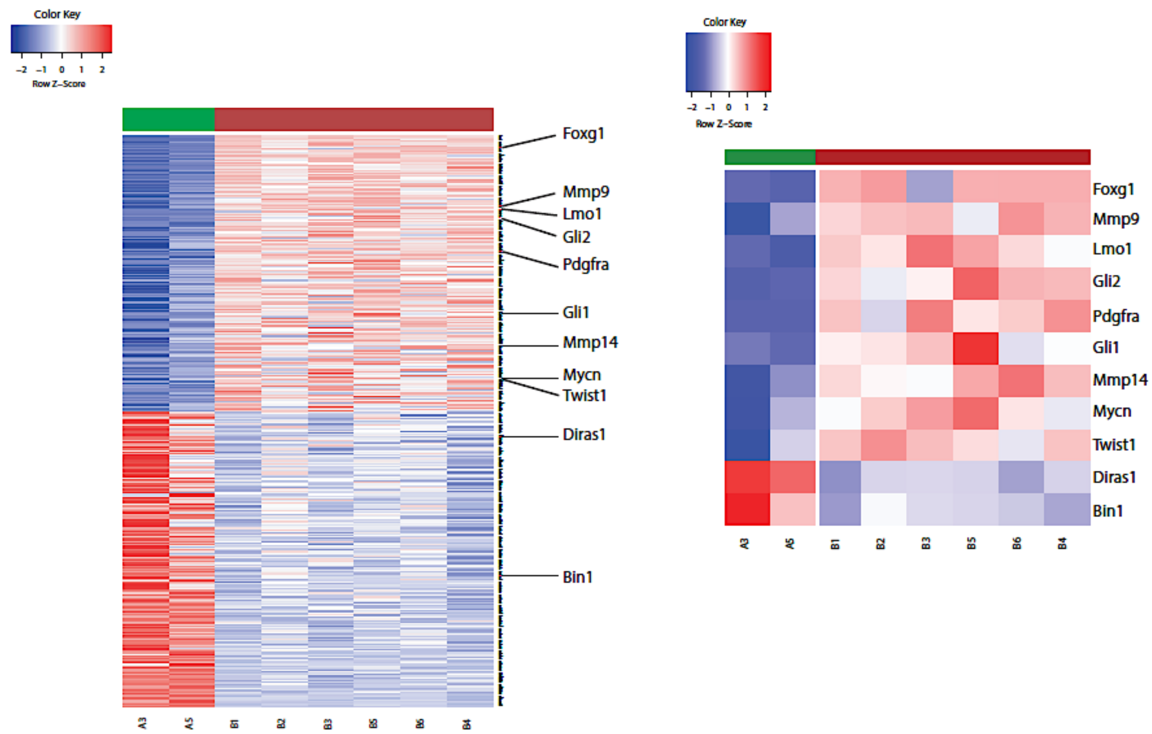

Figure 21. Heatmap of differentially expressed genes in MMs from triple vs double-CKO mice. *Left*, Heatmap depicting differentially expressed genes in same six MMs (B1-B6) from *Bap1;Nf2;Cdkn2a* CKO mice versus two MMs, 375 (A3) and 411 (A5) from *Nf2;Cdkn2a* CKO mice that retained expression of Bap1 shown in Figure 19. Heatmap represents top 390 PRC2 target genes that are differentially expressed with at least 2-fold change and false discovery rate of < 1%, according to DESeq2 analysis. Genes are ranked by significance, with the most significantly up-regulated PRC2 target at the top, and the most significantly down-regulated target at the bottom. *Right*, Magnified view of differentially expressed cancer-related PRC2 target genes in MMs from triple-CKO mice, including upregulated expression of genes implicated in oncogenesis or pro-invasion/metastasis (*Gli2*, *Mmp9*, *Foxg1*, *Lmo1*, *Pdgfra*, *Gli1*, *Mmp14*, *Mycn*, *Twist1*) and downregulation of putative tumor suppressor genes (*Bin1* and *Diras1*).

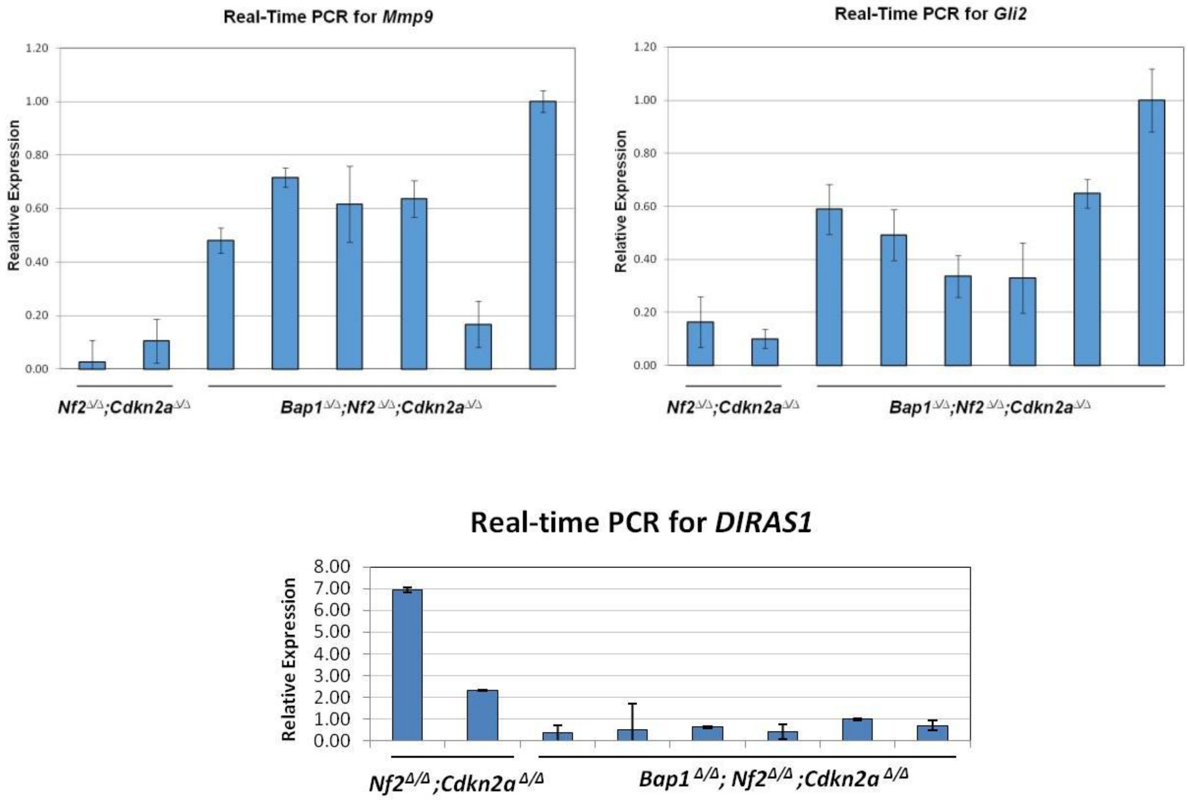

Figure 22. RT-PCR validation of some of the upregulated and downregulated genes found in MMs from *Bap1;Nf2;Cdkn2a* CKO mice. Validation of two upregulated PCR2 target genes, *Mmp9* and *Gli2*, and one downregulated gene *Diras1* in MMs from RNA-seq comparing *Nf2;Cdkn2a* and *Bap1;Nf2;Cdkn2a* CKO mice.

5.3 Discussion

In this investigation, we aimed to induce mesothelial cell-specific homozygous deletions of three tumor suppressor genes (*Bap1*, *Nf2*, and *Cdkn2a*) that have been implicated as major drivers of human MM pathogenesis. While the majority of malignant tumors observed were MMs, additional tumor types also resulted, possibly due to infection of other intrathoracic tissues or by passage of virus via blood vessels to the liver. Notably, HCCs and ICCs were very common later in life in *Bap1;Nf2* CKO mice but were observed in only two CKO mice with any of the other genotypes. Notably, liver-specific deletion of *Nf2* in the developing or adult mouse has been reported to promote a marked, progressive expansion of progenitor cells throughout the liver, with all surviving mice eventually developing both HCC and ICC (99). Interestingly, HCC and ICC were not seen in our *Bap1;Nf2;Cdkn2a* CKO cohort, perhaps because these mice succumbed to MM before hepatic tumors could be detected.

The Kaplan-Meier curves (Figure 15B) indicate that homozygous inactivation of different combinations of *Bap1*, *Nf2*, and *Cdkn2a* affect MM latency differently, with losses of all three genes profoundly accelerating tumor development. Specifically, *Bap1;Nf2;Cdkn2a* CKO mice bearing MM showed much shorter tumor latency than mice in any compound double CKO cohort. Moreover, MMs from triple knockout mice consistently appeared to be high grade, invasive, hypercellular tumors whereas MMs from mice with other genotypes were more variable phenotypically. All MMs observed in our study were sarcomatoid or biphasic, similar to what was reported by Jongsma *et al.* for mice with homozygously floxed conditional compound alleles that were injected IT with Adeno-Cre (63). For example, in their *Nf2;Cdkn2a* CKO mice, 31 MMs were sarcomatoid, 13 had mixed histology, and only 1 was epithelioid (63). It has been speculated that the predominant epithelioid histology seen in human MMs, as opposed to mice, may be the result of species-specific differences or route of induction, including the long latency and exposure to asbestos in the human disease counterpart (63). It is also likely that the particular mouse strain can influence the phenotype observed. For example, in our previous asbestos carcinogenesis work, *Nf2*$^{+/-}$ mice in a 129Sv/Jae genetic background injected IP with asbestos developed roughly equivalent percentages of epithelioid, mixed, and sarcomatoid MMs (60), whereas asbestos-injected *Nf2*$^{+/-}$ mice in a FVB/N background mostly developed sarcomatoid MMs (61).

Heterozygous knockout (+/-) and heterozygous mutant (+/mut) *Bap1* mice injected IP with asbestos exhibit a highly significant increase in the incidence of MMs as compared with asbestos-injected WT littermates, providing in vivo evidence that Bap1 inactivation plays an important role in MM tumorigenesis (48, 94). Similarly, heterozygous Nf2 mice injected with asbestos develop MM with a markedly shorter latency than asbestos-treated WT littermates (60, 88). Heterozygous *Cdkn2a* knockout mice treated with asbestos also develop MM at an accelerated rate compared to asbestos-treated WT mice (80). Furthermore, asbestos-exposed compound *Nf2*$^{+/-}$*;Cdkn2a*$^{+/-}$ mice show further acceleration of asbestos-induced MM and increased presence of cancer stem cells (61). These carcinogenesis studies, in combination with the gene knockout model studies reported here strongly support a working hypothesis that *Bap1*, *Nf2*, and *Cdkn2a* are key drivers of MM pathogenesis and that the collective losses of these three tumor suppressors is sufficient to drive rapidly disseminated, lethal disease, similar to the poor clinical outcome of human pleural MM.

In one study, CKO mice in which only one of these tumor suppressor genes was homozygously deleted developed MM at a low rate, with spontaneous MM-like tumors being identified in 5 of 30 *Nf2*$^{f/f}$ mice and 0/17 *Cdkn2a*$^{f/f}$ mice injected IT with Adeno-Cre (63), supporting the notion that MM development requires the combined involvement of multiple tumor suppressor gene alterations (100). Similarly, in our Bap1 CKO cohort, MM was seen in only 1 of 32 mice. The fact that MM arises spontaneously in a considerable number of CKO mice made deficient for both alleles of two or more tumor suppressor genes, provides compelling support for the role of genetics in MM causation and the need for accumulated genetic and epigenetic alterations for tumor formation (78). As an example, even in the one *Bap1* CKO mice that did develop MM, it is intriguing that there was acquired loss of Nf2 and p16Ink4a expression during tumorigenesis.

The *in vivo* findings presented here with CKO mice closely mimic those found in the human disease counterpart, in which losses of *BAP1*, *CDKN2A*, and *NF2* are frequently seen in various combinations (18, 101). Their frequent occurrence in MM and their individual roles both in various cancer predisposition syndromes and in tumor progression strongly suggest that they are key drivers in MM pathogenesis. Our initial work on BAP1 provided the first demonstration that genetics influences the risk of MM, a cancer linked to mineral fiber carcinogenesis (19). However, there is evidence that germline mutations of CDKN2A and NF2 may also modulate susceptibility to mineral fiber carcinogens. For example, Betti *et al.* recently described a family in which both

MM and cutaneous melanoma cases were found to have a deleterious germline missense mutation in the *CDKN2A* gene, and the family member with MM was determined to be of the low exposure category (102). Additionally, germline mutations in *NF2* have been reported in patients who developed MM. In one case, an individual with neurofibromatosis, type II (NF2) developed peritoneal MM at the relatively young age of 40 (103). Comparative genomic hybridization analysis and IHC staining of the MM tissue revealed loss of the *NF2* gene and protein product, respectively. A second NF2 patient developed a pleural MM at age 75 (104). Both patients were reported to have occupational asbestos exposure.

Our observation that CKO mice with losses of all three critical tumor suppressor genes had much higher MM penetrance and markedly shorter survival than mice with loss of one or two of these genes fits with the model put forward by Vogelstein and Kinzler (105). They proposed that in solid tumors of adults, alterations in a minimum of three mutated driver genes are needed for a cell to evolve into an invasive (malignant) tumor. In our CKO models, loss of one or two tumor suppressors was not consistently sufficient to result in a high incidence of MMs. The exception was the *Nf2;Cdkn2a* CKO model, but even in these mice tumor latency was much longer than in the triple-CKO mouse model. One possibility is that in *Nf2;Cdkn2a* CKO mice, significantly more time is needed in order to accumulate additional genetic and epigenetic alterations sufficient to result in an invasive cancer. In fact, as shown in Figure 19B, 4 of 6 MMs tested from *Nf2;Cdkn2a* CKO mice acquired loss of *Bap1* expression during disease progression. In human MM, tumors are characterized by the presence of multiple somatic genetic and cell signaling alterations. The fact that large spheroids can be reproducibly formed by

Adeno-Cre-induced excision of *Bap1*, *Cdkn2a*, and *Nf2 in vitro*, but not by the excision of only one or two of these genes, also provides experimental support for cooperativity between the inactivation of these three tumor suppressor genes in MM tumorigenesis.

Our RNA-seq analysis of MMs from *Nf2;Cdkn2a* CKO mice that retained expression of *Bap1* expression versus MMs from *Bap1;Nf2;Cdkn2a* CKO mice showed a highly significant statistical difference with regard to the over-expression of some genes directly regulated by PRC2. Some of the upregulated target genes in MMs from the *Bap1;Nf2;Cdkn2a* CKO mice include cancer-related genes such as *Gli2*, which has been reported to foster the proliferation and migration of cancer cells (Zhu, 2018), and Mmp9, which encodes a well-documented promoter of tumor cell invasion (Figure 22), yielding potential mechanisms explaining progression and invasion of our *Bap1*-deficient MMs. A number of other upregulated genes in MMs from *Bap1;Nf2;Cdkn2a* CKO mice have been implicated as oncogenes or pro-invasion/metastasis genes (i.e., *Foxg1, Lmo1, Pdgfra, Gli1, Mmp14, Mycn, Twist1*), whereas the putative tumor suppressor genes *Bin1* and *Diras1* were downregulated (Figure 21). In a study on *Bap1*-deficient myeloid progenitor cells, the majority of differentially expressed genes observed had reduced expression, whereas ~30% of genes were upregulated (35). Similarly, among 1,425 genes identified as differentially expressed with fold-change of at least 2 and false discovery rate <1%, significantly less genes (628, 44%) were upregulated than downregulated (p-value = 8.4 x 10-6, exact binomial test) in MMs from *Bap1*-deficient triple-CKO mice versus Bap1-expressing MMs from double CKO mice. One possible explanation why we observed a highly significant over-representation of upregulated PRC2 target genes may be that the Bap1-containing holo-complex is composed of many subunits, and the exact composition, when bound to positive- or negative-acting regulatory promoter elements, determines the overall influence repression or activation on that target gene. It is also noteworthy that PRC2 subunits such as Ezh2 have been shown to have context-dependent oncogenic or tumor suppressive roles in different cancers (106). LaFave *et al.* demonstrated that BAP1 inactivation leads to EZH2-dependent transformation (35). Although their report did not include RNA-seq analysis on human MM tumors for comparison with our murine findings, they demonstrated that BAP1-deficient MM cells are sensitive to EZH2 pharmacologic inhibition, and our findings add support to their conclusion that such an approach may have clinical efficacy.

Collectively, $Bap1^{f/f};Nf2^{f/f};Cdkn2a^{f/f}$ mice injected IT with Adeno-Cre appear to be useful for modeling an aggressive form of MM. The MMs develop at a high incidence after a short latency period. Moreover, our finding that loss of Bap1 contributes to MM pathogenesis, in part, via loss of PRC2-mediated gene repression of certain oncogenic target genes, suggests a potential avenue for therapeutic intervention that may be rapidly tested in this CKO model.

CHAPTER 6

6 BAP1 INACTIVATION IN PERITONEAL MESOTHELIOMA

6.1 Introduction

Malignant Peritoneal Mesothelioma (MPeM) is confined to the peritoneal cavity (Figure 23) and is less common and has a better prognosis than malignant pleural mesothelioma (MPM). Of all the mesothelioma cases, 10-30% originate from the peritoneum (107). Miller and Wynn reported the first case of MPeM in 1908, describing a 32-year-old male with abdominal pain and ascitic fluid (108). MPeM is not infiltrative but spreads predominantly within the surface of the peritoneum. Asbestos inhalation is linked to MPeM causation in only 33-50% of cases, which is significantly lower than the causal association in MPM (>80%) (109). The survival rate of approximately 50-60 months is longer than in MPM, which is ~ 9-12 months even with chemotherapy (110). Frequently, MPeM is discovered incidentally during surgery or diagnostic imaging (111). Morphologically, as observed in MPM, there are three main subtypes of MPeM: epithelioid, sarcomatoid and/or biphasic subtype. Tandon *et al.* reported the most sensitive immunohistochemical markers for diagnosis MPeM are calretinin (100%), WT1 (94%) and CK5/6 (89%) (91). However, up until recent years there was a problem of not being able to identify malignancy of the cells: none of the markers listed above were considered 100% specific and the malignant character of the cells present would not always be obvious. Consequently, tissue biopsies were necessary to provide evidence of invasive growth (111). A newly introduced method of using immunohistochemical analysis of BAP1 helped in this predicament. Loss of BAP1 expression supports a diagnosis of malignancy, and makes a distinction between MPeM and hyperplasia (91). Therefore, young patients or patients with relevant family history should consider testing for germline *BAP1* mutations.

The gold standard of treatment for MPeM has been cytoreductive surgery (CRS), which potentially delays spread of the tumor, especially if combined with chemotherapy (112). In addition, hypothermic intraperitoneal chemotherapy (HIPEC) delivered during surgery, and normothermic early postoperative chemotherapy (EPIC) that is delivered post CRS are therapeutic options. Sequential chemotherapy (SIC) can be delivered systemically or intraperitoneally and is administered in the postoperative period (113). From a molecular therapy perspective, ALK (anaplastic lymphoma kinase) inhibitor treatments were proposed due to recently reported ALK-rearrangements in a small group of patients (3%) (114). Also, it has been shown that bevacizumab, a humanized antibody against VEGF, in combination with cisplatin and pemetrexed, drastically increased overall survival in a phase III trial (115). Currently, immune checkpoint inhibitors such as anti-CTLA4 and anti-PD1 antibodies are under investigation as possible treatments for MPeM (116, 117).

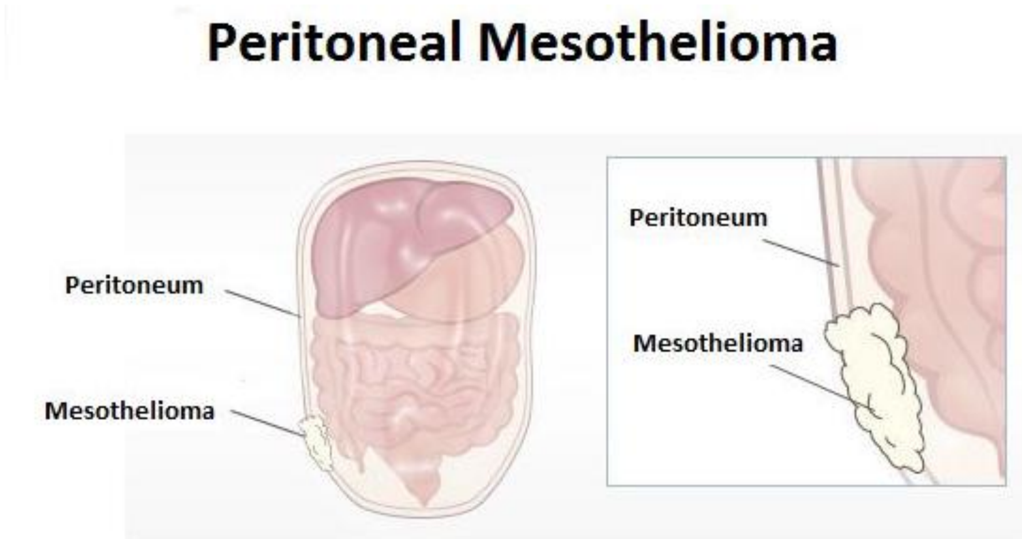

Figure 23. Diagram of the sites of the development of the peritoneal malignant mesothelioma (118). Mesothelioma develops on the peritoneum, a serous membrane forming the lining of the abdominal cavity, composed of a layer of mesothelium and supported by a layer of connective tissue that encapsulates the intra-abdominal organs.

GEM models of disease and cancer are very important tools to understand how cancers develop, as well as providing important preclinical models to test novel therapeutics. Our laboratory and others have used GEM models of asbestos-induced MPeM to provide experimental evidence in support of the critical role of certain TSGs in mesothelioma pathogenesis. However, few conditional GEM models that do not use asbestos but instead adenovirus expressing Cre recombinase to excise TSGs have been reported (63, 65). Since asbestos exposure is not the primary cause of MPeM, it is especially important to have such CKO mouse models mimicking genetic mutations that occur in human patients. Such models permit investigations on mechanisms of tumor development and provide insights into possible MPeM treatments.

As our previously described study (chapter 5) shed light on the development of MPM with various combinations of deletions occurring in human mesothelioma, we were curious to investigate whether a similar phenotype occurs in a mouse model of MPeM. Previously, Guo *et al.* injected Adeno-Cre virus intraperitoneally (IP) or in the bladder of mice with conditional mutants of *Tp53* and/or *Tsc1*, and observed a short latency in MPeM (64). Sementino *et al.* also IP-injected $Pten^{f/f};p53^{f/f}$ mice and observed MPeM development at a much shorter latency and higher incidence when compared to IT-injected littermates. Hence, we hypothesized that all the groups ($Bap1^{f/f}$, $Bap1^{f/f};Nf2^{f/f}$, $Bap1^{f/f};Cdkn2a^{f/f}$, and $Bap1^{f/f};Nf2^{f/f};Cdkn2a^{f/f}$) previously analyzed in IT-injected GEM models will have a shorter tumor latency and higher incidence in IP-injected mice, and based on the data described in chapter 5, the triple-CKO arm would have the fastest tumorigenesis rate.

6.2 Results

As described in chapter 5, we have created mouse models with CKO of different combinations of TSGs. Four different arms of GEM mice were injected IP with Adeno-Cre: 1) *Bap1*$^{f/f}$, 2) *Bap1*$^{f/f}$*;Nf2* $^{f/f}$, 3) *Bap1*$^{f/f}$*;Cdkn2a* $^{f/f}$, and 4) *Bap1*$^{f/f}$*;Nf2*$^{f/f}$*;Cdkn2a*$^{f/f}$ mice (Figure 24).

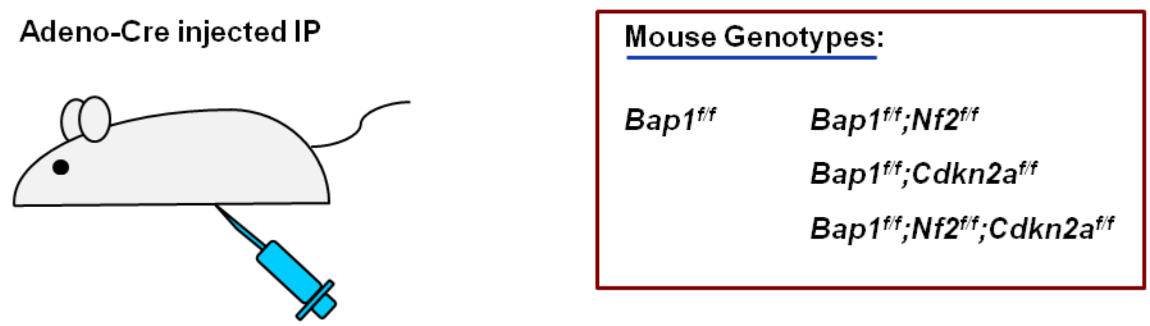

Figure 24. Diagram of the Adeno-Cre IP injection mouse experiment setup. *Left*, Mice were injected intraperitoneally (IP) with Adeno-Cre. *Right*, genotypes of the mice used in this experiment.

Interestingly, all groups of mice injected exhibited higher incidence of MMs than IT-injected animals of the same genotypes tested previously (Figure 25A, Chapter 5). Surprisingly, a high incidence (25/34, 74%) of MPeMs was observed even in mice with CKO of *Bap1* alone. In the other cohorts, 20/24 (83%) of *Bap1*$^{f/f}$;*Cdkn2a*$^{f/f}$ mice, 19/24 (79%) of *Bap1*$^{f/f}$;*Nf2*$^{f/f}$, and 33/33 (100%) of the mice of the triple-CKO arm succumbed to MPeM (Figure 25B, and Table3). Despite a similar high incidence among all the groups, the median survivals differed statistically significantly (log rank test, $p<0.0001$ and $p<0.01$) between the various genotypes of mice tested. The range varied from a median survival of 9 weeks in the triple-CKO group to as long as 34 weeks in the *Bap1*$^{f/f}$, single-gene group, with a p- value of < 0.0001. Kaplan-Meier survival curves are shown along with incidence rates in Figure 25 B.

The majority of tumors that developed in IP-injected mice were MPeMs with the following exceptions: 1) some adenomas and hepatocellular carcinomas were in IP-injected *Bap1*$^{f/f}$ and *Bap1*$^{f/f}$;*Nf2*$^{f/f}$ mice, and 2) granulomas, kidney hydronephrosis, plaques and hepatocarcinoma were observed in IP-injected *Bap1*$^{f/f}$;*Cdkn2a*$^{f/f}$ mice (Table 3).

A

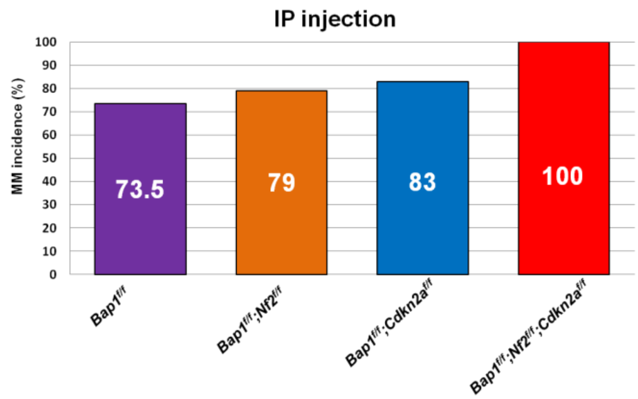

B

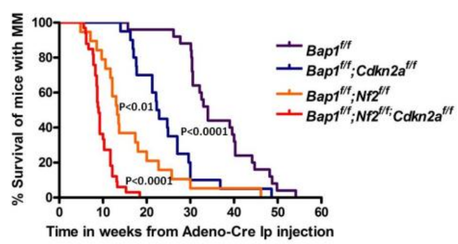

Genotype	% Incidence	Median survival of mice with MM (weeks)
Bap1$^{f/f}$	25/34 (74%)	34
Bap1$^{f/f}$;Cdkn2a$^{f/f}$	20/24 (83%)	23
Bap1$^{f/f}$;Nf2$^{f/f}$	19/24 (79%)	13
Bap1$^{f/f}$;Nf2$^{f/f}$; Cdkn2a$^{f/f}$	33/33 (100%)	9

Figure 25. Incidence and survival of peritoneal malignant mesothelioma (MPeM) in various mouse genotypes following IP injections with Adeno-Cre virus. (A) Incidence of MPeM in the CKO mouse cohorts. **(B)** Kaplan-Meier curves depict survival of mice succumbing to MPeM after IP injections with Adeno-Cre. Note rapid development of MPeM in triple-CKO mice, with median survival being only 9 weeks. The survival differences between each of the cohorts is significant ($p<0.001$ and $p<0.01$).

Table 3. Summary of tumors observed in homozygous conditional knockout (CKO) mice arising after intraperitoneal (IP) injection of Adeno-Cre.

Genotype	*Bap1*	*Bap1;Nf2*	*Bap1;Cdkn2a*	*Bap1;Nf2;Cdkn2a*
No. of mice injected	34	24	24	33
MPeM	25 (74%)	19 (79%)	20 (83%)	33 (100%)
Adenocarcinoma	2[a]	0	0	0
HCC/ICC	1[b]	3[c]	1	0
Other causes of death	9	2	3	0

Abbreviations: HCC, hepatocellular carcinoma; ICC, intrahepatic cholangiocarcinoma; MPeM, malignant peritoneal mesothelioma; a, 1 mouse had both MPeM and adenocarcinoma; b, 1 mouse had both MPeM as well as HCC; c, all three mice had both HCC and ICC.

As it is shown in the Kaplan-Meier curve in Figure 25B, the triple-CKO mice had the shortest tumor latency (9 weeks) and the highest tumor incidence (100%). To further investigate this impressive difference between the triple-CKO mice and the other genotypes, tumor cell proliferation was analyzed in MPeMs from *Bap1*$^{f/f}$ mice or MPeMs from the triple-CKO mice using IHC Ki67 staining. We randomly picked 10 MPeMs from each group and evaluated the percentage of Ki67–positive nuclei in tumor cells making up each MPeM using IHC analysis. Even though standard deviation is high within each group, the triple-knockout CKO MPeM cells have 3-fold more positive nuclei than MPeMs from *Bap1*$^{f/f}$ mice (Figure 26).

Notably, upon dissection of CKO animals, we observed that most of the mice regardless of the genotype exhibited fusion of all internal organs of the abdomen (Figure 27). The National Institute of Health estimates that ~93% of abdominal surgeries lead to adhesions (119). Adhesions develop due to an insult that results in hypoxia and reactive oxygen species damage that in turn promotes inflammation and activation of a coagulation cascade, which results in fibrin bridges between adjacent surfaces (120). Using lineage tracing, Tsai *et al.* demonstrated that a subset of mesothelial cells could be a cell of origin for adhesions in mice and humans (121). From our observations, we see that even *Bap1*$^{f/f}$ mice injected IP with Adeno-Cre developed such peritoneal adhesions, while injections with Adeno-Lacz did not (data not shown). Other investigators, who injected mice with Adeno-Cre IP did not report adhesions in their mice (64, 65). Therefore, we speculate that it is the genetic inactivation of specific TSGs that causes fusion of the peritoneum to the organs and not the virus itself. Our conditional IP GEM models of MPeM described here could also be useful in studies of peritoneal adhesions, which frequently occur in patients post abdominal surgery.

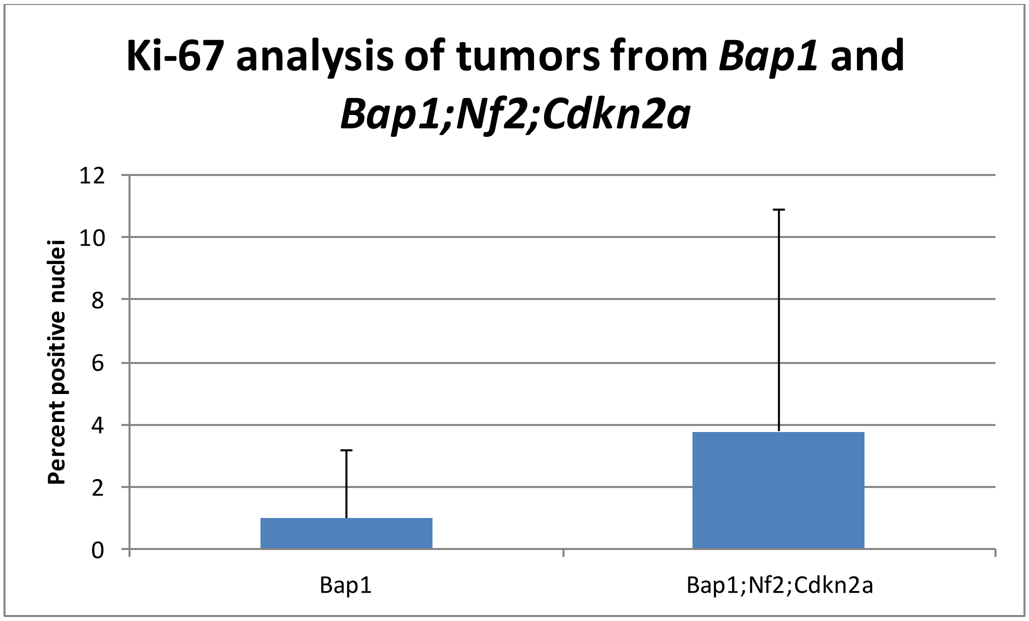

Figure 26. Ki-67 analysis of mesotheliomas from *Bap1* CKO mice vs *Bap1;Nf2;Cdkn2a* CKO mice. Ki-67 staining was performed to analyze the tumor proliferation rate from 10 *Bap1*$^{f/f}$ versus 10 *Bap1*$^{f/f}$;*Nf2*$^{f/}$;*Cdkn2a*$^{f/f}$ triple knockout tumor samples. The percent of positive nuclei stained for Ki-67 was measured and plotted on the graph for each group. Even though the standard deviation is high within each group, tumors from the triple knockout positive nuclei had 3-fold more than those from the *Bap1* CKO mouse group.

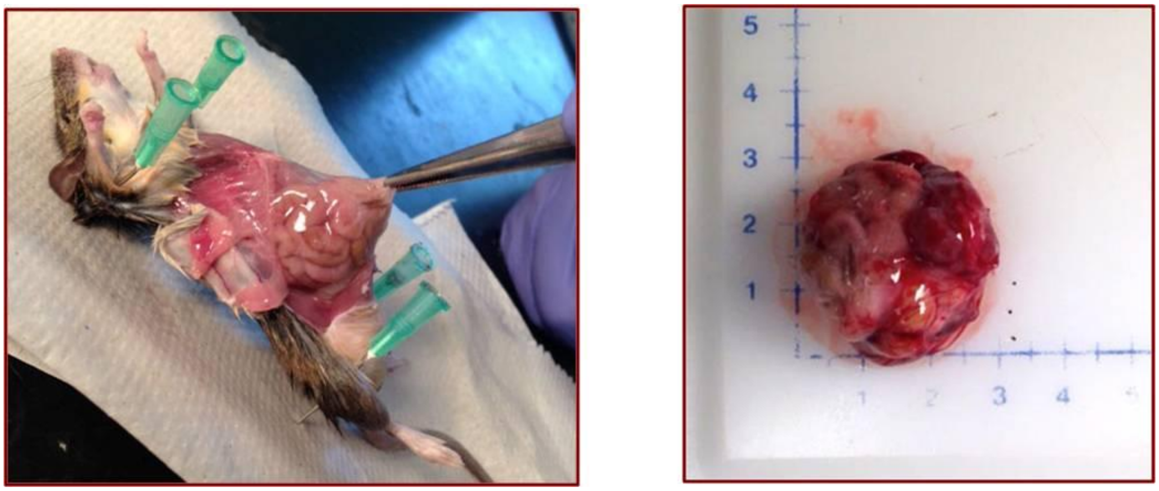

Figure 27. Illustration of peritoneal adhesion and organ fusion in a *Bap1$^{f/f}$;Nf2$^{f/f}$* mouse weeks after injecting IP with Adeno-Cre virus. *Left*, the peritoneal/mesothelial sac with all the organs attached to it. *Right*, representative fused organs dissected out of the abdomen of the mouse.

Since the difference in median survival was so high between *Bap1*$^{f/f}$ alone (34 weeks) and the triple-CKO mice (9 weeks), and the triple-CKO seemed to develop MPeMs more aggressively, we wanted to look into the genetic and pathway differences between the two groups. RNA-seq analysis was conducted on 5 MPeMs tumors from *Bap1* CKO versus 5 tumors from triple-CKO mice versus normal mesothelial cells as a control. Mesothelial markers of the 5 tumors from each group were confirmed via RT-PCR (Figure 30). Notably, when comparing RNA-seq data from normal mesothelial cells to MMs from *Bap1* CKO group, there was an upregulation of the Notch1, Hedgehog and Wnt signaling pathways and downregulation of apoptosis and necrosis pathways. When comparing tumor samples from *Bap1* CKO mice versus triple-CKO mice, there was upregulation in cMET, Pak3 and cell cycle pathways. Additionally, a heatmap of the top 50 most differentially expressed genes was generated and depicted in a Figure 28. Among the upregulated genes were vascular endothelial growth factor (*Vegfd*) and *Pak3* - genes that participate in pathways responsible for angiogenesis, endothelial cell growth, reorganization of actin cytoskeleton, cell motility and anchorage-independent growth (122),(123). Perhaps, these genes could be the drivers of the aggressive and angiogenic phenotype in the triple-CKO tumors (Figure 29). Western blot analysis was performed on tumors from each genotype (*Bap1*$^{f/f}$, *Bap1*$^{f/f}$*;Nf2*$^{f/f}$, *Bap1*$^{f/f}$*;Cdkn2a*$^{f/f}$, and *Bap1*$^{f/f}$*;Nf2*$^{f/f}$*;Cdkn2a*$^{f/f}$) (Figure 31). An interesting phenomenon was observed. Expression of the Nf2 protein was drastically decreased or completely absent in tumors from *Bap1*$^{f/f}$ alone group and *Bap1*$^{f/f}$*;Cdkn2a*$^{f/f}$. Expression of p16Ink4a (encoded by Cdkn2a) protein was decreased in *Bap1*$^{f/f}$ alone samples, and completely lost in *Bap1*$^{f/f}$*;Nf2*$^{f/f}$ tumors. Similar results were described in chapter 5 for MPMs.

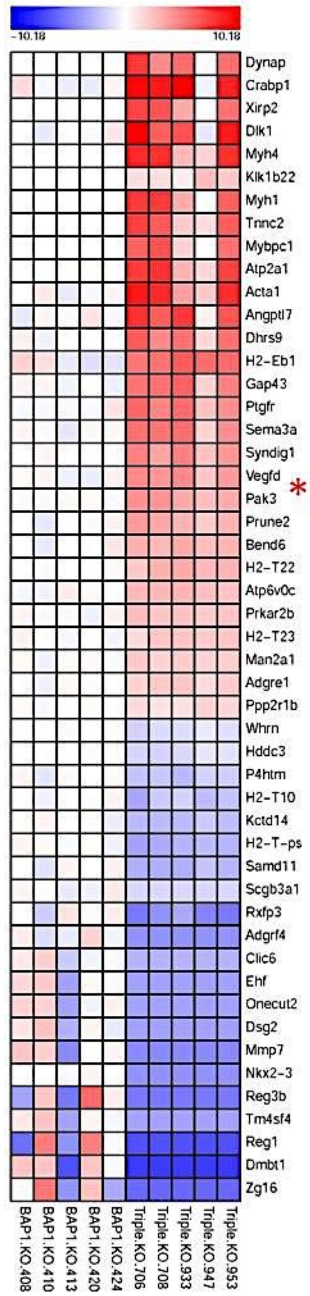

Figure 28. Heatmap of top 50 differentially expressed genes in 5 *Bap1*$^{\Delta/\Delta}$ vs 5 *Bap1*$^{\Delta/\Delta}$;*Nf2*$^{\Delta/\Delta}$;*Cdkn2a*$^{\Delta/\Delta}$ tumors. Included among the upregulated genes are *Vegfd* and *Pak3* marked by an asterisk.

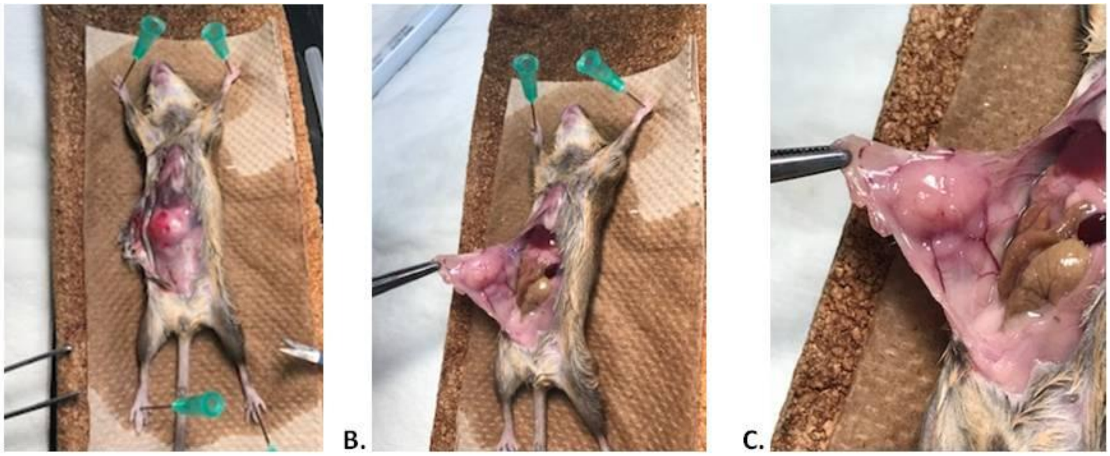

A. B. C.

Figure 29. Photographs of an IP-injected mouse. (A) The mouse is at the initial stage of dissection: the skin is removed around the tumor area. **(B)** Tumor is clearly developed within the peritoneal membrane. **(C)** A magnified illustration of the tumor mass exhibiting clear blood vessels growth.

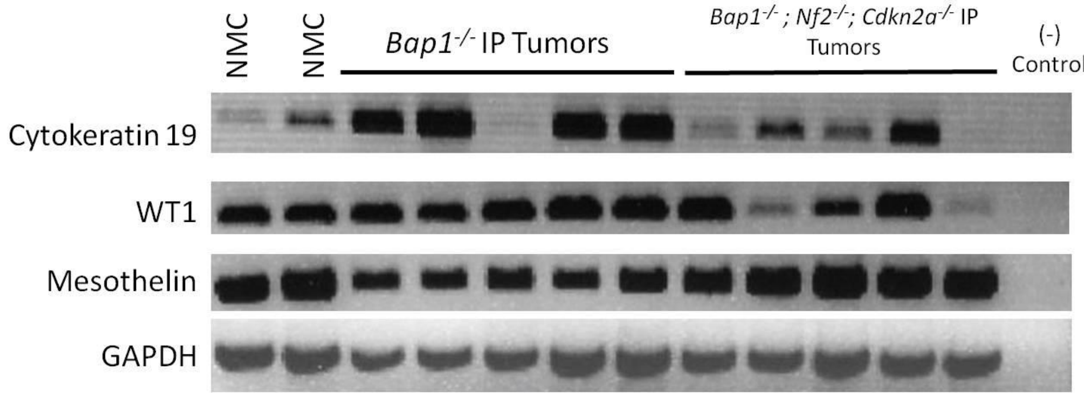

Figure 30. Mesothelioma and mesothelin markers from IP tumors used in RNA-seq analysis. Semi-quantitative RT-PCR was performed to analyze WT1, mesothelin, and GAPDH mRNA expression to show the mesothelial origin of the 5 tumor samples from *Bap1* CKO cohort and 5 tumors from the triple-CKO cohort. Normal mesothelial cell lines were obtained from the non-injected with Adeno-Cre mice.

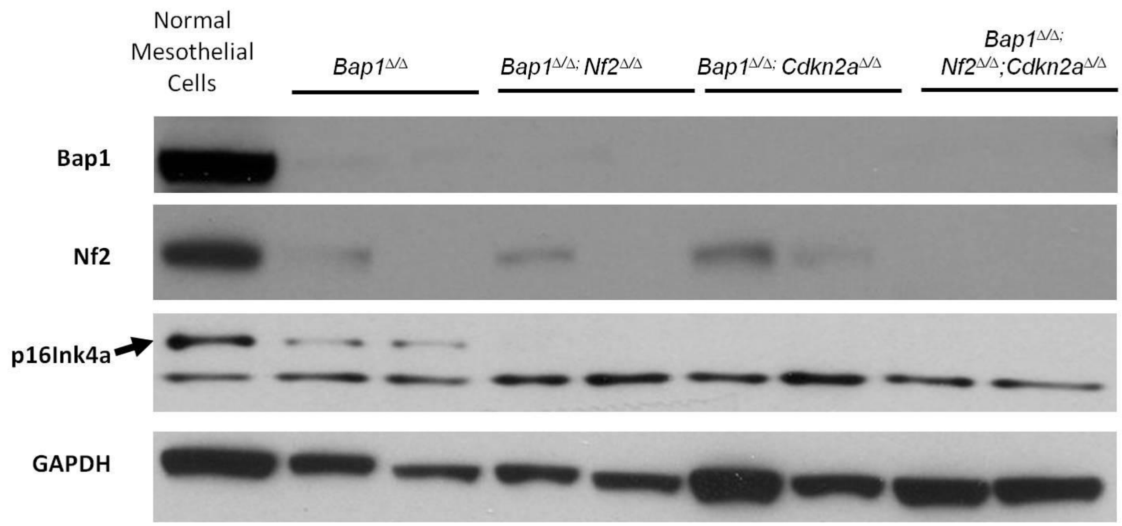

Figure 31. Western blot analysis on MPeM tumor samples from mice injected IP with Adeno-Cre. Western blot analysis of Bap1, Nf2, Cdkn2a (p16Ink4a) and Gapdh protein expression in a panel of MPeMs. Bap1expression is absent in all the samples comparing to the positive control (normal mesothelial cells), as expected. Nf2 expression is lost spontaneously in the *Bap1*$^{\Delta/\Delta}$ and *Bap1*$^{\Delta/\Delta}$*;Cdkn2a*$^{\Delta/\Delta}$ tumors. Cdkn2a (p16Ink4a) expression is lost in the *Bap1*$^{\Delta/\Delta}$ and *Bap1*$^{\Delta/\Delta}$*;NF2*$^{\Delta/\Delta}$ tumor samples. Expression of all three proteins is lost in the triple-CKO group as expected. Gapdh is used as a loading control.

6.3 Discussion

In this study, we sought to determine if inactivation of the three major MM driver tumor suppressor genes (*Bap1*, *Nf2* and *Cdkn2a*) in the peritoneal cavity of CKO mice was sufficient to drive MPeM development, without asbestos, as previously described in the pleural cavity (chapter 5). Nearly all malignant tumors observed in this study, unlike with the IT model, were MMs. The Kaplan-Meier analysis demonstrated that intraperitoneal homozygous deletion of any of the combinations of *Bap1*, *Nf2* and *Cdkn2a* could give rise to MMs with shorter tumor latency than observed in the corresponding IT models, but with a similar trend. One remarkable observation in this study was that MM incidence in *Bap1* CKO mice was much higher in the IP-injected mice than previously observed in IT-injected mice (74% vs. 3%). A possible explanation for this could be that the cell surface of the peritoneal cavity is larger than the thoracic cavity, and hence there are more mesothelial cells for virus to infect. Also, the peritoneum has a large vascular and lymphatic network which could provide a growth advantage for IP MM model versus the IT MM model.

In both the IP and IT models, *Bap1;Nf2;Cdkn2a* CKO mice developed MMs fastest, followed by *Bap1;Nf2*, *Bap1;Cdkn2a*, and then *Bap1*CKO mice. The data indicate that *Bap1* loss cooperates tumorigenically with *Nf2* loss more efficiently than it does with *Cdkn2a* loss in both the peritoneal and pleural cavities. Interestingly however, MMs from all the genotypes tested in the IP model showed a somatic decrease or complete loss of p16Ink4a in all the groups (Figure 31). This suggests that just like in pleural MMs, inactivation of all three genes often occur in combination in MM (Figure

16 and 19) and depending on different TSG combinations of the CKO mouse, it can take more or less time for a spontaneous loss of p16Ink4a to occur.

The shortest tumor latency was in the triple-CKO mice (9 weeks). This cohort also had the highest MPeM incidence (100%) and had the highest percentage of Ki-67-positive cells. Among the top 50 differentially expressed genes from the RNA-seq analysis, *Vegfd* and *Pak3* are the ones involved in angiogenesis formation and cell motility. Consequently, this could possibly explain the aggressive phenotype of the triple-CKO tumors.

CHAPTER 7

7 GENERAL DISCUSSION/FUTURE DIRECTIONS

BAP1 is a tumor suppressor with multifaceted functions. It acts as a deubiquitinating enzyme that regulates histone modification, gene transcription, DNA damage repair and cell death (45). Somatic mutations of *BAP1* can act as driver events in numerous cancers, in particular malignant mesothelioma (MM) and both cutaneous melanoma (CM) and uveal melanoma (UM). Over the last decade, research on *BAP1* has increased exponentially: according to PubMed, the number of articles published on *BAP1*-related topics increased 17.5-fold between 2010 and 2018, with BAP1 protein interactions, cellular functions, and role in tumor development continuing to emerge. Still, there remains a big gap in our knowledge about BAP1. This thesis addresses gene vs. environment and gene vs. gene interactions with the goal of understanding mechanisms underlying *BAP1*-related cancer predisposition and how environmental and genetic effects combine to drive cancer pathogenesis.

In chapter 3, we introduced a mouse model of melanoma with a germline *Bap1* knock-in mutation ($Bap1^{+/Lou}$) identical to the mutation found in patients from a BAP1 syndrome family living in Louisiana. This mouse model was crossed to a well-established transgenic mouse model of melanoma (HGF^{Tg} mice) to interrogate the role of *Bap1* haploinsufficiency in melanomagenesis. We speculated that because this BAP1 family lived in the subtropical state of Louisiana, members of this family would likely be exposed to year-round intense UVR, and that due to the *BAP1* mutation, carriers would be more susceptible to the development of UM, CM and other skin tumors. Therefore, we hypothesized that *Bap1*$^{+/Lou}$ mice exposed to UVR would develop CM and that crossing these mice to *HGF*^{Tg} animals to create *Bap1*$^{+/Lou}$*;HGF*^{Tg} animals would shorten tumor latency and increase the incidence of melanomagenesis. Interestingly, *Bap1*$^{+/Lou}$ alone mice developed melanomas (2 mice at 14 and 26 months), demonstrating that after a single dose of UVR, a single copy mutation of *Bap1* is sufficient to give rise to CM in some animals. In the *Bap1*$^{+/Lou}$*;HGF*^{Tg} cohort, only 2 mice developed CM after UVR exposure, and tumor latency (~14 months) was similar to that of *HGF*^{Tg} mice treated with UVR. The experiment was compromised because *HGF*^{Tg} mice exhibited rectal prolapses/intestinal obstructions and had to be euthanized before CMs could arise. In future experiments, we would propose to use multiple doses of UVR instead of a single neonatal dose, better mimicking the long term exposures sustained by humans. Additionally, we would cross the *Bap1*$^{+/Lou}$ model to mice with inactivation of tumor suppressor genes involved in CM and MM-prone families, such as *CDKN2A*. We hypothesize that giving multiple doses of UVR would induce more melanomas in *Bap1*$^{+/Lou}$ mice, and that *Bap1*$^{+/Lou}$*;Cdkn2a*$^{+/-}$ mice would develop an even higher incidence and more rapid progression of CMs compared to animals with inactivation of only one gene.

One of the fairly recently discovered functions of BAP1 is its involvement in homologous recombination (HR) in DNA double-strand break repair (40). In chapter 4, we explore the mechanism by which BAP1 is involved in UV-induced DNA damage repair, namely nucleotide excision repair (NER). We hypothesized that cells lacking BAP1 would have increased amounts of unrepaired DNA damage caused by UVR. We established stable sh*BAP1* knockdown in human melanocytes, which are relevant to cancers characteristic of the BAP1 TPDS. In these germane cells, we show decreased accumulation of BRCA1 and RAD51 proteins at the DNA damage caused by UVR, which confirms observations made by others in chicken cells exposed to ionizing radiation (40). Our results demonstrate that BAP1 is indeed necessary for NER in cells relevant to cancers associated with BAP1 inactivation. We also demonstrate an increase of UVR-induced adducts (cyclobutane pyrimidine dimers or CPDs) and increased comet assay "tail" lengths in the UVR-treated BAP1-deficient cells, also consistent with a role of BAP1 in NER. Since there was an increase of damaged DNA in UVR-treated BAP1-deficient cells, we hypothesized that these cells are not able to efficiently repair DNA and thereby may stall in S-phase of the cell cycle, where NER usually occurs. To test this possibility, cell cycle progression was also evaluated by flow cytometry after UVR in both *BAP1*-deficient and *BAP1*-competent cells. When 293HEKT cells with stable *BAP1* knockdown were treated with UVR, more cells were in S-phase, suggesting an inability to repair DNA damage and progress to the next stage of the cell cycle. Overall, our data are consistent with BAP1 playing a role in cell cycle progression, DNA damage and DNA adduct repair in various types of cells. However, further experimentation is necessary to understand the exact mechanism of how and with which partners BAP1 functions in NER. We speculate that perhaps due to BAP1's ability to modify chromatin and to regulate gene expression via its deubiquitinating function, it could have an effect both in the initiation of NER and the recruitment of repair pathway proteins. It would be interesting to analyze the ubiquitin status of histones at the sites of DNA damage and/or to test whether BAP1 is bound to chromatin at sites of DNA damage in UVR-treated cells.

As described above, *BAP1* is implicated in numerous familial cancers, particularly MM, CM and UM. Most human MMs exhibit somatic alterations of *BAP1*, *NF2* and/or *CDKN2A*. However, it is not known if inactivation of *BAP1* cooperates with loss of *NF2* and/or *CDKN2A* to drive an aggressive MM phenotype. There are multiple established mouse models that have been generated to study MM pathogenesis; however, most of these models have been used to evaluate gene vs. environment interactions, involving the loss of one or more tumor suppressor genes (TSGs). Here, we describe the first pleural MM conditional knockout (CKO) mouse model investigating cooperation between deletion of *Bap1* and deletion of other TSGs implicated in human MM, *i.e.*, *Nf2* and *Cdkn2a*. In chapter 5, we describe results of various crosses between a homozygous *Bap1* CKO mouse ($Bap1^{f/f}$) and $Nf2^{f/f}$ and/or $Cdkn2a^{f/f}$ mice, thereby making double-CKO combinations and $Bap1^{f/f};Nf2^{f/f};Cdkn2a^{f/f}$ triple-CKO mice. These mice were subsequently injected with Adeno-Cre intrathoracically (IT) to knock out the floxed TSGs in the mesothelial lining of the pleural cavity. Notably, homozygous deletion of single genes, gave rise to few MMs. In contrast, 22% of double-CKO *Bap1;Cdkn2a* mice developed MM with a median survival of 27 weeks, and 17% of *Bap1;Nf2* mice developed MM with a median survival of 21 weeks. The highest incidence and shortest median survival was seen in the triple-CKO mice (85%; 12 weeks). MMs from the triple-CKO cohort were highly aggressive and invasive compared to those observed in the double-CKO combinations. To gain some insights with regard to these marked phenotypic differences, immunoblot analyses were performed on MMs from triple-CKO and double-CKO *Nf2;Cdkn2a* mice. Surprisingly, we found that 4 out of 6 MMs from *Nf2;Cdkn2a* CKO mice lost expression of Bap1. This observation suggested that acquired loss of Bap1 may be favored in MM development. To clarify what Bap1 loss itself conveys in the MM tumorigenic process, we turned to RNA-seq analysis to assess the contribution of Bap1 inactivation. We thus investigated specifically RNA expression differences between the two samples from the double *Nf2*$^{f/f}$*;Cdkn2a*$^{f/f}$ tumors that retained Bap1 expression, and the 6 tumors from the *Bap1*$^{f/f}$*;Nf2*$^{f/f}$*;Cdkn2a*$^{f/f}$ mice with complete loss of Bap1. Interestingly, we found that upregulated expression of a set of polycomb repressive complex 2 (PRC2) genes was significantly higher in MMs from the triple-CKO mice. These results are consistent with previous studies that implicated BAP1 as an antagonist of PRC2 gene expression. Among this gene set, there was upregulation of multiple oncogenes and pro-invasion/metastasis genes (i.e., *Foxg1, Lmo1, Pdgfra, Gli1, Gli2*, *Mmp9*, *Mmp14*, *Mycn*, *Twist1*), and downregulation of putative tumor suppressor genes (*Bin1* and *Diras1*). Thus, loss of BAP1 may contribute to MM tumorigenesis, in part, via deregulation of PRC2-mediated gene repression of specific oncogenic genes.

In addition, we showed that the collective inactivation of all three TSGs (*Bap1*, *Nf2*, *Cdkn2a*) in normal mesothelial cells consistently led to the formation of large spheroids, suggestive of a cancer stem cell-like phenotype. Together, the RNA data and the spheroid formation imply that Bap1 loss is a critical driver of the aggressive MM phenotypes seen *in vivo*. We speculate that this capability may be due to Bap1's ability to modify gene expression, whether via epigenetic or transcriptional regulation. In future research, it would be worthwhile to modify different domains of Bap1 to determine if its deubiquitinating function is responsible for providing a stem cell-like phenotype and tumor aggressiveness. One could also employ inhibitors of genes shown to be upregulated in these aggressive tumors and test whether their inhibition would lead to less proliferative and/or less invasive tumors. If successful, these results could lead to novel therapeutic targets in pleural MM.

How loss of *Bap1*, *Nf2* and *Cdkn2a* cooperate to drive MM pathogenesis is not yet fully understood. However, one might opine that *Cdkn2a* loss would result in deregulation of the pRb and p53 cell cycle pathways, and *Nf2* loss would lead to altered Hippo, Pak and mTOR signaling. Collectively, these alterations would be expected to cooperate in driving MM pathogenesis, as *Cdkn2a* loss would mechanistically result in two acquired hallmarks of cancer, insensitivity to antigrowth signals (p16Ink4a loss) and evasion of apoptosis (p19Arf loss), whereas Nf2/Merlin loss would be expected to result in processes such as evasion of apoptosis and tissue invasion/metastasis. Based on the upregulated oncogenes (e.g., *Lmo1, Gli1/2*) and downregulated tumor suppressor genes (*Bin1*, *Diras1*) identified in MM cells with *Bap1* loss, other possible effects on hallmarks of cancer such as Lmo1-induced ECM and integrin-related self-sufficiency in growth signals, Gli1/2-related maintenance of cancer stem cells, and *Mmp9/14*-induced invasiveness may be mechanistically connected with Bap1 inactivation and could be explored in future studies.

In chapter 6, we present the first peritoneal (IP) MM mouse model with conditional inactivation of three major TSGs implicated in human MM. The mouse model used is similar to the one described in chapter 5. However, in this study only 1) $Bap1^{f/f}$, 2) $Bap1^{f/f}$;$Nf2^{f/f}$, 3) $Bap1^{f/f}$;$Cdkn2a^{f/f}$, and 4) $Bap1^{f/f}$;$\mathrm{Nf2}^{f/f}$;$\mathrm{Cdkn2a}^{f/f}$ genotypes were used for IP Adeno-Cre injections. In this IP model, we observed peritoneal MMs with a tumor latency consistently shorter than in the IT model, but resembling the trend found in the IT model: *Bap1;Cdkn2a* CKO mice (40 weeks IT; 23 weeks IP); *Bap1;Nf2* CKO mice (21 weeks IT; 13 weeks IP); and *Bap1;Nf2;Cdkn2a* CKO mice (12 weeks IT, 9 weeks IP). One of the most interesting findings is that MM incidence in the *Bap1*$^{f/f}$ cohort was much higher when injected with Adeno-Cre IP than when injected IT: 74% vs 3%, respectively. We speculate this difference might be due to the much larger mesothelial cell surface of the peritoneum as compared to the thoracic cavity and, hence, that there are more cells for the virus to infect. This might also be one reason why deaths due to MM in each of the double- and triple-CKO mouse cohorts consistently occurred more rapidly in the IP-injected mice than in IT-injected mice. The triple-CKO genotype exhibited 100% MM incidence and had the shortest survival (9 weeks in IP-injected mice vs. 12 weeks in the IT cohort). Ki-67 analysis confirmed a high proliferative phenotype of the IP tumors. We also performed a RNA-seq analysis on MMs from *Bap1* CKO mice versus *Bap1;Nf2;Cdkn2a* CKO mice, and among the top 50 differentially expressed genes we found *Vegfd* and *Pak3* to be upregulated. These two genes are involved in angiogenesis formation and cell motility, respectively, and upregulation of these pathways could explain, in part, the aggressive phenotype of tumors from the triple-CKO mice. Overall the IP triple-CKO mouse model shows 100% penetrance and very short tumor latency, making it a potentially invaluable tool for preclinical studies. We could also use cell lines derived from the mouse MMs to perform invasion/migration assays to confirm the invasive phenotype of tumors *in vitro*.

Even though there is still much to decipher about the functions of *BAP1* and how it is involved in the formation of MM and other tumor types, our data contribute valuable insights, and take another step towards answering such questions. As PubMed shows that the publications on the topic of *BAP1* are clearly on the rise, our mouse models of MM may serve as valuable resources for translational research and aid in discovering novel therapeutics against this fatal disease.

REFERENCES

1. Mott FE. Mesothelioma: a review. Ochsner J. 2012;12(1):70-9.

2. Center MaAA. Malignant Mesothelioma | Causes, Symptoms, Prognosis 2019 [Available from: https://www.maacenter.org/mesothelioma/.

3. Cancer.org. What Is Malignant Mesothelioma? : Cancer. org; 2019 [Available from: https://www.cancer.org/cancer/malignant-mesothelioma/about/malignant-mesothelioma.html.

4. Asbestos.com. Mesothelioma: What Is Malignant Mesothelioma Cancer? 2019 [Available from: https://www.asbestos.com/mesothelioma/.

5. Organization WH. Asbestos 2019 [Available from: https://www.who.int/ipcs/assessment/public_health/asbestos/en/.

6. Donaldson K, Murphy FA, Duffin R, Poland CA. Asbestos, carbon nanotubes and the pleural mesothelium: a review of the hypothesis regarding the role of long fibre retention in the parietal pleura, inflammation and mesothelioma. Part Fibre Toxicol. 2010;7:5.

7. Yang H, Testa JR, Carbone M. Mesothelioma epidemiology, carcinogenesis, and pathogenesis. Curr Treat Options Oncol. 2008;9(2-3):147-57.

8. Benedetti S, Nuvoli B, Catalani S, Galati R. Reactive oxygen species a double-edged sword for mesothelioma. Oncotarget. 2015;6(19):16848-65.

9. Carbone M, Ly BH, Dodson RF, Pagano I, Morris PT, Dogan UA, et al. Malignant mesothelioma: facts, myths, and hypotheses. J Cell Physiol. 2012;227(1):44-58.

10. Hanahan D, Weinberg RA. Hallmarks of cancer: the next generation. Cell. 2011;144(5):646-74.

11. Cheng JQ, Jhanwar SC, Klein WM, Bell DW, Lee WC, Altomare DA, et al. p16 alterations and deletion mapping of 9p21-p22 in malignant mesothelioma. Cancer Res. 1994;54(21):5547-51.

12. Gil J, Peters G. Regulation of the INK4b–ARF–INK4a tumour suppressor locus: all for one or one for all. Nature Reviews Molecular Cell Biology. 2006;7:667.

13. Cheng JQ, Lee WC, Klein MA, Cheng GZ, Jhanwar SC, Testa JR. Frequent mutations of NF2 and allelic loss from chromosome band 22q12 in malignant mesothelioma: evidence for a two-hit mechanism of NF2 inactivation. Genes Chromosomes Cancer. 1999;24:238-42.

14. Bianchi AB, Mitsunaga SI, Cheng JQ, Klein WM, Jhanwar SC, Seizinger B, et al. High frequency of inactivating mutations in the neurofibromatosis type 2 gene (NF2) in primary malignant mesotheliomas. Proc Natl Acad Sci U S A. 1995;92(24):10854-8.

15. Petrilli AM, Fernandez-Valle C. Role of Merlin/NF2 inactivation in tumor biology. Oncogene. 2016;35(5):537-48.

16. Xio S, Li D, Vijg J, Sugarbaker DJ, Corson JM, Fletcher JA. Codeletion of p15 and p16 in primary malignant mesothelioma. Oncogene. 1995;11:511-5.

17. Lu YY, Jhanwar SC, Cheng JQ, Testa JR. Deletion mapping of the short arm of chromosome 3 in human malignant mesothelioma. Genes Chromosomes Cancer. 1994;9(1):76-80.

18. Bott M, Brevet M, Taylor BS, Shimizu S, Ito T, Wang L, et al. The nuclear deubiquitinase BAP1 is commonly inactivated by somatic mutations and 3p21.1 losses in malignant pleural mesothelioma. Nature Genetics. 2011;43:668.

19. Testa JR, Cheung M, Pei J, Below JE, Tan Y, Sementino E, et al. Germline BAP1 mutations predispose to malignant mesothelioma. Nat Genet. 2011;43(10):1022-5.

20. Wiesner T, Obenauf AC, Murali R, Fried I, Griewank KG, Ulz P, et al. Germline mutations in BAP1 predispose to melanocytic tumors. Nat Genet. 2011;43(10):1018-21.

21. Abdel-Rahman MH, Pilarski R, Cebulla CM, Massengill JB, Christopher BN, Boru G, et al. Germline BAP1 mutation predisposes to uveal melanoma, lung adenocarcinoma, meningioma, and other cancers. J Med Genet. 2011;48(12):856-9.

22. Walpole S, Pritchard AL, Cebulla CM, Pilarski R, Stautberg M, Davidorf FH, et al. Comprehensive Study of the Clinical Phenotype of Germline BAP1 Variant-Carrying Families Worldwide. J Natl Cancer Inst. 2018;110(12):1328-41.

23. Jensen DE, Proctor M, Marquis ST, Gardner HP, Ha SI, Chodosh LA, et al. BAP1: a novel ubiquitin hydrolase which binds to the BRCA1 RING finger and enhances BRCA1-mediated cell growth suppression. Oncogene. 1998;16:1097-112.

24. Ladanyi M, Zauderer MG, Krug LM, Ito T, McMillan R, Bott M, et al. New strategies in pleural mesothelioma: BAP1 and NF2 as novel targets for therapeutic development and risk assessment. Clin Cancer Res. 2012;18(17):4485-90.

25. Kadariya Y, Cheung M, Xu JF, Pei JM, Sementino E, Menges CW, et al. Bap1 Is a Bona Fide Tumor Suppressor: Genetic Evidence from Mouse Models Carrying Heterozygous Germline Bap1 Mutations. Cancer Research. 2016;76(9):2836-44.

26. Ventii KH, Devi NS, Friedrich KL, Chernova TA, Tighiouart M, Van Meir EG, et al. BRCA1-associated protein-1 is a tumor suppressor that requires deubiquitinating activity and nuclear localization. Cancer Research. 2008;68(17):6953-62.

27. Machida YJ, Machida Y, Vashisht AA, Wohlschlegel JA, Dutta A. The deubiquitinating enzyme BAP1 regulates cell growth via interaction with HCF-1. J Biol Chem. 2009;284(49):34179-88.

28. Eletr ZM, Wilkinson KD. An emerging model for BAP1's role in regulating cell cycle progression. Cell Biochem Biophys. 2011;60:3-11.

29. Narayanan A, Ruyechan WT, Kristie TM. The coactivator host cell factor-1 mediates Set1 and MLL1 H3K4 trimethylation at herpesvirus immediate early promoters for initiation of infection. P Natl Acad Sci USA. 2007;104(26):10835-40.

30. Tyagi S, Chabes AL, Wysocka J, Herr W. E2F activation of S phase promoters via association with HCF-1 and the MLL family of histone H3K4 methyltransferases. Mol Cell. 2007;27(1):107-19.

31. Chittock EC, Latwiel S, Miller TC, Muller CW. Molecular architecture of polycomb repressive complexes. Biochem Soc Trans. 2017;45(1):193-205.

32. Simon JA, Kingston RE. Mechanisms of polycomb gene silencing: knowns and unknowns. Nat Rev Mol Cell Biol. 2009;10(10):697-708.

33. Scheuermann JC, de Ayala Alonso AG, Oktaba K, Ly-Hartig N, McGinty RK, Fraterman S, et al. Histone H2A deubiquitinase activity of the Polycomb repressive complex PR-DUB. Nature. 2010;465(7295):243-7.

34. Kemp CD, Rao M, Xi SC, Inchauste S, Mani H, Fetsch P, et al. Polycomb Repressor Complex-2 Is a Novel Target for Mesothelioma Therapy. Clin Cancer Res. 2012;18(1):77-90.

35. LaFave LM, Beguelin W, Koche R, Teater M, Spitzer B, Chrarniec A, et al. Loss of BAP1 function leads to EZH2-dependent transformation. Nat Med. 2015;21(11):1344-9.

36. Harper JW, Elledge SJ. The DNA damage response: ten years after. Mol Cell. 2007;28(5):739-45.

37. Price BD, D'Andrea AD. Chromatin Remodeling at DNA Double-Strand Breaks. Cell. 2013;152(6):1344-54.

38. Chapman JR, Taylor MR, Boulton SJ. Playing the end game: DNA double-strand break repair pathway choice. Mol Cell. 2012;47(4):497-510.

39. Shao G, Lilli DR, Patterson-Fortin J, Coleman KA, Morrissey DE, Greenberg RA. The Rap80-BRCC36 de-ubiquitinating enzyme complex antagonizes RNF8-Ubc13-dependent ubiquitination events at DNA double strand breaks. P Natl Acad Sci USA. 2009;106(9):3166-71.

40. Yu H, Pak H, Hammond-Martel I, Ghram M, Rodrigue A, Daou S, et al. Tumor suppressor and deubiquitinase BAP1 promotes DNA double-strand break repair. Proc Natl Acad Sci U S A. 2014;111(1):285-90.

41. Ismail IH, Davidson R, Gagne JP, Xu ZZ, Poirier GG, Hendzel MJ. Germline mutations in BAP1 impair its function in DNA double-strand break repair. Cancer Res. 2014;74(16):4282-94.

42. Bononi A, Giorgi C, Patergnani S, Larson D, Verbruggen K, Tanji M, et al. BAP1 regulates IP3R3-mediated Ca(2+) flux to mitochondria suppressing cell transformation. Nature. 2017;546(7659):549-53.

43. Zhang Y, Shi J, Liu X, Feng L, Gong Z, Koppula P, et al. BAP1 links metabolic regulation of ferroptosis to tumour suppression. Nat Cell Biol. 2018;20(10):1181-92.

44. Affar EB, Carbone M. BAP1 regulates different mechanisms of cell death. Cell Death Dis. 2018;9(12):1151.

45. Carbone M, Yang H, Pass HI, Krausz T, Testa JR, Gaudino G. BAP1 and cancer. Nat Rev Cancer. 2013;13(3):153-9.

46. Popova T, Hebert L, Jacquemin V, Gad S, Caux-Moncoutier V, Dubois-d'Enghien C, et al. Germline BAP1 mutations predispose to renal cell carcinomas. Am J Hum Genet. 2013;92(6):974-80.

47. Klebe S, Driml J, Nasu M, Pastorino S, Zangiabadi A, Henderson D, et al. BAP1 hereditary cancer predisposition syndrome: a case report and review of literature. Biomark Res. 2015;3:14.

48. Xu J, Kadariya Y, Cheung M, Pei J, Talarchek J, Sementino E, et al. Germline mutation of Bap1 accelerates development of asbestos-induced malignant mesothelioma. Cancer Res. 2014;74(16):4388-97.

49. Jhappan C, Noonan FP, Merlino G. Ultraviolet radiation and cutaneous malignant melanoma. Oncogene. 2003;22(20):3099-112.

50. Hoban PR, Ramachandran S, Strange RC. Environment, phenotype and genetics: risk factors associated with BCC of the skin. Expert Rev Anticancer Ther. 2002;2(5):570-9.

51. Goudar RK. Review of pemetrexed in combination with cisplatin for the treatment of malignant pleural mesothelioma. Ther Clin Risk Manag. 2008;4(1):205-11.

52. Boyer A, Pasquier E, Tomasini P, Ciccolini J, Greillier L, Andre N, et al. Drug repurposing in malignant pleural mesothelioma: a breath of fresh air? Eur Respir Rev. 2018;27(147).

53. Wu L, Allo G, John T, Li M, Tagawa T, Opitz I, et al. Patient-Derived Xenograft Establishment from Human Malignant Pleural Mesothelioma. Clin Cancer Res. 2017;23(4):1060-7.

54. Maronpot RR, Nyska A, Foreman JE, Ramot Y. The legacy of the F344 rat as a cancer bioassay model (a retrospective summary of three common F344 rat neoplasms). Crit Rev Toxicol. 2016;46(8):641-75.

55. Bomhard E. Frequency of spontaneous tumours in NMRI mice in 21-month studies. Exp Toxicol Pathol. 1993;45(5-6):269-89.

56. Peters RL, Rabstein LS, Spahn GJ, Madison RM, Huebner RJ. Incidence of spontaneous neoplasms in breeding and retired breeder BALB-cCr mice throughout the natural life span. Int J Cancer. 1972;10(2):273-82.

57. Shirai M, Maejima T, Tanimoto T, Kumagai K, Makino T, Kai K, et al. Mixed Type of Malignant Mesothelioma in an Aged Male ICR Mouse. J Toxicol Pathol. 2011;24(3):169-72.

58. Jean D, Jaurand MC. Mesotheliomas in Genetically Engineered Mice Unravel Mechanism of Mesothelial Carcinogenesis. Int J Mol Sci. 2018;19(8).

59. Altomare DA, Menges CW, Pei J, Zhang L, Skele-Stump KL, Carbone M, et al. Activated TNF-alpha/NF-kappaB signaling via down-regulation of Fas-associated factor

1 in asbestos-induced mesotheliomas from Arf knockout mice. Proc Natl Acad Sci U S A. 2009;106(9):3420-5.

60. Altomare DA, Vaslet CA, Skele KL, De Rienzo A, Devarajan K, Jhanwar SC, et al. A mouse model recapitulating molecular features of human mesothelioma. Cancer Research. 2005;65:8090-5.

61. Menges CW, Kadariya Y, Altomare D, Talarchek J, Neumann-Domer E, Wu Y, et al. Tumor suppressor alterations cooperate to drive aggressive mesotheliomas with enriched cancer stem cells via a p53-miR-34a-c-Met axis. Cancer Research. 2014;74(4):1261-71.

62. Dey A, Seshasayee D, Noubade R, French DM, Liu J, Chaurushiya MS, et al. Loss of the tumor suppressor BAP1 causes myeloid transformation. Science. 2012;337(6101):1541-6.

63. Jongsma J, van Montfort E, Vooijs M, Zevenhoven J, Krimpenfort P, van der Valk M, et al. A conditional mouse model for malignant mesothelioma. Cancer Cell. 2008;13(3):261-71.

64. Guo Y, Chirieac LR, Bueno R, Pass H, Wu W, Malinowska IA, et al. Tsc1-Tp53 loss induces mesothelioma in mice, and evidence for this mechanism in human mesothelioma. Oncogene. 2014;33(24):3151-60.

65. Sementino E, Menges CW, Kadariya Y, Peri S, Xu J, Liu Z, et al. Inactivation of Tp53 and Pten drives rapid development of pleural and peritoneal malignant mesotheliomas. J Cell Physiol. 2018;233(11):8952-61.

66. Noonan FP, Recio JA, Takayama H, Duray P, Anver MR, Rush WL, et al. Neonatal sunburn and melanoma in mice - Severe sunburn in newborn, but not adult, mice is linked with melanoma in later life. Nature. 2001;413(6853):271-2.

67. Noonan FP, Zaidi MR, Wolnicka-Glubisz A, Anver MR, Bahn J, Wielgus A, et al. Melanoma induction by ultraviolet A but not ultraviolet B radiation requires melanin pigment. Nat Commun. 2012;3:884.

68. Takayama H, Takagi H, Larochelle WJ, Kapur RP, Merlino G. Ulcerative proctitis, rectal prolapse, and intestinal pseudo-obstruction in transgenic mice overexpressing hepatocyte growth factor/scatter factor. Lab Invest. 2001;81(3):297-305.

69. Sgul.ac.uk. Cell Culture Media 2019 [Available from: http://www.sgul.ac.uk/depts/anatomy/pages/Dot/Cell%20Bank%20conditions.htm.

70. Bot J, Whitaker D, Vivian J, Lake R, Yao V, McCauley R. Culturing mouse peritoneal mesothelial cells. Pathology - Research and Practice. 2003;199:341-4.

71. Baumann F, Flores E, Napolitano A, Kanodia S, Taioli E, Pass H, et al. Mesothelioma patients with germline BAP1 mutations have 7-fold improved long-term survival. Carcinogenesis. 2015;36(1):76-81.

72. Love MI, Huber W, Anders S. Moderated estimation of fold change and dispersion for RNA-seq data with DESeq2. Genome Biol. 2014;15(12):550.

73. Noonan FP, Dudek J, Merlino G, De Fabo EC. Animal models of melanoma: an HGF/SF transgenic mouse model may facilitate experimental access to UV initiating events. Pigment Cell Res. 2003;16(1):16-25.

74. Choi YS, Fisher DE. UV and melanoma: the TP53 link. Cell Res. 2014;24(10):1157-8.

75. Webster JD, Pham TH, Wu X, Hughes NW, Li Z, Totpal K, et al. The tumor suppressor BAP1 cooperates with BRAFV600E to promote tumor formation in cutaneous melanoma. Pigment Cell Melanoma Res. 2019;32(2):269-79.

76. Pathania S, Nguyen J, Hill SJ, Scully R, Adelmant GO, Marto JA, et al. BRCA1 Is Required for Postreplication Repair after UV-Induced DNA Damage. Molecular Cell. 2011;44(2):235-51.

77. Henley SJ, Larson TC, Wu M, Antao VC, Lewis M, Pinheiro GA, et al. Mesothelioma incidence in 50 states and the District of Columbia, United States, 2003-2008. Int J Occup Environ Health. 2013;19(1):1-10.

78. Murthy SS, Testa JR. Asbestos, chromosomal deletions, and tumor suppressor gene alterations in human malignant mesothelioma. Journal of Cellular Physiology. 1999;180:150-7.

79. Sekido Y, Pass HI, Bader S, Mew DJY, Christman MF, Gazdar AF, et al. Neurofibromatosis type 2 (*NF2*) gene is somatically mutated in mesothelioma but not in lung cancer. Cancer Res. 1995;55:1227-31.

80. Altomare DA, Menges CW, Xu J, Pei J, Zhang L, Tadevosyan A, et al. Losses of both products of the Cdkn2a/Arf locus contribute to asbestos-induced mesothelioma development and cooperate to accelerate tumorigenesis. PLoS One. 2011;6:e18828.

81. Hmeljak J, Sanchez-Vega F, Hoadley KA, Shih J, Stewart C, Heiman D, et al. Integrative Molecular Characterization of Malignant Pleural Mesothelioma. Cancer Discov. 2018;8(12):1548-65.

82. Frizelle SP, Grim J, Zhou J, Gupta P, Curiel DT, Geradts J, et al. Re-expression of p16INK4a in mesothelioma cells results in cell cycle arrest, cell death, tumor suppression and tumor regression. Oncogene. 1998;16:3087-95.

83. Yang CT, You L, Yeh CC, Chang JW, Zhang F, McCormick F, et al. Adenovirus-mediated p14(ARF) gene transfer in human mesothelioma cells. J Natl Cancer Inst. 2000;92:636-41.

84. Xiao GH, Gallagher R, Shetler J, Skele K, Altomare DA, Pestell RG, et al. The NF2 tumor suppressor gene product, merlin, inhibits cell proliferation and cell cycle progression by repressing cyclin D1 expression. Molecular and cellular biology. 2005;25(6):2384-94.

85. Lopez-Lago MA, Okada T, Murillo MM, Socci N, Giancotti FG. Loss of the tumor suppressor gene NF2, encoding merlin, constitutively activates integrin-dependent mTORC1 signaling. Molecular and cellular biology. 2009;29(15):4235-49.

86. Xiao GH, Beeser A, Chernoff J, Testa JR. p21-activated kinase links Rac/Cdc42 signaling to merlin. J Biol Chem. 2002;277:883-6.

87. Poulikakos PI, Xiao GH, Gallagher R, Jablonski S, Jhanwar SC, Testa JR. Re-expression of the tumor suppressor NF2/merlin inhibits invasiveness in mesothelioma cells and negatively regulates FAK. Oncogene. 2006;25:5960-8.

88. Fleury-Feith J, Lecomte C, Renier A, Matrat M, Kheuang L, Abramowski V, et al. Hemizygosity of Nf2 is associated with increased susceptibility to asbestos-induced peritoneal tumours. Oncogene. 2003;22:3799-805.

89. Misaghi S, Ottosen S, Izrael-Tomasevic A, Arnott D, Lamkanfi M, Lee J, et al. Association of C-terminal ubiquitin hydrolase BRCA1-associated protein 1 with cell cycle regulator host cell factor 1. Mol Cell Biol. 2009;29:2181-92.

90. Yu H, Mashtalir N, Daou S, Hammond-Martel I, Ross J, Sui G, et al. The ubiquitin carboxyl hydrolase BAP1 forms a ternary complex with YY1 and HCF-1 and is a critical regulator of gene expression. Molecular and cellular biology. 2010;30(21):5071-85.

91. Tandon RT, Jimenez-Cortez Y, Taub R, Borczuk AC. Immunohistochemistry in Peritoneal Mesothelioma: A Single-Center Experience of 244 Cases. Arch Pathol Lab Med. 2018;142(2):236-42.

92. Baughman JM, Rose CM, Kolumam G, Webster JD, Wilkerson EM, Merrill AE, et al. NeuCode Proteomics Reveals Bap1 Regulation of Metabolism. Cell Rep. 2016;16(2):583-95.

93. Gezgin G, Dogrusoz M, van Essen TH, Kroes WGM, Luyten GPM, van der Velden PA, et al. Genetic evolution of uveal melanoma guides the development of an inflammatory microenvironment. Cancer Immunol Immunother. 2017;66(7):903-12.

94. Napolitano A, Pellegrini L, Dey A, Larson D, Tanji M, Flores EG, et al. Minimal asbestos exposure in germline BAP1 heterozygous mice is associated with deregulated inflammatory response and increased risk of mesothelioma. Oncogene. 2016;35(15):1996-2002.

95. Ohar JA, Cheung M, Talarchek J, Howard SE, Howard TD, Hesdorffer M, et al. Germline BAP1 Mutational Landscape of Asbestos-Exposed Malignant Mesothelioma Patients with Family History of Cancer. Cancer Res. 2016;76(2):206-15.

96. Harbour JW, Onken MD, Roberson ED, Duan S, Cao L, Worley LA, et al. Frequent mutation of BAP1 in metastasizing uveal melanomas. Science. 2010;330:1410-3.

97. Pena-Llopis S, Vega-Rubin-de-Celis S, Liao A, Leng N, Pavia-Jimenez A, Wang S, et al. BAP1 loss defines a new class of renal cell carcinoma. Nat Genet. 2012;44(7):751-9.

98. Sashida G, Wang C, Tomioka T, Oshima M, Aoyama K, Kanai A, et al. The loss of Ezh2 drives the pathogenesis of myelofibrosis and sensitizes tumor-initiating cells to bromodomain inhibition. J Exp Med. 2016;213(8):1459-77.

99. Benhamouche S, Curto M, Saotome I, Gladden AB, Liu CH, Giovannini M, et al. Nf2/Merlin controls progenitor homeostasis and tumorigenesis in the liver. Gene Dev. 2010;24(16):1718-30.

100. Taguchi T, Jhanwar SC, Siegfried JM, Keller SM, Testa JR. Recurrent deletions of specific chromosomal sites in 1p, 3p, 6q, and 9p in human malignant mesothelioma. Cancer Res. 1993;53:4349-55.

101. Cheung M, Testa JR. BAP1, a tumor suppressor gene driving malignant mesothelioma. Transl Lung Cancer Res. 2017;6(3):270-8.

102. Betti M, Aspesi A, Biasi A, Casalone E, Ferrante D, Ogliara P, et al. CDKN2A and BAP1 germline mutations predispose to melanoma and mesothelioma. Cancer letters. 2016;378(2):120-30.

103. Baser ME, De Rienzo A, Altomare D, Balsara BR, Hedrick NM, Gutmann DH, et al. Neurofibromatosis 2 and malignant mesothelioma. Neurology. 2002;59:290-1.

104. Baser ME, Rai H, Wallace AJ, Evans DG. Neurofibromatosis 2 (NF2) and malignant mesothelioma in a man with a constitutional NF2 missense mutation. Fam Cancer. 2005;4:321-2.

105. Vogelstein B, Kinzler KW. The path to cancer —three strikes and you're out. N Engl J Med. 2015;373(20):1895-8.

106. Vo BT, Li C, Morgan MA, Theurillat I, Finkelstein D, Wright S, et al. Inactivation of Ezh2 Upregulates Gfi1 and Drives Aggressive Myc-Driven Group 3 Medulloblastoma. Cell Rep. 2017;18(12):2907-17.

107. Price B. Analysis of current trends in United States mesothelioma incidence. Am J Epidemiol. 1997;145(3):211-8.

108. Miller J, Wynn WH. A malignant tumour arising from the endothelium of the peritoneum and producing a mucoid ascitic fluid. J Pathol Bacteriol. 1908;12:267-U69.

109. Garcia-Fadrique A, Mehta A, Mohamed F, Dayal S, Cecil T, Moran BJ. Clinical presentation, diagnosis, classification and management of peritoneal mesothelioma: a review. J Gastrointest Oncol. 2017;8(5):915-24.

110. Bridda A, Padoan I, Mencarelli R, Frego M. Peritoneal mesothelioma: a review. MedGenMed. 2007;9(2):32.

111. Broeckx G, Pauwels P. Malignant peritoneal mesothelioma: a review. Transl Lung Cancer Res. 2018;7(5):537-42.

112. Helm JH, Miura JT, Glenn JA, Marcus RK, Larrieux G, Jayakrishnan TT, et al. Cytoreductive surgery and hyperthermic intraperitoneal chemotherapy for malignant peritoneal mesothelioma: a systematic review and meta-analysis. Ann Surg Oncol. 2015;22(5):1686-93.

113. Verma V, Sleightholm RL, Rusthoven CG, Koshy M, Sher DJ, Grover S, et al. Malignant Peritoneal Mesothelioma: National Practice Patterns, Outcomes, and Predictors of Survival. Ann Surg Oncol. 2018;25(7):2018-26.

114. Hung YP, Dong F, Watkins JC, Nardi V, Bueno R, Dal Cin P, et al. Identification of ALK Rearrangements in Malignant Peritoneal Mesothelioma. JAMA Oncol. 2018;4(2):235-8.

115. Zalcman G, Mazieres J, Margery J, Greillier L, Audigier-Valette C, Moro-Sibilot D, et al. Bevacizumab for newly diagnosed pleural mesothelioma in the Mesothelioma Avastin Cisplatin Pemetrexed Study (MAPS): a randomised, controlled, open-label, phase 3 trial. Lancet. 2016;387(10026):1405-14.

116. Calabro L, Maio M. Immune checkpoint blockade in malignant mesothelioma: A novel therapeutic strategy against a deadly disease? Oncoimmunology. 2014;3(1):e27482.

117. Scherpereel A, Mazieres J, Greillier L, Lantuejoul S, Do P, Bylicki O, et al. Nivolumab or nivolumab plus ipilimumab in patients with relapsed malignant pleural mesothelioma (IFCT-1501 MAPS2): a multicentre, open-label, randomised, non-comparative, phase 2 trial. Lancet Oncol. 2019;20(2):239-53.

118. Medifee.com. 2019 [cited 2019 04/17]. Available from: http://www.medifee.com/blog/wp-content/uploads/2016/06/peritoneal-mesothelioma-medifee.png.

119. Schnuriger B, Barmparas G, Branco BC, Lustenberger T, Inaba K, Demetriades D. Prevention of postoperative peritoneal adhesions: a review of the literature. Am J Surg. 2011;201(1):111-21.

120. Liakakos T, Thomakos N, Fine PM, Dervenis C, Young RL. Peritoneal adhesions: Etiology, pathophysiology, and clinical significance - Recent advances in prevention and management. Digest Surg. 2001;18(4):260-73.

121. Tsai JM, Sinha R, Seita J, Fernhoff N, Christ S, Koopmans T, et al. Surgical adhesions in mice are derived from mesothelial cells and can be targeted by antibodies against mesothelial markers. Sci Transl Med. 2018;10(469).

122. Shibuya M. Vascular Endothelial Growth Factor (VEGF) and Its Receptor (VEGFR) Signaling in Angiogenesis: A Crucial Target for Anti- and Pro-Angiogenic Therapies. Genes Cancer. 2011;2(12):1097-105.

123. Asano Y, Jimenez-Dalmaroni A, Liverpool TB, Marchetti MC, Giomi L, Kiger A, et al. Pak3 inhibits local actin filament formation to regulate global cell polarity. HFSP J. 2009;3(3):194-203.